THE HIGH TEMPERATURE, HIGH VACUUM VAPORIZATION AND THERMODYNAMIC PROPERTIES OF URANIUM DIOXIDE

by

Raymond J. Ackermann
A.B., University of Kansas, 1952

Submitted to the Department of Chemistry and the Faculty of the Graduate School of the University of Kansas in partial fulfillment of the requirements for the degree of Doctor of Philosophy

October, 1955

TABLE OF CONTENTS

TABLE OF CONTENTS

TABLE OF CONTENTS

TABLE OF CONTENTS

TABLE OF CONTENTS

TABLE OF CONTENTS

THE HIGH TEMPERATURE, HIGH VACUUM VAPORIZATION AND THERMODYNAMIC PROPERTIES OF URANIUM DIOXIDE

by

Raymond J. Ackermann

I. INTRODUCTION

The investigation of phenomena at temperatures in excess of 1000°C has only recently assumed a position of prominence in the broad field of physical chemistry. The recent interest in high temperature industrial processes and the application of atomic energy to both military and civilian projects has brought about a pressing demand for a knowledge of high temperature chemistry.

One might be led to believe that the prime obstacle to the utilization of high temperature processes would be the difficulty in development of materials of construction for use in high temperature systems. To be sure, this is certainly true to a very large extent when one is dealing with temperatures greater than 2000°C. The more fundamental difficulty lies in the lack of information about the types of compounds that can exist at high temperatures and, therefore, about the kinds of reactions that are likely to occur at these elevated temperatures.

This research was concerned with the high temperature properties of the uranium-oxygen system above 1000°C. The reasons for studying this system were to attempt to clarify some of the apparent complexities of the system and to gain information about its high temperature behavior.

In this system there are well established compounds at the compositions UO_2, U_4O_9, U_3O_8, and UO_3. Considerable work on the chemistry of the compounds, the phase relationships in the system, the thermodynamic properties of the compounds, the various crystal structures, and the decomposition behavior of the higher oxides has been previously accomplished.

The purpose of this investigation has been to establish the vaporization processes and the thermodynamic properties of the lower uranium oxides at high temperatures. The difficulties of calorimetric techniques at high temperatures have precluded a straightforward determination of heats and entropies of formation of many solid, liquid and gaseous substances. Lacking such information, chemists have found studies of the volatilities of various refractory substances to be the best approach to the problem of high temperature chemistry.

The principal experiments that were performed to show the high temperature behavior of the lower uranium oxides included the establishment of the vapor pressure of the dioxide, UO_2, by effusion measurements, the measurement of the volatility of uranium-uranium dioxide mixtures, and X-ray studies of residues and sublimates resulting from vaporization experiments.

Effusion measurements on UO_2 were carried out over a temperature range of 1200°, extending from 1300°C to about 2500°C. The calculated vapor pressures ranged from 10^{-8} mm to about 6 mm, a range greater than 10^8. These temperature and pressure ranges are about three times the usual ranges reported in the literature. No measurements over such wide ranges of pressure and temperature have ever been reported previously.

The results of the measurements show that $UO_2(s)$ vaporizes congruently. Its heat of sublimation and the stability and dissociation energy of $UO_2(g)$ have been established. The results of the mixture experiments have been used to show that fragmentation is unimportant in the vaporization of $UO_2(s)$. Pronounced curvature of a log p vs. $1/T$ plot at temperatures above 2200°K can be interpreted in terms of the existence of a gaseous dimer, $U_2O_4(g)$.

II. VAPORIZATION PROCESSES OF METAL OXIDES

For the purpose of discussing the results of this investigation, it is convenient to arbitrarily classify the high vacuum vaporization processes of all metal oxides studied to date. Five classes result.

Oxides belonging to the first class vaporize predominantly to the gaseous elements in accordance with the general equation

$$M_xO_y(s) \longrightarrow xM(g) + y\,(1 - \alpha)/2\ O_2(g) + y\alpha O(g), \qquad (1)$$

where α is the degree of dissociation of oxygen. An oxide belonging to this class may vaporize either congruently, as shown in Eq. (1), or incongruently. If congruent vaporization occurs, the composition of the vapor phase will remain identical with that of the condensed phase during the course of vaporization. The oxide, NiO, vaporizes congruently to the elements.[8] If, however, incongruent vaporization occurs, the composition of the vapor phase will not be the same as that of the solid phase during the course of vaporization, since either metal or oxygen is preferentially lost. The composition of the condensed phase will therefore become progressively richer in the component that is less readily lost. This enrichment can be accommodated by the condensed phase either in the form of a solid solution or by the appearance of a second solid phase.

The second class consists of oxides which decompose upon heating to yield oxygen and a lower oxide with no appreciable loss of the metal to the vapor phase:

$$M_xO_y(s) \longrightarrow M_xO_{y-z}(s) + z\alpha\, O(g) + z(1 - \alpha)/2\ O_2(g). \qquad (2)$$

Vaporization of such an oxide occurs incongruently since the condensed phase constantly changes in composition. The iron oxide, $Fe_2O_3(s)$, vaporizes thus to form $Fe_3O_4(s)$ and oxygen.[8]

The third class of oxides, which has only recently been studied, is composed of oxides which predominantly vaporize without decomposition:

$$M_xO_y(s) \longrightarrow M_xO_y(g) \qquad (3)$$

Since no decomposition occurs, the vaporization process is congruent. An example of an oxide showing this behavior is TiO.[71]

The fourth class of oxides contains those which vaporize either congruently or incongruently by disproportionation according to the general expression

$$M_{a+x}O_{b+y}(s) \longrightarrow M_aO_b(g) + M_xO_y(s, \text{ or } g). \qquad (4)$$

Examples of oxides exhibiting congruent disproportionation are SiO_2 and possibly Ti_2O_3. The oxide SiO_2 vaporizes to form SiO(g) and oxygen[8] while it has been postulated that Ti_2O_3 vaporizes to TiO(g) and TiO_2(g).[25] An example of an incongruent disproportionation is furnished by WO_2, which vaporizes to W(s) and WO_3(g).

The fifth class contains oxides which form gaseous dimers or polymers according to the expression

$$aM_xO_{y+z}(s) \longrightarrow (M_xO_y)_a(g) + az(1-\alpha)/2\ O_2(g) + az\alpha\ O(g). \qquad (5)$$

This kind of vaporization process is exemplified by the oxide B_2O_3 which vaporizes congruently to form predominantly B_2O_2(g) and oxygen.[11]

In order to ascertain how a given oxide vaporizes, one can gain considerable information from vapor pressure measurements of the oxide. When one attempts to measure the equilibrium vapor pressure of a given oxide, the exact nature of the phase diagram is important. The phase law states that unique values of the vapor pressure will be obtained if, and only if, the system is invariant. In a two-component system, such as the uranium-oxygen system, meaningful vapor pressure measurements at a given temperature may be carried out only on the following invariant systems:

(1) a system that is congruently vaporizing, ~~and~~ or

(2) a system which possesses two condensed phases plus a vapor phase.

Under certain experimental conditions one may be able to perform quasi-equilibrium vapor pressure measurements on a single condensed phase that is not congruently vaporizing, provided the composition of the condensed phase, and consequently the pressure, does not appreciably change during the time of measurement. Such a system is frequently referred to as a pseudo-invariant system.

Whether a vaporization process is invariant at a given temperature may be established by observing the constancy of the volatility as a function of time and by examination of the residue and sublimate for the phase or phases present by conventional X-ray diffraction techniques. Chemical analyses of residues and sublimates are quite useful in supplementing X-ray data.

Oxides belonging to the first class, provided they vaporize congruently, can be identified rather easily if the free energy of formation of the oxide and the vapor pressure of the metal are known. A knowledge of these thermodynamic quantities enables one to calculate the decomposition pressure of the oxide at a given temperature. If this calculated

decomposition pressure agrees with the experimentally measured volatility, one must conclude that the oxide vaporizes predominantly to the gaseous elements. If, however, the measured volatility of the oxide is considerably larger than the calculated decomposition pressure, one must then conclude that gaseous oxide molecules are important in the equilibrium vapor above the condensed phase, and vaporization occurs via one or more processes as shown by equations (3), (4), and (5).

Once the invariance of the vaporization process of a given oxide is established, one can then carry out meaningful vapor pressure measurements, which enable one to calculate a heat of sublimation or vaporization, ΔH, using the well-known form of the Clapeyron equation:

$$\frac{\partial(\ln p)}{\partial(1/T)} = -\Delta H/R. \qquad (6)$$

The change in entropy accompanying sublimation or vaporization, which is also obtainable from vapor pressure measurements, gives additional insight into the type of vaporization process that occurs. If oxide molecules are important in the vapor phase, heats of vaporization and/or sublimation may be combined with heats of formation and other thermodynamic data to yield a value of the dissociation energy of a particular gaseous molecule. Such combinations of thermodynamic data are frequently referred to in the literature as thermodynamic cycles. If, however, a spectroscopic value of the dissociation energy is known, one then may calculate a value for the heat of formation of the compound under study. If vapor pressure measurements are carried out over both the solid and liquid states of a substance, it may then be possible to evaluate the heat of fusion of the solid. However, since the heat of fusion is sometimes only a few thousand calories per mole, the necessary break in the vapor pressure plot may be obscured by experimental error, and the heat of fusion may then only be estimated.

Conventional measurements of vapor pressures are usually restricted to a narrow range of temperature amounting to only a few hundred degrees, and the logarithm of the vapor pressure is a linear function of the reciprocal of the absolute temperature within the error of measurement. Vapor pressure measurements that extend over a temperature range that is many-fold the conventional range may enable one to detect real curvature in a log p vs. $1/T$ plot. If the curvature if due to the variation of ΔH with temperature, i.e., the difference ΔC_p between the heat capacities of the vapor and condensed phases is not zero, then the heat of vaporization and/or sublimation may be calculated as a function of temperature and, provided the heat capacity of the condensed phase is known, the heat capacity of the vapor phase may be evaluated and not merely estimated. It should be pointed out, however, that the establishment of

ΔC_p by measurement of the vapor pressure is far from being an easy task because of the extreme precision required in the measurements to detect the very slight curvature in a plot of log p vs. $1/T$.

It should be emphasized that real curvature in the vapor pressure plot may result from a number of simultaneously important processes, thus adding to the complexity of high temperature investigations of chemical systems. Hence, it is sometimes impossible to prove unequivocally a particular process to be the cause of this curvature unless other independent data are known or obtained by further investigation. Data obtained from mass spectrometry, high temperature heat capacity measurements, spectroscopy, velocity selectors and momentum detectors may then be necessary to supplement vapor pressure data and to complete the study of high temperature systems.

III. PRIOR INVESTIGATIONS IN THE URANIUM-OXYGEN SYSTEM

A. The Oxides of Uranium

The uranium-oxygen system is no doubt the most complex of the actinide-oxygen systems studied to date. The three most common oxides of uranium, UO_2, U_3O_8, and UO_3, have been known for almost a century, but it has been only recently that systematic investigations have been carried out in the system. Biltz and Mueller[2] were the first to study in detail systems of oxygen composition greater than UO_2, and their data have been copiously quoted throughout the chemical literature. More recent investigations[4, 1, 27, 56, 55, 24, 59, 19, 30] have yielded considerable new information about the system, while comprehensive surveys and reports[36,7] have appeared in the literature within the last few years. A complete X-ray diffraction study of unit cell structures and dimensions of all known oxides of uranium has been carried out by Rundle, et al.[59]

Recent controversy has arisen concerning the existence of the solid monoxide UO. The only evidence for the formation of this phase has been obtained by X-ray diffraction techniques which have yielded a cubic lattice parameter a_0 varying from 4.91 to 4.93 Å units. All attempts to prepare the monoxide free from the isomorphous monocarbide, UC, and the mononitride, UN, have met with failure.[59] Attempts to prepare the monoxide by heating UO_2, or a higher oxide, with uranium metal at high temperatures have usually been disappointing, although Dawson and Lister[19] claim to have prepared UO by such a procedure, but make no mention of possible carbide or nitride contamination. Rundle, et al.[59] have proposed that carbon is necessary either to promote the reaction of a higher oxide with uranium to form the UO phase, or that some UC and UN must be present for the UO phase to form. They find that a_0 for UN is 4.880 Å units and a_0 for UC is 4.951 Å units. It is significant that the lattice parameter of what is assumed to be the UO phase lies between those of the monocarbide and the mononitride, which are isomorphous and readily form solid solutions. In all probability the UO phase should be described as UX where X is carbon, nitrogen and perhaps oxygen in somewhat varying proportions.

The dioxide UO_2 is a dark brown crystalline solid possessing a face-centered cubic (fluorite structure) unit cell. Rundle, et al.[59] have measured the lattice parameter of this unit cell to be 5.4581 ± 0.0005 kx units. This value of the lattice parameter yields a theoretical density of 10.97 g/cm^3. The compound UO_2 readily takes up oxygen at low temperatures (150 to 200°C) to form solid solutions having the general designation UO_{2+x}, where x varies from 0.00 up to a reported maximum of about 0.34.[36, 24] Alberman and Anderson[1] have measured the lattice parameter of the UO_{2+x} phase as a function of increasing oxygen content and found that the size of the unit cell remained constant within their experimental error. The existence of a UO_{2-x} cubic phase has also been claimed

by numerous investigators on the basis of X-ray evidence. However, the evidence for the existence of such a metal rich solid solution phase is very meager and a more thorough investigation is demanded.

Above 500°C the UO_{2+x} phase separates into two cubic phases, a lower oxide phase having a somewhat variable composition ranging from $UO_{2.00}$ to $UO_{2.07}$, and a higher oxide phase having a fixed composition of $UO_{2.25}$.[27] This higher oxide phase shows no appreciable oxygen solubility and should probably be designated as a compound U_4O_9. This compound has been incorrectly referred to in the literature as β-UO_2. Although rather limited investigation has been carried out in this region of the uranium-oxygen system, it is suspected that the two cubic phases merge at somewhat higher temperature and high oxygen pressure. At temperatures below 800°K, the system is further complicated by the presence of a tetragonal phase having a composition that varies between $UO_{2.42}$ and $UO_{2.29}$. Most of this variation in composition occurs between 400°K and 500°K.[27]

The composition region from $UO_{2.56}$ to $UO_{2.67}$ has been recently studied by Hoekstra, et al.[30] using high-temperature X-ray diffraction techniques.

In the composition region between U_3O_8 and UO_3 only Biltz and Mueller[2] have carried out any systematic investigation. Their work indicates a two-phase region at temperatures below about 850°K and probably a UO_{3-x} homogeniety range extending from about $UO_{2.9}$ up to $UO_{3.0}$.

Uranium trioxide, UO_3, exists in an amorphous form and in at least four crystalline modifications.[36] The transition temperatures and heats of transition between these various crystalline modifications have not been reliably established to date.

The condensed phase diagram of the uranium-oxygen system was sketched on the basis of these previous investigations carried out with the system and is shown in Fig. 1.

B. Previous High Temperature Investigations with UO_2

Only very limited investigations of the high temperature behavior of UO_2 have been carried out prior to this work. Greenwood[23] proposed that UO_2 loses oxygen above 1600°C in vacuo. His statement is not supported by experimental proof but results from an analogy drawn between UO_2 and MnO_2. Rehn and Cefola[56] measured the vapor pressure of UO_2 at only five temperatures over the range 1600°C to 2000°C. Their measurements were carried out by means of the effusion method with alpha counting used as the analytical means for assay of collected sublimates. Their data yield a heat of sublimation for UO_2 of 137 kcal $mole^{-1}$ and a vapor pressure of 1.4×10^{-6} atm at 2000°K.

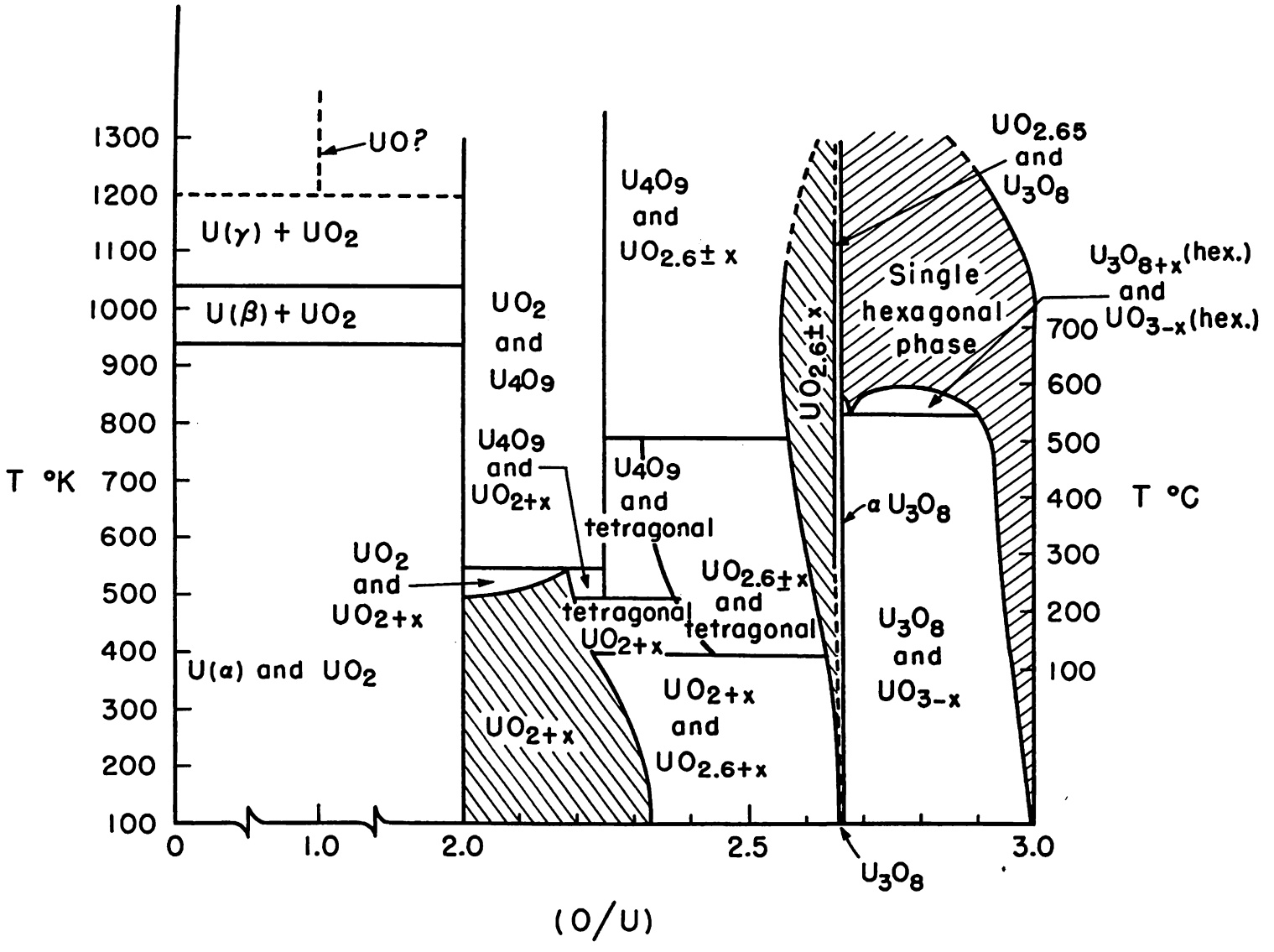

Figure 1

The Tentative Condensed Phase Diagram of the Uranium-Oxygen System for Composition vs. Temperature

(The lined areas represent single phase regions)

During the course of their investigation of the vapor pressure of liquid uranium, Rauh and Thorn[55] observed a marked suppression of the volatility of the liquid metal upon introducing residual pressures of oxygen of the order of 10^{-6} to 10^{-7} mm. They interpreted this phenomenon as being caused by the formation of an oxide coating, which they designated as UO_x, which partially covered the liquid metal surface. Extrapolation of the data to complete coverage of the liquid by the impervious oxide coating gave a result which was interpreted as the vapor pressure of UO_x. The heat of vaporization of UO_x obtained from the slope of log p vs. $1/T$ was 1.34 kcal $mole^{-1}$ and the vapor pressure was 6×10^{-7} atm at 2000°K. This UO_x is about a factor of two less volatile than UO_2 as measured by Rehn and Cefola. If x = 2, a discrepancy exists between the two investigations.

Brewer, et al.[6] gave, in their compilation of thermodynamic data, an estimated value for the vapor pressure of UO_2 of 10^{-8} atm at 2000°K. Brewer[7] also lists a value of D_O, the dissociation energy of UO_2 to gaseous atoms at 0°K, as being 355 kcal $mole^{-1}$.

Another high temperature physical property of UO_2 that has undergone limited investigation is the melting point, and there have been as many values of it as there have been investigators. Ruff and Gocke[58] reported the melting point of UO_2 under a nitrogen atmosphere to be 2176°C, while Friederich and Sittig[21] reported 2500° to 2600°C in a nitrogen atmosphere. The most recent value is given by Lambertson and Gunzel[45] as 2878 ± 22°C in a helium atmosphere.

Wahlin[69] heated a tungsten wire containing UO_2 to a temperature of about 1800°C and observed three types of ions: U^+, W^+, and UO^+, using a magnetic deflection method. No data were given concerning the relative intensities of these species and no mention of UO_2^+ was indicated.

The low temperature heat capacity of $UO_2(s)$ from 0° to 300°K has been determined by Jones, Gordon, and Long.[35] The high temperature heat content and the heat capacity of $UO_2(s)$ were measured over the temperature range 298° to 1500°K by Moore and Kelley[51] using a "drop" calorimeter. No solid phase transitions were observed over this temperature range. The heat of formation of $UO_2(s)$ at 298°K has been measured by Huber, Holley, and Meierkord.[31] These thermodynamic data have been used by Coughlin[16] to compile heats and free energies of formation of $UO_2(s)$ from 298° to 1500°K.

IV. THEORY AND METHODS PERTINENT TO THIS INVESTIGATION

A. The Effusion Method of Measuring Vapor Pressures

Vapor pressures in the range 10^{-8} mm to 10^{-1} mm are usually determined by one of two conventional methods, the Langmuir rate of evaporation method[46] and the Knudsen effusion method.[41, 42, 43, 44, 67] Both methods are similarly based on the kinetic theory of gases. In the case of the effusion method the vapor flows from a space, where it is in equilibrium at some given temperature with the condensed phase, through an orifice into a high vacuum. This rate of flow through the orifice can be simply related to the vapor pressure of the condensed phase. Since the effusion method was employed throughout this investigation, and since vapor pressures as large as 6 mm down to 10^{-8} mm were measured, it is of significant interest to derive and discuss the relationships employed by this method.

1. Theory

Let us consider a saturated vapor in thermal and mechanical equilibrium contained in space A as shown in Fig. 2. Any given molecular velocity must be equally distributed in all directions, otherwise mass transfer would occur in the gas, contrary to our assumption of mechanical equilibrium. Consider a small circular plane element of area dS drawn anywhere in the space of the gas. Molecules will be crossing dS continually in both directions; consider only those which cross dS toward one side only. Of the $\underline{n}$ molecules per unit volume, $4\pi nA\, v^2\, e^{-B^2v^2}\, dv$ are moving with speeds in a particular speed range between v and v + dv, where $A = B^3/\pi^{3/2}$ and $B^2 = M/2RT$. Since the molecules are moving equally in all directions, i.e., the gas is isotropic, $d\omega/4\pi$ will be the fraction moving in directions lying within the element of solid angle $d\omega$. Of these molecules, as many will cross dS during a time dt as lie at the beginning of dt within a cylinder having a base dS and a slant height v dt, and therefore a volume $v\,dt \cdot dS \cos\theta$. Hence, the number of molecules crossing dS in time dt within a given solid angle $d\omega$ is $4\pi A\, nv^2\, e^{-B^2v^2} \frac{d\omega}{4\pi} v\,dt\,dS\cos\theta$. Substitution of $d\omega = \sin\theta\, d\theta d\phi$, division by dS and dt, and integration over ϕ from 0 to 2π yield for the number of molecules in the speed range v to v + dv crossing unit area in unit time in the specified direction θ, $2\pi n A\, v^3\, e^{-B^2v^2}\, dv \sin\theta\cos\theta\, d\theta$. The total number of molecules per unit time per unit area, $\underline{Z}$, crossing a given section toward one side regardless of speed and direction is obtained by integrating the last expression over θ from 0 to $\pi/2$, and from 0 to ∞ over $\underline{v}$:

$$Z = 2\pi \underline{n} A \int_0^\infty v^3\, e^{-B^2v^2}\, dv \int_0^{\pi/2} \sin\theta\, \cos\theta\, d\theta. \qquad (7)$$

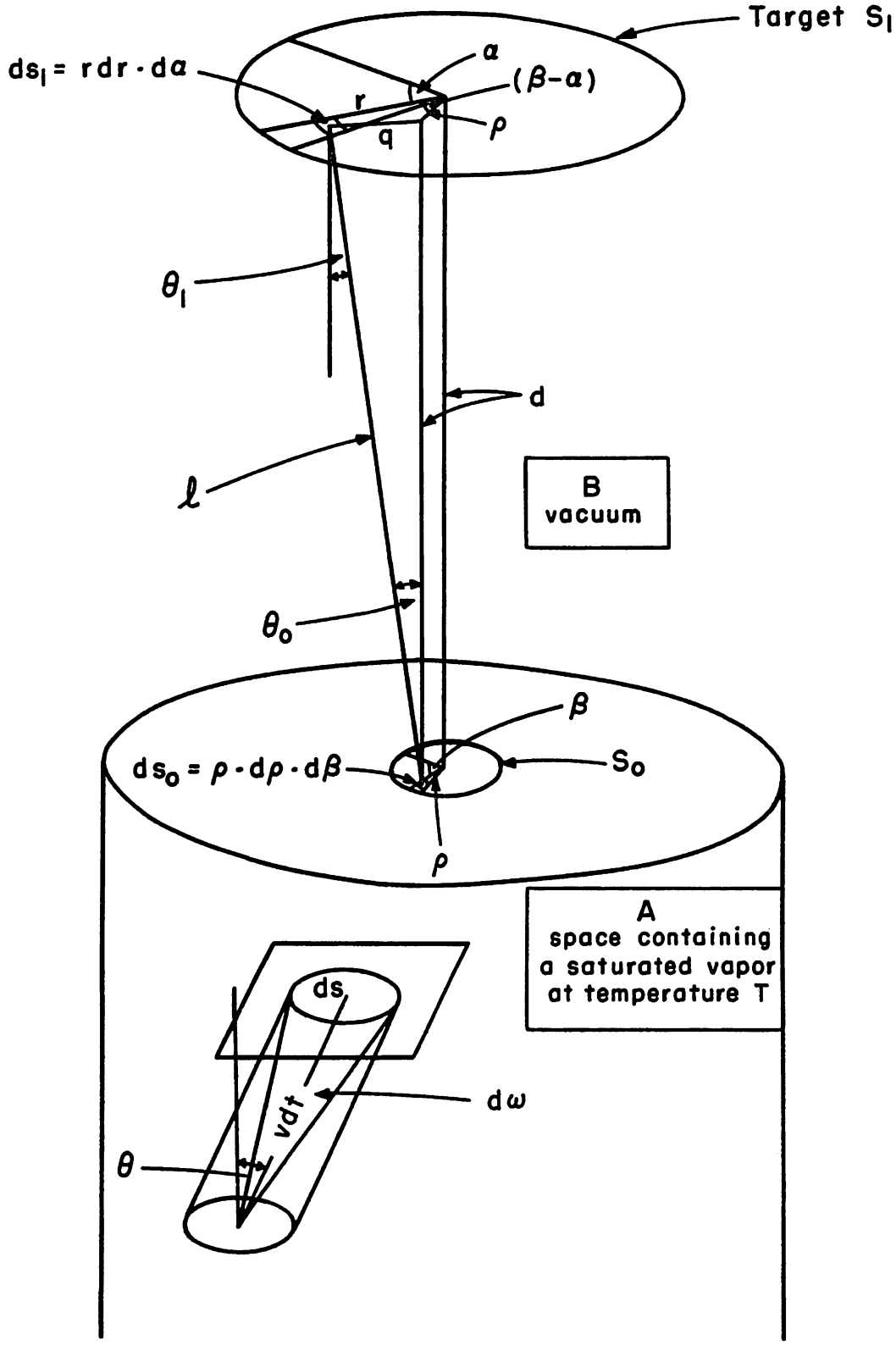

Figure 2

Effusion Through a Thin-Edged Orifice and the Cosine Law

Evaluation of the first integral by the method of parts yields $1/2B^4$. The second integral integrates to 1/2. Hence, $Z = \pi nA/2B^4$ molecules per unit area per unit time.

Substitution for B and A yields, upon rearrangement,

$$Z = (1/4)\, n \left(\frac{8}{\pi}\frac{RT}{M}\right)^{1/2} = \frac{n\bar{c}}{4} \quad \text{molecules cm}^{-2}\,\text{sec}^{-1} \ , \tag{8}$$

where $\bar{c}$ is the average Maxwellian velocity. At pressures less than 0.1 mm one can assume the vapor to behave ideally. Then

$$n = P/kT \ . \tag{9}$$

Referring now to Fig. 2, let us suppose that S_0 is a small circular orifice located in the wall of container A. Above the plane of the orifice is a region of high vacuum, B, and a collector plate, S. To simplify matters we shall consider orifice S_0 to be ideal, that is, its presence does not disturb the velocity distribution of the molecules in container A, and every molecule which strikes S_0 is transmitted into region B. In reality this assumption of an ideal orifice would be justified provided the orifice area were very small and its circumference were knife-edged.

Since $(n\bar{c}/4)S_0$ molecules strike S_0 per second and are transmitted into region B, it is of interest to calculate how many of these molecules will strike a plane circular area S_1 parallel to S_0 and perpendicular to a line joining its center with that of S_0.

The number of molecules leaving dS_0 and arriving at dS_1, an elemental area located in S_1 a distance ℓ from dS_0, is given by

$$dz = \frac{(Z)}{\pi}\ \frac{\cos\theta_0\, dS_0\, \cos\theta_1\, dS_1}{\ell^2} \ . \tag{10}$$

The $\cos\theta$'s enter in Eq. (10) from purely geometrical considerations and π enters in a proportionality factor. Equation (10) is a general statement of Lambert's cosine law.

By inspection of Fig. 2, one finds that

$$q^2 = r^2 + \rho^2 - 2r\rho\, \cos\,(\beta-\alpha) \quad , \tag{11}$$

where q is a line in the target joining the projection of dS_0 along d with dS_1, r and α are the polar coordinates in the target S_1 and ρ and β are the polar coordinates in the orifice S_0. Also by inspection one writes that

$$\ell^2 = d^2 + q^2 = d^2 + r^2 + \rho^2 - 2r\rho\, \cos\,(\beta-\alpha), \tag{12}$$

$$\theta_0 = \theta_1 \quad , \tag{13}$$

and

$$\cos\theta_1 = d/\ell \quad . \tag{14}$$

Substitution of the above quantities into Eq. (10) gives

$$dz = \frac{Z\, d^2\rho \cdot d\rho \cdot d\beta \cdot r \cdot dr \cdot d\alpha}{\pi[\, d^2 + r^2 + \rho^2 - 2r\rho\, \cos\,(\beta-\alpha)\,]^2} \quad . \tag{15}$$

Integration over the four variables r, ρ, α, β gives the number of molecules leaving an orifice of radius ρ and arriving at a collector plate of radius r located a distance d from the orifice.

$$\int dz = \frac{Z}{\pi} \int_0^{2\pi} \int_0^{2\pi} \int_0^{r} \int_0^{\rho} \frac{d^2 \cdot \rho \cdot d\rho \cdot d\beta \cdot r \cdot dr \cdot d\alpha}{[d^2 + r^2 + \rho^2 - 2r\rho\cos(\beta-\alpha)]^2} \tag{16}$$

The integration cannot be performed exactly, but approximate methods[33, 63] have been worked out and the error resulting in their use is not great. In general, as was the case in this research, it is possible to consider S_0 as being very small. If this assumption is valid then, $\rho << r$ and $\rho^2 - 2r\rho\cos(\beta-\alpha)$ can be neglected compared with $d^2 + r^2$ in the denominator of Eq. (16). Removal of $\rho\ d\rho\ d\beta\ (=S_0)$ from under the integral sign is also certainly justified if the above condition is fulfilled. Then after integration over $d\alpha$ Eq. (16) simplifies to

$$\int dz = \frac{Z}{\pi} S_0\, d^2\, 2\pi \int_0^{r} \frac{r\, dr}{(d^2 + r^2)^2} \quad . \tag{17}$$

Performing the simple integration one finds

$$\int dz = Z\, S_0 \left(\frac{r^2}{d^2 + r^2}\right) = N \text{ molecules sec}^{-1} \quad . \tag{18}$$

The resulting bracketed term represents the fraction of the total effusate intercepted by a plane target of radius r located a perpendicular distance d from an ideal orifice.

Upon expressing N in moles per sec and making the necessary substitution for Z in terms of Eq. (8), one finds that

$$p = \frac{W}{S_0 t}\left(\frac{2\pi RT}{M}\right)^{1/2}\left(\frac{d^2 + r^2}{r^2}\right) \qquad (19)$$

where:

W = mass of vapor striking target S_1 in grams,

S_0 = area of orifice in cm^2,

t = time in seconds,

R = gas constant in appropriate units,

T = the absolute temperature,

M = the molecular weight of the vapor.

Hence, the measurement of the vapor pressure of a solid or liquid requires a determination of the four fundamental quantities: mass, length, time, and temperature.

In order that the equilibrium vapor pressure of the condensed phase contained in the effusion cell be obtained from the measured fundamental quantities, it is necessary that certain conditions be fulfilled. These are:

(1) The cell and the condensed phase must remain at a constant, known temperature.

(2) The molecular weight of the vaporizing species must be known.

(3) The condensation coefficient of the vapor molecules striking the target must be known.

(4) Appreciable re-evaporation of vapor molecules off the surfaces of the vacuum system onto the target must not occur.

(5) No appreciable scattering of the vapor molecules must occur between the orifice and target.

(6) The orifice must be knife-edged.

(7) The equilibrium vapor pressure must exist within the effusion cell.

(8) The condensed phase under investigation must react neither with the effusion cell material nor with residual gases in the vacuum.

That conditions (1) through (4) must be met is self-evident from Eq. (19), and the specific way in which each of these conditions was fulfilled is reserved for a later section of this thesis. Some discussion should be given, at this time to the remaining conditions.

Condition (5) may be easily achieved by maintaining region B (see Fig. 2) at a very low pressure. Molecules issuing from S_0 experience almost no collisions and travel in straight lines forming what is commonly known as a "molecular beam." (64) The probability that a vapor molecule in the molecular beam will experience a collision in traversing a distance ℓ in the vacuum containing residual gas molecules is given by $e^{-\ell/\lambda}$, where λ is the mean free path of a beam molecule in the residual gas of pressure p. Since this mean free path will not differ greatly from the mean free path of a residual gas molecule, it may be calculated approximately from the classical expression(50)

$$\lambda = \frac{kT}{\sqrt{2}\,\pi\sigma^2 p}\,, \tag{20}$$

where k is Boltzmann's constant, T is the absolute temperature of the residual gas molecules, σ is the mean collision diameter of the colliding molecules, and p is the pressure in dynes cm^{-2}.

If condition (6) is not fulfilled, then the probability of transmission of a vapor molecule through an orifice that is not knife-edged is less than unity and depends in a rather complicated manner on the radius and thickness of the orifice. Clausing(12, 13, 14) has studied this problem in great detail and was able to calculate a so-called transmission probability for a circular orifice of given dimensions.

Condition (8) may be considered as a special example of condition (7). If reaction occurs between the condensed phase and the effusion cell material or residual gases in the vacuum system, the equilibrium pressure of the condensed phase will be disturbed. In order to fulfill the requirement demanded by condition (7) let us consider an effusion cell having an orifice S_0 and containing a condensed phase with evaporating area S_a. The weight loss in grams of the substance per unit time, m, is given by

$$m/S_0 = p(M/2\pi RT)^{1/2}\,, \tag{21}$$

where p is the actual pressure existing in the effusion cell. The number of grams of vapor condensing on the substance per unit area in unit time is given by

$$\alpha p(M/2\pi RT)^{1/2}\,,$$

where α is the condensation coefficient. If η grams of the substance vaporize per unit area in unit time, then from a mass balance one obtains

$$m/S_a = \eta - \alpha p(M/2\pi RT)^{1/2} \quad , \tag{22}$$

because the net mass which leaves the substance in unit time must equal the mass escaping out the orifice in unit time. But when $m = 0$, $p = \overset{\circ}{p}$, the saturated vapor pressure, because then the number of molecules striking the condensed phase exactly equals the number leaving it. Hence,

$$\eta = \alpha \overset{\circ}{p} (M/2\pi RT)^{1/2} \quad , \tag{23}$$

and

$$m/S_a = \alpha(\overset{\circ}{p}-p) (M/2\pi RT)^{1/2} \quad . \tag{24}$$

Simple algebraic rearrangement yields

$$p = \overset{\circ}{p}/[1 + (S_0/\alpha S_a)]. \tag{25}$$

Therefore, if $S_a >> S_0$ (α is generally very close to unity), then $p \cong \overset{\circ}{p}$ and the error involved in assuming the observed vapor pressure to be the saturated vapor pressure is insignificant.

The necessary conditions for the precise and accurate determination of vapor pressures up to 0.1 mm by the effusion method have been discussed. Since effusion measurements in this research were carried out at pressures somewhat higher than the generally accepted upper limit of the method, it is of interest to review the experimental attempts to establish this upper limit; no adequate theoretical treatment concerning this upper limit has been thus far advanced.

2. Experimental Attempts to Establish the Limiting Conditions of the Effusion Method

The first vapor pressure measurements of a slightly volatile substance were carried out by Knudsen[43] in 1909. Since then, numerous investigators have attempted to establish the limitations of the method. In particular, studies have been undertaken to ascertain the effect of increasing the source pressure to the point where molecular flow no longer prevails, i.e., the number of gas-phase collisions becomes appreciable. The flow of gases through orifices at very high pressures can be adequately treated with hydrodynamics, whereas the flow of gases at extremely low pressures must be treated on the basis of kinetic theory. The intermediate region between hydrodynamic and molecular flow is then of interest from the standpoint of both theoretician and experimentalist in that it affords a continuous transition between the two limiting kinds of flow. Theoretical attempts to formulate the

behavior of gases at these intermediate pressures (of the order of millimeters) have been largely empirical in nature, and experimental investigations of the flow of gases at these pressures have been somewhat contradictory. Five investigations have been carried out to study the nature of flow of gases at pressures intermediate between molecular and hydrodynamic flow. The first investigation dealt with the total flow of various gases through thin-edged orifices, whereas the remaining four investigations concerned the flow in specific directions in the 2π solid angle above the plane of a thin-edged orifice.

a. The Experiments of Knudsen - Knudsen[42] first undertook the investigation of the behavior of total flow through a thin-edged orifice as a function of increasing source pressure. From kinetic theory it can be shown that the net weight of gas per second effusing through a thin-edged orifice of area a is given by the expression

$$m = a(2\pi)^{-1/2} (M/RT)^{1/2} (p' - p'') \quad , \tag{26}$$

where p' is the source pressure and p'' is the pressure outside the orifice. Knudsen defined the quantity

$$T_K = mRT/M (p' - p'') \quad , \tag{27}$$

which is independent of pressure at a given temperature T°K. Knudsen then proceeded to investigate the constancy of T_K as the mean free path became small compared to the orifice diameter.

Two different orifices were used throughout the investigation. Orifice No. 1 was produced in a 2.5- mil platinum sheet by carefully forcing a hole with a hard-pointed object; this resulted in an orifice that was not entirely round. The area of the orifice was measured to be 5.21×10^{-6} cm^2. Orifice No. 2 was produced in a similar manner; its area was measured to be 66.0×10^{-6} cm^2. The mass of gas effusing through a given orifice was determined by the initial measurement of the pressure on both sides of the orifice and repetition of the pressure measurement after a known time of flow. The measurement of pressure was effected by means of a McLeod gauge at low pressures and an ordinary mercury manometer at higher pressures.

The experimental results showed that the derived formulae for molecular flow held to close approximation when the mean free path, given by the classical expression [see Eq. (20)], was large compared to the orifice diameter. The values of T_K remained constant until the mean free path had decreased to about ten times the orifice diameter. A further decrease in the mean free path caused T_K to increase slowly until the mean free path became as small as one-tenth the orifice diameter. At this point

T_K reached the limiting value predicted by the laws of hydrodynamic flow. Further decrease in the mean free path caused no appreciable change in T_K. The source pressures at which deviations from molecular flow occurred amounted to a few tenths of a millimeter.

The flow of hydrogen, oxygen, and carbon dioxide through both orifices showed the same qualitative behavior.

Hence, Knudsen's experiments indicate that the total amount of gas effusing through a thin-edged orifice is greater than that expected from kinetic theory calculation once the mean free path has attained a value of the order of the orifice diameter. Knudsen's experiments are inherently complex since flow through the orifice occurred in both the forward and reverse directions, and, in view of more recent work, they appear to be rather crude in that they suffer from a lack of sensitive pressure measurement.

b. The Experiments of Knauer and Stern - Knauer and Stern[40] investigated the rate of the effusion as a function of source pressure of water vapor, supplied by a condensed phase, through a source slit having the dimensions 0.6 cm x 0.0022 cm. An image slit of similar dimensions defined a molecular beam which was intercepted by a liquid air-cooled silver target. The minimum time of appearance of the trace, which amounted to about 30 seconds or less, was recorded for increasing source pressures. This experiment of Knauer and Stern is contrasted with the total flow measurements of Knudsen in that the rate of flow in the forward direction was observed as a function of source pressure.

It can be shown from previously developed equations that the product of the pressure and minimum time, t_{min}, of appearance of the trace is proportional to the square root of the temperature but independent of the pressure, so long as molecular flow occurs through the orifice. Hence for short temperature ranges the quantity $p \cdot t_{min}$ should be approximately constant as the source pressure is changed.

Their results with water vapor showed that no deviation from molecular flow occurred up to source pressures of 0.5 mm Hg. At the oven pressure of 0.5 mm, the calculated mean free path of the water vapor molecules is 0.06 mm, or about 3 times the width of the source slit. At still higher pressures, the plot of pt_{min} vs p formed a curve that is convex toward the pressure axis. This means that the intensity in the forward direction falls off with increasing pressures of the source. Knauer and Stern interpreted these data in terms of a vapor cloud, located outside the orifice, which forms as a result of a large fraction of vapor phase collisions in the neighborhood of the orifice.

The above-cited experiment using water as the effusing species constitutes one of the most frequently cited reasons for limiting molecular effusion experiments to pressures less than a few tenths of a millimeter. Knauer and Stern also, however, carried out a similar experiment using mercury as the effusing vapor. A plot of pt_{min} vs p in this case passes through a definite minimum at p = 0.5 mm, in contrast to the results of the experiment using water vapor. They did not find a constant value of $p \cdot t_{min}$ even at low pressures.

The principal error associated with these experiments lies in the precise measurement of the minimum time of appearance of the trace when viewed with a microscope on the condensation target. Both physiological and psychological factors are inherent, since the measurement of time depends upon the eye response of the observer. Knauer and Stern estimated an error of 10% under the most favorable of their experimental conditions, and it remains quite possible that the intensity decrease in the water vapor experiments at higher pressures resulted from experimental error alone.

c. The Experiments of Johnson - Johnson[34] devised a molecular beam experiment to test whether an ionization gauge measures accurately the intensity of the beam. His experiments may be used to set a minimum for the upper pressure limit at which molecular flow occurs. Mercury atoms, effusing through a source slit having the dimensions of 0.01 cm x 0.1 cm, passed through a collimator and were detected by means of an ionization gauge. Johnson expressed his results in terms of ionization current as a function of pressure. The current was expressed in units of $i/e \times 10^6$, where i is the ionization current formed by the electron current e in the ionization gauge detector. Observations of ionization current were made over a range of source pressures between 0.1 and 143 mm Hg. From 0.1 mm up to about 35 mm the ionization current in the forward direction increased linearly. Beyond this pressure, the rate of increase of ionization current in the forward direction decreased until a maximum current was obtained at a source pressure of about 100 mm Hg. At this pressure, the calculated mean free path was 0.01 the width of the source slit. At pressures exceeding 100 mm, the ionization current decreased.

Consider, first, the pressure range below 35 mm. The most reasonable interpretation of the results in this region appears to be that since the ionization current is a linear function of the source pressure, then the beam intensity must also be a linear function of the source pressure. Such a relationship is exactly what is predicted by the equations of molecular flow. One concludes, therefore, that these equations should describe adequately the flow in the forward direction at pressures such that the mean free paths are greater than 0.01 the slit width.

The maximum in the ionization current is not uniquely explainable. Therefore the results at pressures above 35 mm cannot be used to deduce the upper limit of the effusion method.

It appears that Johnson's data are in serious disagreement with those of Knauer and Stern. In view of his results, Johnson rejected Knauer and Stern's concept of a cloud formation in front of the orifice. Johnson proposed, instead, that in Knauer and Stern's experiment an absorbing atmosphere built up in the space outside the source slit because they did not cool the apparatus sufficiently to condense the effused gases.

d. The Experiments of Mayer - The work of Mayer[48, 49] is probably the most thorough investigation dealing with the effusion of gases through thin edge orifices. Permanent gases at a constant pressure and temperature were allowed to effuse through orifices ranging in dimensions from 6×10^{-7} cm^2 to 9×10^{-4} cm^2. The intensity at various points in the 2π solid angle above the plane of the orifice was measured by a detector consisting of an aluminum vane (Flügel) 1 mm x 6 mm attached to a quartz fiber 10 cm long and about 0.001 mm thick.

The ability of the detector device to measure molecular intensity is based on the principle of the torsion balance. The force which the incident molecules or atoms exert against the surface of the aluminum vane sets up a torque which twists the quartz fiber and builds up a restoring force. The magnitude of this force is determined by measuring the deflection of the vane.

With this arrangement Mayer was able to check the cosine law at a given source pressure at arbitrary distances from the orifice by moving the vane in a straight path at right angles to the forward direction of the effusing molecular beam. It was also possible to move the vane at various distances parallel to the normal to the plane of the orifice. At each new value of the pressure the deflection of the vane was observed and the deflection corrected for the change in distance from the orifice resulting from the deflection and for the change in solid angle subtended at the orifice by the vane as a result of the deflection.

The pressure behind the source was varied between 0.4 to 4.5 mm Hg, while the pressure outside the source was always less than the vapor pressure of mercury at 18° to 20°C (<0.001 mm Hg).

It can be demonstrated from kinetic theory and the cosine law that the number of molecules arriving at an elementary area dS_1 through a solid angle $d\omega$ subtended by an element of orifice area dS_0 is given by

$$\frac{dn}{dS_1} = \frac{Z}{\pi} \frac{d^2}{(d^2 + r^2)^2} dS_0 \quad , \tag{28}$$

where d is the perpendicular distance from the orifice to the vane and r is the radius of the vane. The quantity Z is defined by Eq. (8). Mayer's data

gave excellent confirmation of the cosine law equation at distances from the orifice of 4 to 8 mm. At the maximum source pressure (4.5 mm Hg) the mean free path of the effusing molecules was approximately equal to the slit width (0.01 mm).

Another series of measurements was carried out using an aluminum vane having a diameter of 3 mm and located a distance of 7 mm in front of the orifice. The source pressure was increased from 0.072 mm Hg to 1.34 mm Hg. The pressure outside the source was maintained constant at about 10^{-4} mm Hg. The quotient of the corrected deflections of the vane and the difference in pressure inside and outside the source were constant, independent of pressure. Hence, the intensity in the forward direction was linear with pressure over the range investigated, and Mayer's results are also in contradiction with the work of Knauer and Stern.

Summarizing the work of Mayer one observes two important results: (1) a cosine law distribution occurs outside a thin-edged orifice at least up to 4.5 mm Hg corresponding to a mean free path about equal to the orifice diameter, and (2) the intensity in the forward direction is a linear function of pressure for the same orifice over a pressure range of 0.072 to 1.34 mm Hg. The ratio of mean free path to orifice diameter at this highest pressure is about 3.0.

e. The Experiments of Clower and Phipps - Clower and Phipps[15] allowed cadmium atoms to effuse from a glass oven through an orifice having the approximate shape of a hyperboloid of one sheet. The minimum diameter of the orifice was measured to be 0.29 mm. The vapor pressure of the cadmium was varied from 0.0145 to 0.562 mm Hg. For this range of pressure, the Knudsen number, which they defined as the ratio of the mean free path to the orifice diameter, assumed values between 25 and 0.6. A liquid nitrogen-cooled, optically flat, plate was supported in front of, and parallel to, the plane of the orifice at a distance of 10.39 mm. The variation in thickness of the cadmium deposits collected on this optically flat plate was then measured by an interferometer method. This variation in thickness was interpreted in terms of a probability density of the atoms effusing at an angle θ to the normal axis to the orifice.

It was found that, even with the smallest pressures, the fraction of atoms issuing from the orifice in the forward direction decreased as the pressure of the cadmium vapor behind the orifice increased. The decrease in this fraction in the forward direction was associated with an increase in angles, $\theta > 0°$. This increase appeared to reach a maximum at about 30°. No measurements were carried beyond $\theta = 45°$. Clower and Phipps give no satisfactory explanation for this observed phenomenon. The situation is complicated by the non-ideality of the orifice. Hence, these results appear to bear little relationship to the effusion measurements carried out in this research.

3. Concluding Remarks Regarding the Limits of the Effusion Method

In view of Mayer's work, one is justified in carrying out vapor pressure measurements by the effusion method at least up to pressures where the mean free path becomes approximately equal to three times the orifice diameter. Johnson's work would indicate the feasibility of effusion measurements at still higher pressures, where the mean free path may become only one-tenth or less the orifice diameter. This author views the experiments of Knudsen and those of Knauer and Stern with some skepticism since the inherent errors associated with them are no doubt large. The work of Clower and Phipps may not apply where thin-edged orifices are concerned.

B. Materials, and Analytical Methods and Results

1. History, Treatment, and Analysis of Original Samples

Four distinct isotopic distributions of uranium in uranium dioxide were used in this work: natural, U^{235} enriched, U^{233} enriched, and U^{238} enriched.

All samples of UO_2 containing uranium of natural isotopic abundance that were used throughout this investigation were taken from one of two sources. The first was very pure material, having a maximum impurity of 10 ppm of silicon as determined by spectrographic analysis. The second was pure material prepared by the decomposition of uranyl nitrate. The uranyl nitrate crystals were obtained from the Special Materials Division at Argonne National Laboratory. The isotopic abundance of the natural material was measured by mass spectrometric analysis, which yielded the following composition in mole per cent: $99.275 \pm 0.009\%$ U^{238}, $0.720 \pm 0.009\%$ U^{235}, and $0.0052 \pm 0.0009\%$ U^{234}.

The relative stabilities of uranyl nitrate, $UO_2(NO_3)_2$, and the oxides UO_3, U_3O_8, and UO_2 under certain conditions of temperature and pressure, enable one to devise the following method of preparing UO_2:

$$UO_2(NO_3)_2\,(s) \xrightarrow[\text{atm pressure}]{200^\circ - 300^\circ C} UO_3(s) + 2NO_2(g) + 1/2\,O_2(g), \tag{29}$$

$$3UO_3\,(s) \xrightarrow[\text{atm pressure}]{750^\circ - 850^\circ C} U_3O_8(s) + 1/2\,O_2(g), \tag{30}$$

$$U_3O_8\,(s) \xrightarrow[10^{-4}\ \text{mm}\ O_2]{1300^\circ C} 3\,UO_2\,(s) + O_2\,(g) \tag{31}$$

Uranium wire, enriched to ~90% U^{235}, was obtained from the Special Materials Division. Spectrographic analysis of this uranium wire showed carbon with 115.0 ppm present, to be the principal impurity. Other impurities found to be present were 45 ppm of silicon and 25.0 ppm of iron. To convert the metal to the oxide, the wire was dissolved in nitric acid and converted to the dioxide by the method outlined above.

A small amount of uranyl nitrate containing U^{233} (ca. 30 mg) in one cc of nitric acid solution was obtained from Dr. F. Hagemann of Argonne National Laboratory. The uranyl nitrate solution as received was thought to contain appreciable daughter activity, so an ether extraction of the uranyl nitrate was performed to separate it chemically from the daughter elements. The following procedure was devised from the somewhat general method given by Rodden and Warf.[57]

Step 1. The one cc of solution containing the 30 mg of uranyl nitrate was introduced into a 100-ml Kjeldahl flask No. 1.

Step 2. To flask No. 1 was added about 30 cc of diethyl ether and about 5-10 cc of saturated ammonium nitrate solution. Careful agitation of the two liquid phases effected distribution equilibrium.

Step 3. Flask No. 1 and contents was then lowered into an acetone-solid CO_2 bath and the aqueous layer frozen out.

Step 4. The ether layer was immediately poured off in Kjeldahl flask No. 2 and placed in the bath so as to freeze out any small amount of the aqueous layer which may have been transferred.

Step 5. The ether layer in flask No. 2 was then poured into flask No. 3, which contained about 15 cc of distilled water. Distribution equilibrium was insured by again agitating the two liquid phases.

Step 6. The aqueous layer was again frozen out and the ether layer poured back into flask No. 1, and the whole procedure was repeated. Three extractions in all were performed.

In Step 2 the addition of a small amount of saturated ammonium nitrate solution served as a "salting-out agent," which enhanced the concentration of uranium in the ether layer. In Step 5 the uranium in the ether layer was re-extracted into a relatively large amount of distilled water. This step allowed one to use the same ether throughout the three extractions, which decreased the danger of working with larger amounts of ether. The progress of the ether extraction could be visually followed by observing the intensity of the yellow-green color imparted to the ether layer by the presence of the uranyl ion, UO_2^{++}, and the gradual disappearance of this color from the aqueous salt layer. The entire series of extractions was carried out in a well-ventilated, completely enclosed hood equipped with rubber glove attachments to decrease the radioactivity hazard. After extraction of the uranium was complete, the 15 cc of aqueous solution was evaporated to about 2 cc with a heat lamp. The 2 cc of very concentrated uranyl nitrate solution was then quantitatively transferred into a tungsten cup in tantalum effusion cell No. 2 and evaporated to dryness. The crucible lid was pressed on by means of a special jig and the crucible was introduced into the Pyrex vapor pressure apparatus to be described later. The solid uranyl nitrate contained in the crucible was then easily converted to UO_2 by vacuum heating. The reactions listed previously account for the formation of $UO_2(s)$.

Depleted U_3O_8 was obtained from Dr. James Gindler of the Chemistry Division at Argonne National Laboratory. It was converted to UO_2 by heating at 1400°C in vacuo.

2. Determination of Composition of Original Samples and Residues

a. Uranium Assay. The standard gravimetric method for the determination of uranium consists of dissolving a weighed sample of oxide in nitric acid and adding sufficient ammonium hydroxide to precipitate diammonium uranate, $(NH_4)_2UO_4$. This precipitate is then washed, dried, and ignited to U_3O_8 at 800°C to a constant weight. A precision of 0.1 to 0.2% can be obtained if samples of about 0.5 gram are employed.

b. Oxygen-to-Uranium Ratio by Direct Combustion to U_3O_8. A UO_y sample of the order of 0.2 to 0.5 gram may be burned in an oxygen atmosphere or in air at 750 to 850°C according to the equation

$$3UO_y(s) + \frac{8-3y}{2} O_2(g) \longrightarrow U_3O_8(s) \quad . \tag{32}$$

From the initial weight of the sample, m, and from the change in weight, Δm, one can calculate the magnitude of y within a precision of 0.1 - 1.0% for 0.2 - 0.5- gram samples. The relationship between y and the previously mentioned quantities is

$$\frac{\Delta m}{m} = \frac{[(8 - 3y)/2]32}{3(238.07 + 16.00\ y)} \quad , \tag{33}$$

from which y can be conveniently computed.

c. Oxygen-to-Uranium Ratio by the Method of Hoekstra and Katz. Uranium oxides react with bromine trifluoride according to the following equation:(29)

$$UO_y(s) + 2BrF_3(\ell) \longrightarrow Br_2(g) + UF_6(g) + \frac{y}{2} O_2(g) \quad . \tag{34}$$

The reaction is carried out in a closed system fitted with the appropriate traps and pumps; the bromine and uranium hexafluoride gas may be frozen out in liquid nitrogen traps while the oxygen is pumped off and its volume measured at a given temperature and pressure. The quantity y, the oxygen-uranium ratio, can be calculated from the initial mass of UO_y and the moles of oxygen formed. A precision of better than 0.2% may be obtained if samples of the order of 50 to 100 mg are employed.

d. Oxygen Analysis by the Argon Fusion Method. This modified vacuum-fusion method consists of sealing from 100 to 1000 μg of an oxide in a small, cleaned platinum capsule and dropping this capsule into molten platinum contained in a graphite crucible. The oxide reacts with the dissolved carbon and yields carbon monoxide. The carbon monoxide is carried away by a stream of argon and converted to carbon dioxide by an appropriate oxidizing agent, such as I_2O_5. The carbon dioxide is carried through the system by the stream of argon and frozen out at a liquid nitrogen trap. After flushing the system thoroughly with argon, the CO_2 is allowed to sublime and come to room temperature and its volume at atmospheric pressure, and hence the amount, is read off from a calibrated manometer. A precision of 0.2 to 0.4% is claimed, but actual experience has shown that such a precision is not generally obtainable. The method, however, is excellently adapted to the analysis of very small quantities of uranium dioxide.

e. Oxygen-Uranium Ratio by X-ray Lattice Parameter Measurement. Provided that the material to be analyzed is not amorphous, the phase or phases present in a given sample may be determined by analyzing the characteristic spacing of X-ray diffraction lines obtained by the Debye-Scherrer technique. The composition of a given sample of the UO_{2+x} phase may be determined by measuring the lattice parameter a_0 of the unit cell. The lattice parameter of the face-centered cubic (fluorite) structure UO_{2+x} decreases with increasing oxygen content in a linear fashion as predicted by Vegard's law. Hence, the X-ray method is applicable for the rapid determination of the ratio, O/U, once the lattice parameter vs composition diagram is established. Figure 3 shows the decrease in lattice parameter of the UO_{2+y} phase with increasing oxygen content as established by this research. The analyses, whereby the ratio O/U was obtained, were

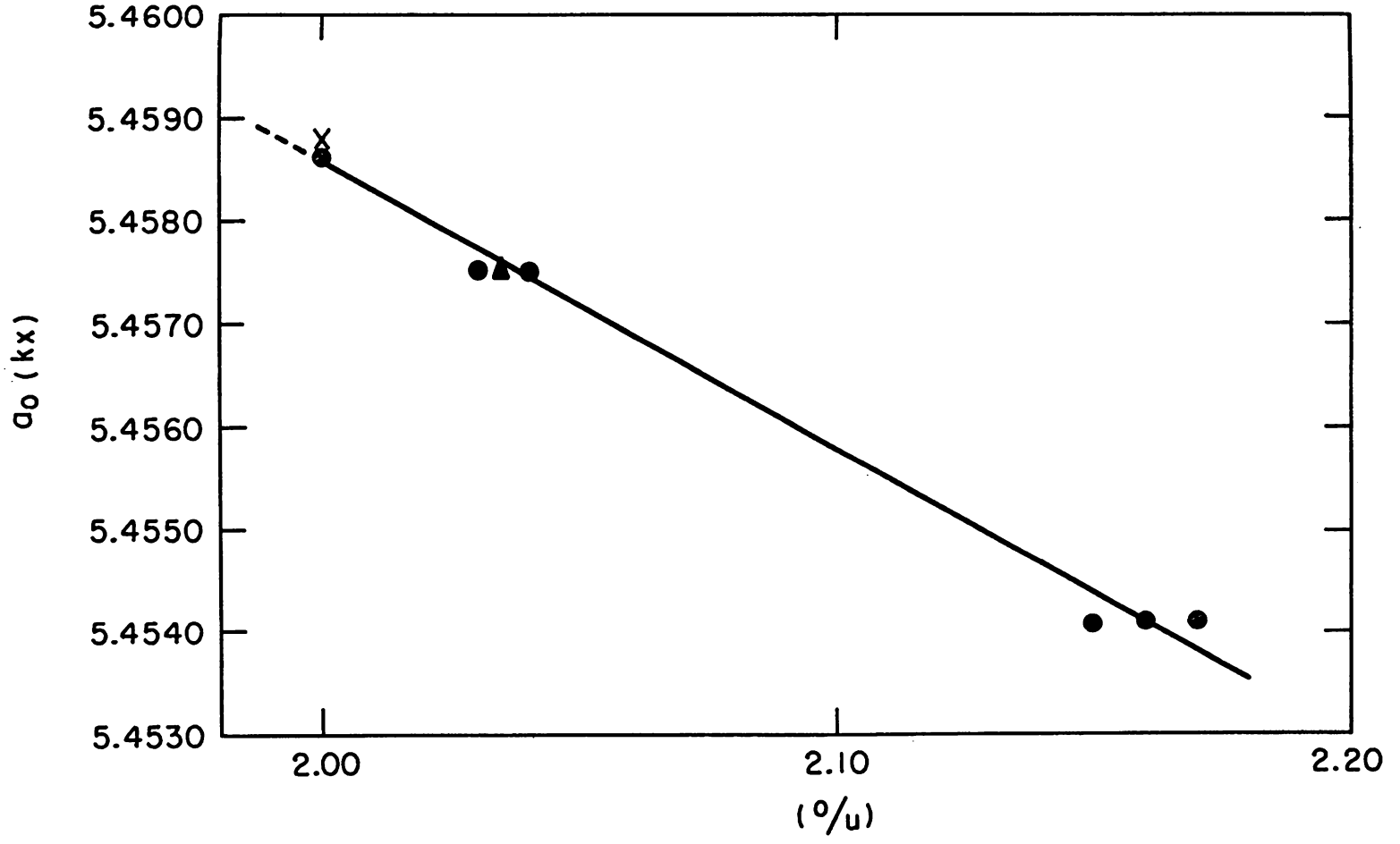

Figure 3

The Lattice Parameter-Composition Diagram for the UO_{2+x} Phase

Three different notations are used to depict different methods of sample analysis: the dots, ● , represent the argon-fusion method; the triangle, ▲ , represents uranium assay; the X represents the Hoekstra and Katz method of oxygen analysis.

carried out by three independent methods; the dots indicate the fusion method, the solid triangle indicates the gravimetric method, and the cross indicates the BrF_3 method.

Alberman and Anderson,[1] however, claim that the size of the UO_{2+x} unit cell remains constant over the composition range of $x = 0.00$ to 0.20. Their values of a_0 are given to only the third place beyond the decimal, and within their quoted error a_0 would obviously be constant since the lattice parameter is a slightly varying function of oxygen content, varying only in the third and fourth decimal places as shown by this investigation.

3. Analysis of Collected Sublimates

Since, in general, collected sublimates were obtained in quantities less than a milligram, the analytical methods described for original samples and residues are not all applicable for determination of composition of such small amounts of material. At first glance, both the X-ray and Argon Fusion methods would seem practicable. In the case of collected sublimates, however, the X-ray diffraction patterns obtained are of little quantitative value because vapors that are condensed on very cold surfaces usually deposit in an orientated, strained, and finely divided state. Therefore, the crystalline size ($>5\,\mu$) necessary for the attainment of clear, sharp X-ray diffraction lines is not obtained, and broad, fuzzy lines result which can be used only for qualitative identification of the phase or phases present. Hence, the argon fusion method is the only direct way of determining the chemical composition of a collected sublimate.

Additional analytical methods were utilized in this research to ascertain the composition of the effusing species. Spectroscopic analysis of a collected sublimate furnished some information concerning reaction of the effusing vapor or the condensed phase with the effusion cell. The absorption spectrum of a thin film of sublimate condensed on a quartz target was also useful in the qualitative identification of the sublimate.

4. Determination of Quantity of Collected Sublimates

a. Direct Weighing. The most fundamental and direct method of determining the amount of a collected sublimate is to weigh it on a microbalance. A microbalance should enable one to weigh an object precisely within about 10 micrograms, provided the set of weights and the rider employed are accurately calibrated and provided the sensitivity of the balance can be reproducibly established. It is also imperative that the zero point of the balance not drift with time. In view of these restrictions, a precise and accurate determination of the weight of an object cannot be carried out unless the weight of the object exceeds 0.2 mg. This would give a precision within 5% or less. In general, most of the collected sublimates of this research were less than the above-quoted amount and the method of direct weighing was applicable only to the very heaviest of the collected sublimates.

b. Alpha Counting. The use of radioactive isotopes in analytical procedures is steadily gaining in importance, since radioactive elements and compounds have numerous applications in many fields of investigation. The usefulness of these isotopes is due mainly to the sensitivity of radioactive measurements and the basic properties of the radioactive atoms. These radioactive species can be detected and quantitatively determined in exceedingly small amounts. Under proper conditions of half-life, type, and energy of the emitted particle, they are determinable by measurement of activity in concentrations many times smaller than by any other known chemical or physical method. This extreme sensitivity and ease of detection make the application of radioactive isotopes very convenient, for example, in solubility, exchange, and vapor pressure measurements. Since atoms having the property of spontaneous disintegration differ from the stable nuclei by only a slight shift in atomic weight, this difference does not ordinarily play a measurable role in the process under study, except, of course, for the process of isotopic separation. This is particularly true of the heavier elements since the effect of various isotopes on the process under study varies with the square root of the ratio of masses involved.

The total disintegration rate of a sample containing a mixture of radioactive species is statistically given by

$$\frac{dN_t}{dt} = 0.693 \sum_i (N/t_{\frac{1}{2}})_i \qquad (35)$$

where $N = N_0 W_i / M_i$ is the number of atoms or molecules of the i^{th} species and $t_{1/2}$ is the corresponding half-life of the i^{th} species. The quantity N_0 is Avogadro's number, $\underline{W}$ is the weight in grams, and $\underline{M}$ is the atomic or molecular weight.

In the absolute measurement of the counting rate of α-particles, a number of factors must be quantitatively evaluated, whereas in relative counting these factors are eliminated. The observed counting rate, c/m, is given by the expression

$$\frac{c}{m} = S \cdot A \cdot R \cdot G \cdot E \frac{dN_t}{dt} \quad , \qquad (36)$$

where S = backscattering factor ($\geqslant 1$), A = self-absorption factor ($\leqslant 1$), R = resolution loss factor ($\lesssim 1$), G = geometry factor (< 1), and E = counter efficiency ($\lesssim 1$) The first two factors in Eq. (36) are dependent upon the particular alpha-emitting species and the type of sample backing used, whereas the last three factors are dependent only upon the type of counter employed.

Both experimental and theoretical investigation have established that some of the α-particles which are emitted into the backing plate of the sample are scattered by the backing plate at small angles to the surface and

consequently are included in the observed count. Theory[17] predicts that about 3% of the Pu^{239} alphas are back-scattered off a flat platinum backing plate, i.e., S = 1.03. Experiments[61] have yielded a back-scattering factor of about 1.04 for Pu^{239} α's backed by platinum. Back-scattering is known to increase slightly as the α-energy is decreased so that the back-scattering resulting from U^{238} alphas may be somewhat larger.[61] However, in general, a value of S = 1.04 will introduce only a small error for almost any α-emitter backed by platinum.

When an alpha emitter is mounted on a platinum plate for counting in a chamber, the alpha emission may be dispersed and absorbed by the emitting material itself. Such a phenomenon is known as self-absorption. The number of alpha particles lost by self-absorption obviously depends on the sample thickness and the energy of the alpha particle. If a sample of weight W in mg is uniformly distributed over an area s, then the fraction F of the alpha particles, having a range r in the solid sample material, that are self-absorbed is given by[18]

$$F = 1/2\ W/rs. \tag{37}$$

For the heaviest sublimate collected, W was 0.595 mg; r was about 9 mg cm^{-2} and s was 3 cm^2. Substitution of these quantities into Eq. (37) gives a maximum value of 0.011 for F. Autoradiograms taken of collected sublimates of various thicknesses showed absolutely no non-uniformity. In view of this fact and the small percentage self-absorption, A was considered to be unity.

All collected sublimates were assayed for uranium by means of a Nuclear Measurements Corporation Proportional Counter, Converter Model PCC-10. Collected sublimates on flat 5-mil platinum were placed between the electrodes in a manner such that a geometry factor G = 0.50 was attained. Methane flowed constantly through the counting chamber. The voltage was maintained constant at the alpha plateau of 900 volts. The resolution losses of this instrument are partly a function of the amplifier and scaler circuits but can be easily made less than 0.01% per 1000 c/m. Hence R is also very close to unity. The remaining factor, E, the counter efficiency for alpha particles, is invariably assumed to be unity. Since alpha particles produce an enormous number of ion pairs in traversing matter, all alphas are certain to be counted if they reach the chamber without losing too much of their energy due to self-absorption. However, it is of importance to periodically check the constancy of the counter efficiency. This can be accomplished conveniently by periodic reference to an alpha counting standard.

Equation (36) now reduces to the expression

$$c/m = 0.52\ (dN_t/dt)\ , \tag{38}$$

from which the weight of material on a given target can be determined once the half-lives and percentage abundances of the isotopes contained therein have been established.

Because the decay of radioactive atoms is a random process the error associated with the measurement of a counting rate can be calculated from an assumed distribution of randomness. Provided the half-life of the radioactive species is very large compared to the counting time and the number of counts is large, then the probable error in a measured number of counts $\underline{c}$ is $\pm\ 0.6745\ c^{1/2}$. This means that there is a probability of 0.5 that the true member of counts, c_0, lies between the limits $c \pm 0.6745 c^{1/2}$. Measurement of the time can usually be made with great accuracy. Hence, any error in the measured counting rate, c/m, can be considered to result from statistical error in $\underline{c}$ only, and the probable error in c/m is given by $\pm\ 0.6745 \left(\frac{c/m}{t}\right)^{1/2}$.

c. Photofluorometric Assay. Price, Ferretti, and Schwartz[54] have devised a sensitive method of uranium detection that utilizes the fluorescence spectrum of uranium fused in sodium fluoride. About 20 mg of a solution containing uranium in the form of the uranyl ion, UO_2^{++}, is carefully pipetted into a small platinum dish and evaporated to dryness either under a heat lamp or in a desiccator. To the dry residue in the dish is added approximately 0.3 g of 90% sodium fluoride - 10% sodium carbonate and the mixture is fused by holding the dish in the flame of a Meeker burner. A milky-white button of the flux containing the uranium is obtained and the fluorescence is then caused by irradiating the button with the 365 mμ line of mercury. The resulting yellow-green fluorescence is measured by a photoelectric fluorophotometer. The reliable range of the method is from 10^{-9} to 10^{-6} gram of uranium, although more recent instruments claim a reliable sensitivity as low as 10^{-10} gram of uranium. Blanks generally give a reading corresponding to less than 10^{-10} gram.

The fluorometric method was used to assay collected sublimates by mounting the small platinum dishes in an inverted position as condensation targets and collimating the molecular beam so that only the bottom of the dish collected effusate. However, the method did not yield the desired precision for vapor pressure measurements and was discarded in favor of other methods of uranium assay. The method did, however, prove useful in measuring the condensation coefficient of effusate on liquid nitrogen-cooled targets which will be discussed later.

V. EXPERIMENTAL PROCEDURE AND DATA

A. Procedures and Equipment Common to All Measurements

1. The Measurement of Temperature

All temperatures were determined by means of a Leeds and Northrup disappearing filament type optical pyrometer designated as pyrometer No. 2 (serial no. 1045528). The pyrometer was sighted in the black-body hole located in the bottom of a given effusion cell to obtain a temperature reading. For each effusion cell used the temperature of the black-body hole was compared with the cavity temperature at different temperatures in a preliminary experiment. These corrections were later applied to the observed black-body temperatures in the effusion measurements. All temperature readings were corrected for the transmissivity of the interposed window and prism. Pyrometer No. 2 was calibrated at the copper point and the calibration extended up to about 2600°C by means of rotating sectors.[68] Assuming Wien's radiation law to be valid over this temperature range, the pyrometer was calibrated by observing the temperature of a graphite black-body with and without the rotating sector in position. Wien's law, in its most useful form, states that

$$1/T_s - 1/T = -\frac{\lambda_e}{c_2} \ell n\tau \qquad (39)$$

where T_s is the observed temperature of the black-body measured through a sector of transmissivity τ. The quantity T is the true temperature of the black-body, c_2 is Wien's second radiation constant, and λ_e is the effective wavelength of the pyrometer to be used when temperatures T and T_s are employed in the equation. Values of λ_e may be calculated from a knowledge of the transmissivity of the pyrometer filter as a function of wavelength, the normal eye sensitivity, and Wien's law. A plot of calibration corrections for the pyrometer at various temperatures was readily constructed from the differences in the temperatures calculated from the Wien's law equation and the temperatures of the black-body observed without the sector. The initial sector measurement was based upon the pyrometer reading corrected at the copper point, and the entire calibration was then extended to higher temperatures by regulating successive T_s's for temperatures at which the calibration correction had been determined.

As a check on the validity of extending rotating sector measurements beyond the copper point, the freezing point of pure platinum was determined. A small discrepancy of only 3.0° was found to exist between the corrections obtained by means of the sectors and the observed platinum point. Since no primary or secondary points on the 1948 Temperature Scale[66] exist above the freezing point of platinum, the calibration was considered valid at higher temperatures as based on the agreement at the platinum point and the validity of the radiation laws.

2. Production and Maintenance of High Vacua

Figure 4 shows the type of high vacuum pumping system used during this research. A divergent nozzle mercury diffusion pump, backed by a two-stage mercury diffusion pump, and a Welch Duo-Seal mechanical pump could produce and maintain vacua as low as 5×10^{-8} mm Hg. A liquid nitrogen trap was employed to freeze out condensable gases and to keep mercury from distilling into the vapor pressure apparatus.

3. Induction Heating of the Effusion Cells

Heating of the effusion cells was accomplished with a 20-kva Thermonic high-frequency induction furnace having Powerstat power control. A General Electric constant voltage transformer supplied constant power to the furnace. Consequently, the temperature of the effusion cells could be maintained constant within ±1° over periods of time of at least one hour.

B. Establishment of the Congruency of Vaporization of Uranium Dioxide

Strong evidence that $UO_2(s)$ forms an invariant system at a fixed temperature is furnished by the constant volatility as a function of time as shown by series I-2 in Table VI (p.68). Further evidence that the system is not only invariant, but congruently vaporizing, is furnished by room temperature X-ray diffraction patterns of the residues after exposure to the atmosphere. Only the face-centered cubic UO_2 phase was found in all residues. This UO_2 phase always gave a value for the lattice parameter of $a_0 = 5.4588 \pm 0.0004$ kx units. Reference to Fig. 3 indicated a solid composition of $UO_{2.00}$ corresponding to this value of the lattice parameter. Hence, it appears that the vapor pressure of $UO_2(s)$ is unique at a fixed temperature and true equilibrium measurements can be carried out with $UO_2(s)$.

C. The High Temperature (Series B) Effusion Measurements with Uranium Dioxide

Effusion measurements on UO_2 were carried out over three distinct, but overlapping, ranges of temperature, and they will be presented in chronological order.

The so-called high temperature measurements over the range 1750° to 2400°C were carried out in the fused silica apparatus shown in Fig. 5. The effusion cell was fabricated from sintered tungsten obtained from the Fansteel Corporation and had a density of about 11 g/cc before additional sintering. Machining of this sintered tungsten material could be accomplished with conventional, hardened steel machine tools. After machining, the

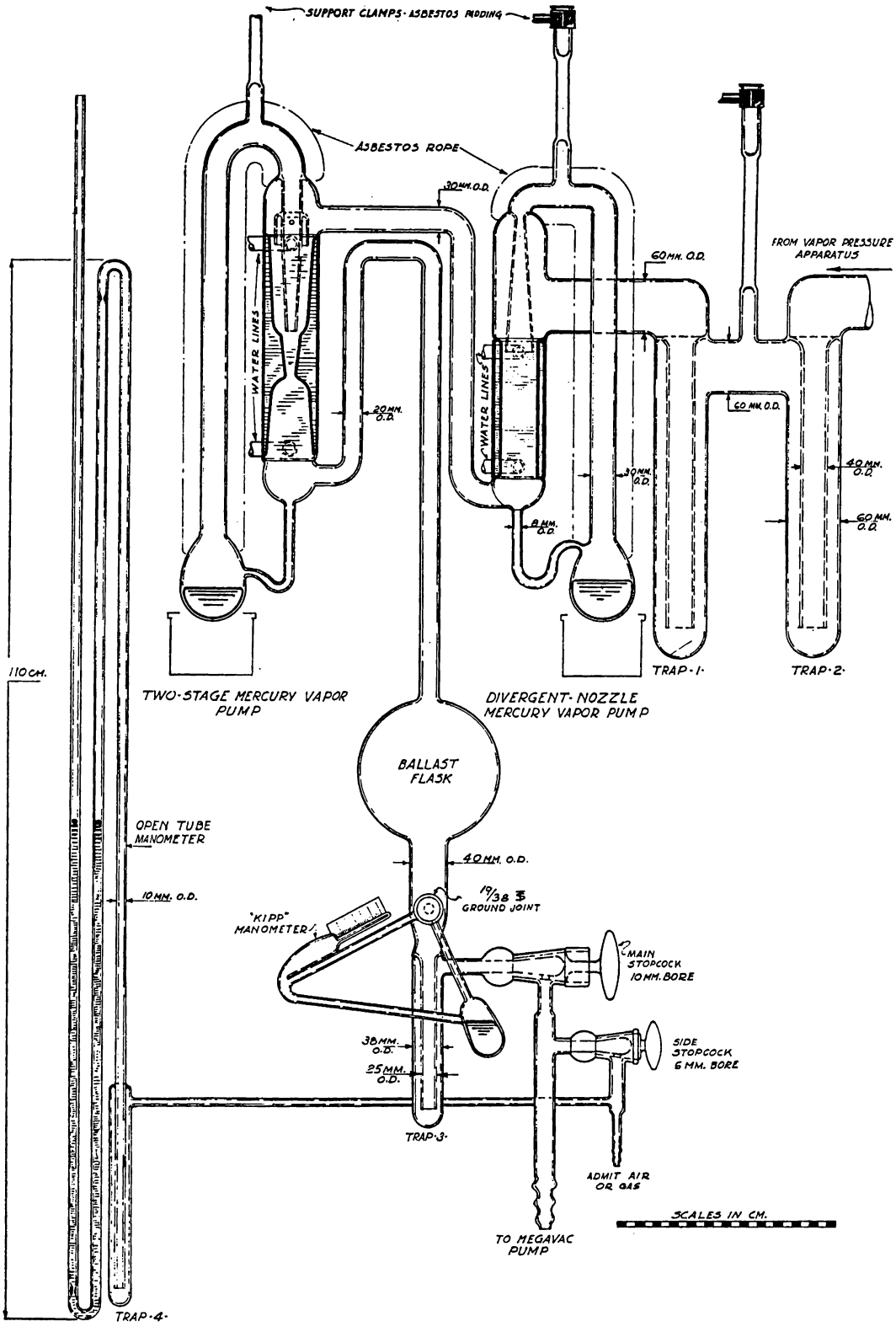

Figure 4

Schematic Diagram of the Type of High Vacuum Pumping System Used in This Research

(Only one of the two traps was cooled)

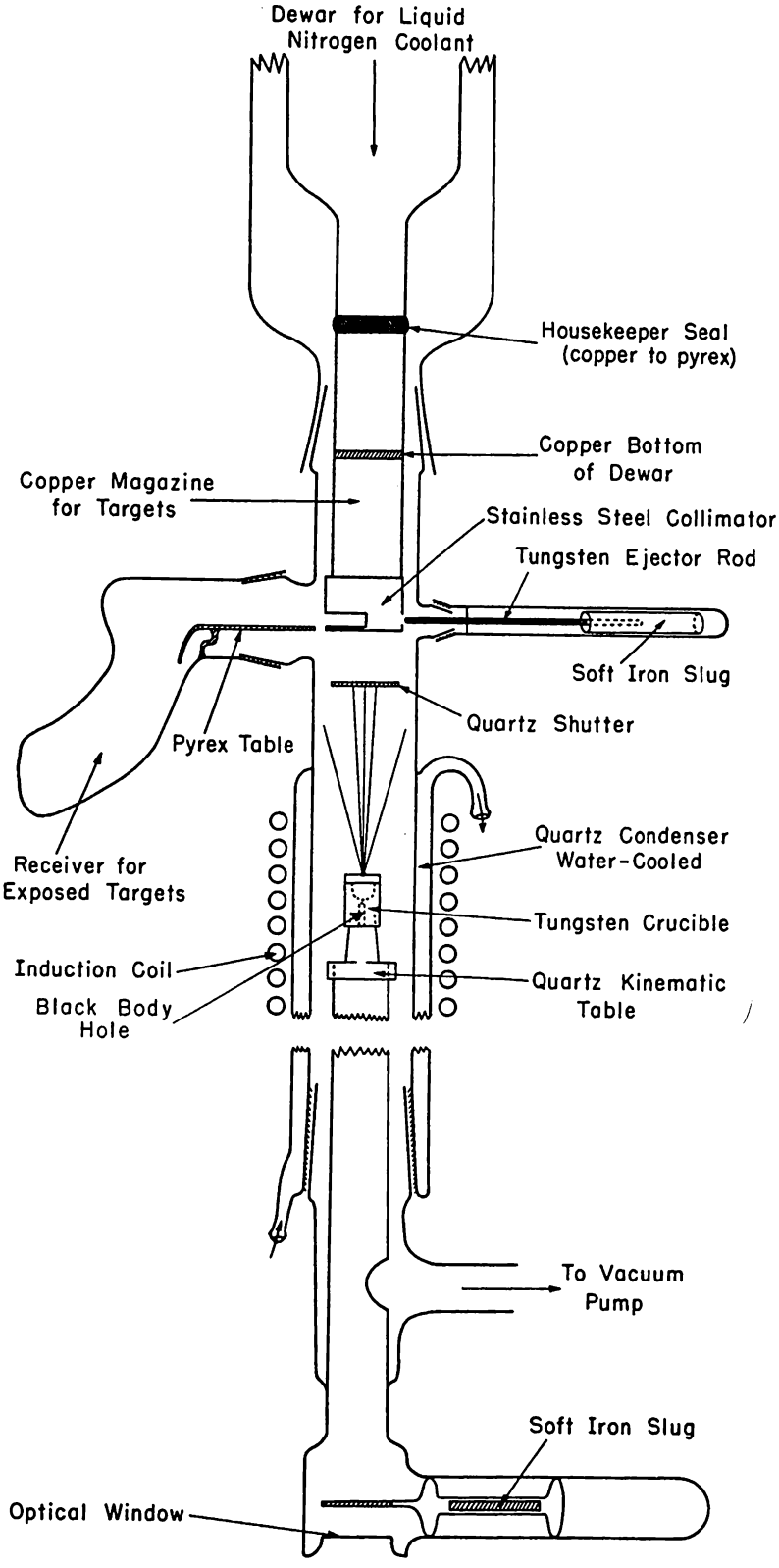

Figure 5

Schematic Diagram of the Fused Silica Vapor Pressure Apparatus used for Effusion Measurements at Temperatures above 2000°K

crucible was further sintered at about 2400°C, during which time the crucible dimensions shrunk about 10%. After this sintering treatment, further machining of the crucible could be accomplished only with carbide-tip machine tools. Sintering and outgassing of the crucible were carried out until constant dimensions were obtained. The choice of tungsten as a crucible material depended on the three following requirements: (1) the chemical inertness toward UO_2 at high temperatures; (2) the ability of the crucible material itself to withstand very high temperatures; and (3) the relatively low vapor pressure of tungsten at the high temperatures at which it was employed. X-ray analysis and spectrographic analysis gave no indication of reaction of any kind between UO_2 and tungsten.

Figure 6 is a schematic diagram of tungsten effusion cell No. 1 used in making the high temperature measurements. The cell was supported by three 40-mil tungsten legs which rested on a quartz semi-kinematic table. The tungsten legs were pointed at the ends to reduce the area of contact between the legs and the quartz table, thus reducing leakage of heat. The quartz table directly below the cell served as a radiation shield and helped to offset the small heat leak caused by the tungsten legs. The orifice was machined in the crucible lid and was made thin-edged by grinding and polishing the top surface of the lid.

A problem that one invariably faces in measuring the rate of flow of condensable gases through a thin-edged orifice is the problem of orifice clogging. When induction heating is employed, the heat is generated largely in the outer periphery of the susceptor. As a result, the inner portion of the susceptor is heated mainly by conduction. Consequently the region of a thin-edged orifice is not as effectively heated because the heat energy flowing inward is geometrically reduced by the thinness of the orifice and radiation losses above the orifice. As a result, partial condensation of the vapor arising from the oven charge will eventually clog the orifice.

To overcome this difficulty, close-fitting annular radiation shields, fabricated from 2-mil tungsten sheet,were placed directly above the top of the crucible. The shields were held tightly against the lid of the crucible by a slotted tantalum shield which did not heat inductively. In this way, warming of the orifice was adequately accomplished and no appreciable interception of the effusate resulted. The presence of the close-fitting radiation shields made it possible to carry out the vapor pressure measurements at higher pressures with no fear of orifice clogging. However, their presence tended to increase the temperature of the crucible lid some fifty degrees and make uncertain the effective evaporating temperature of the oven charge. This difficulty was apparent in preliminary runs in which partial melting of the oven charge occurred on the outer and uppermost edges of the charge. Most metal oxides, including UO_2, are poor thermal conductors and the unevenness of radiation from the crucible lid, being

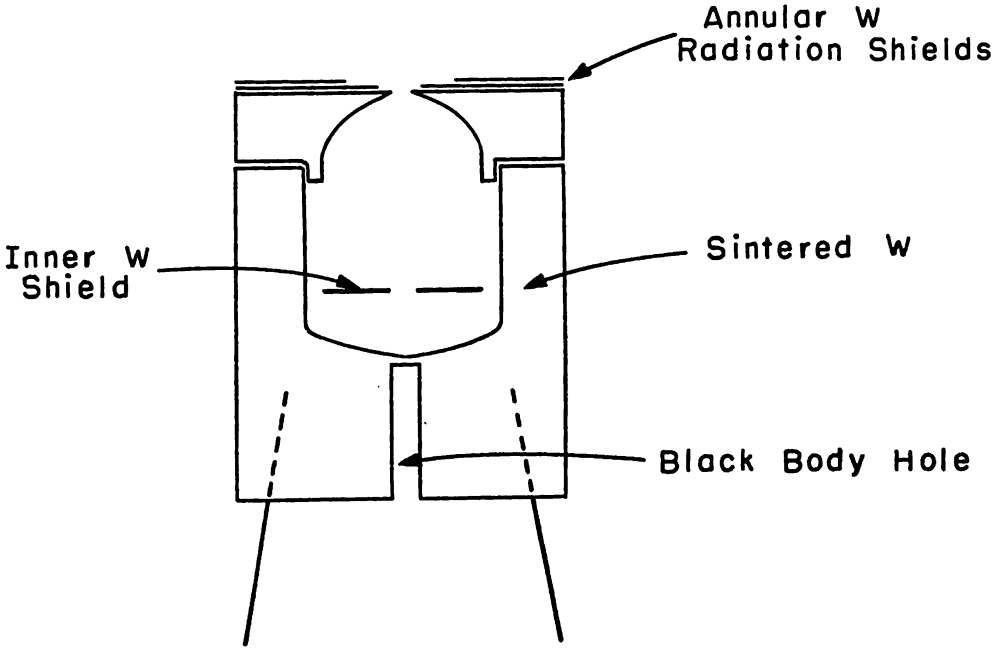

Figure 6

Schematic Diagram of Effusion Cell No. 1
Used with Fused Silica Vapor Pressure Apparatus

hotter at the outer edge, caused this observed phenomenon. Therefore, an inner radiation shield, fabricated from 5-mil tungsten (which is a good thermal conductor), was inserted in the cavity of the effusion cell to reduce the effect of the unevenness of radiation from the lid. This shield had a central hole and an irregularly shaped periphery. The ratio of orifice area to exposed UO_2 surface was 0.15. The effect of this inner radiation shield on the rate of effusion was corrected for in the final vapor pressure calculations.

As many as 25 condensation targets could be exposed in a single experiment. All condensation targets were fabricated from 5-mil platinum and were of 15/16" diameter. The targets were contained in aluminum cassettes having an o.d. 1/32" less than the i.d. of the copper magazine. Small phosphor-bronze springs held the platinum targets in the cassettes. Before insertion into the cassettes and into the apparatus, the platinum targets were chemically cleaned in hot nitric acid and then heated inductively in air at about 1000°C to remove any impurity film that might hinder complete condensation of the effusate. The copper magazine, which was liquid nitrogen-cooled, served to hold the condensation targets in fixed position at a fixed distance from the oven orifice. The molecular beam could be easily shut off from the target by means of a magnetically operated shutter. After a given time of exposure, measured by a Precision Scientific Company "Time-It" clock, the shutter was closed and the target ejected magnetically onto a Pyrex table and into the receiver for exposed targets. Collimation of the molecular beam was accomplished by means of a stainless steel collimator which was soldered to the copper magazine to insure good thermal contact. The amount of material condensed on a given target at a given temperature during a given time of exposure was determined by alpha counting.

1. Measurement of the Condensation Coefficient of the Effusate on Liquid Nitrogen-Cooled Platinum Targets

Two experiments were performed to ascertain whether the fraction of incident molecules condensing was unity. The target temperature was measured as a function of the oven temperature by spot-welding a 1-mil chromel-alumel thermocouple to a platinum target. The target was placed in the apparatus so that the thermocouple was on the lower face. Figure 7 gives a plot of the results obtained. The target temperature, even at the highest of oven temperatures, should have been sufficiently low to condense all effusate molecules.

To test further the fraction condensing, a so-called "bouncing" experiment was performed. Two platinum targets were involved. The upper one was mounted in its normal orientation, one cassette thickness higher than if it were to be exposed in the usual fashion. The lower one was mounted in an inverted orientation facing the upper target. The two

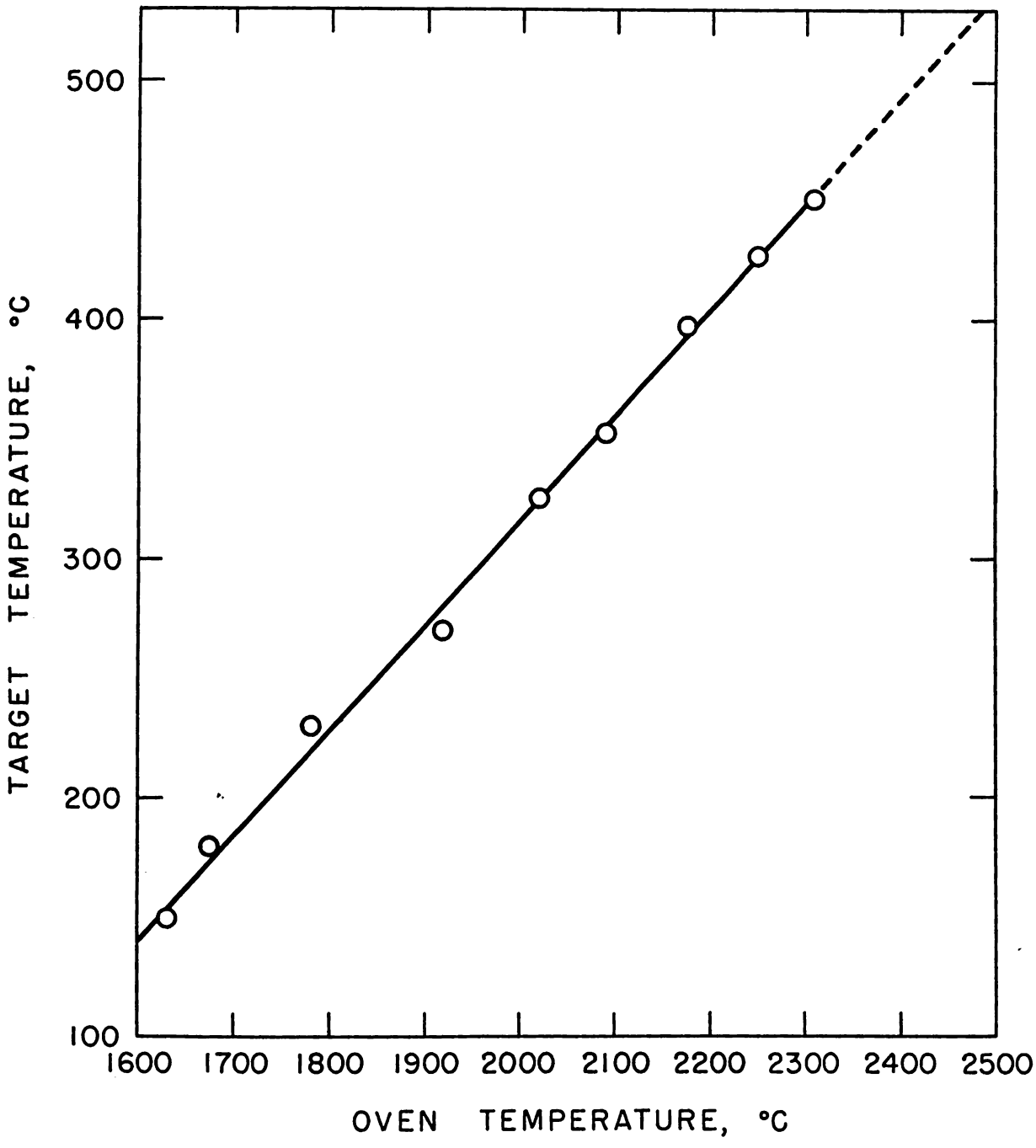

Figure 7

Plot of Target Temperature vs. Oven Temperature for the Fused Silica Vapor Pressure Apparatus

targets were separated by a distance of 1/4". A 0.5" diameter hole was drilled in the center of the lower target and cassette, thus allowing effusate to strike the upper target. If any appreciable bouncing occurred, the lower target should have contained uranium. The twin targets were then exposed to the effusate at an oven temperature corresponding to a target temperature of about 400°C. The sublimate on the upper target was assayed by alpha counting, which showed 98.0×10^{-6} gram UO_2 to be present. The lower annular target was removed and placed in a small amount of hot nitric acid to dissolve any uranium which it might have collected via bouncing. The nitric acid solution was then quantitatively transferred to a small platinum dish and the analysis for uranium was carried out by the fluorophotometric method. The analysis showed about 1.17×10^{-7} gram uranium present. Even after applying the appropriate geometry factor to correct for the presence of the hole in the lower target, the observed bouncing effect was less than 0.3%, which is insignificant in view of the other errors involved in the vapor pressure measurements.

2. The Inner Shield (Series E and F) Measurements: Effect of Size and Location of the Evaporating Area

The effect of the inner tungsten radiation shield on the rate of effusion of vapor out of the orifice of effusion cell No. 1 was determined in two series of measurements. The series designated as the E-series was carried out by inserting, one at a time, four 5-mil tungsten shields of different size into the crucible cavity and determining the weight gain by alpha counting of several condensation targets at 2190°C. The shields used in these measurements had successively smaller outer diameters which defined successively larger annular evaporating areas of the oven charge. The F-series of measurements was carried out in identical fashion at the same temperature of all the E-series of measurements, but the F-series of shields contained successively larger holes in their centers. The outer diameters were turned to give a snug fit with the circumference of the crucible cavity; thus in effect successively larger central evaporating areas of the oven charge were defined by the presence of the respective shields. The data are presented in Table I and Fig. 8. The reciprocals of the weights of material, W, collected by the condensation targets are plotted along the ordinate, while the quantity (S_0/S_a) is plotted along the abscissa; here S_0 is the area of the orifice of effusion cell No. 1 and S_a is the area of the evaporation surface of the oven charge defined by the respective inner shields. A linear least-squares treatment of the data of each series shown in Table I gave the following expressions:

$$(10^4/W)_E = (1.162 \pm 0.045)\,(S_0/S_a) + (0.399 \pm 0.046) \quad ; \qquad (40)$$

$$(10^4/W)_F = (0.3555 \pm 0.004)\,(S_0/S_a) + (0.445 \pm 0.003) \quad . \qquad (41)$$

Table I

THE INNER SHIELD DATA

The Effect of Size and Location of the Evaporating Area

Orifice area, $S_0 = 0.0366\ cm^2$.

Preliminary experiments indicated that a value of 29° should be added to the black-body temperature to give the cavity temperature. The corrected temperature for these experiments is 2190°C.

Series E (Annular area S_a)

No.*	$\frac{1}{W}(10^{-4}$ gram)	S_0/S_a
15	1.28	0.80
16	1.42	0.80
17	0.70	0.29
18	0.75	0.29
21	1.16	0.72
22	1.31	0.72
27	2.37	1.71

Series F (Central area S_a)

No.*	$\frac{1}{W}(10^{-4}$ gram)	S_0/S_a
23	0.97	1.48
24	0.98	1.48
28	0.78	0.95
30	0.70	0.74
32	0.63	0.53

* Order of exposure

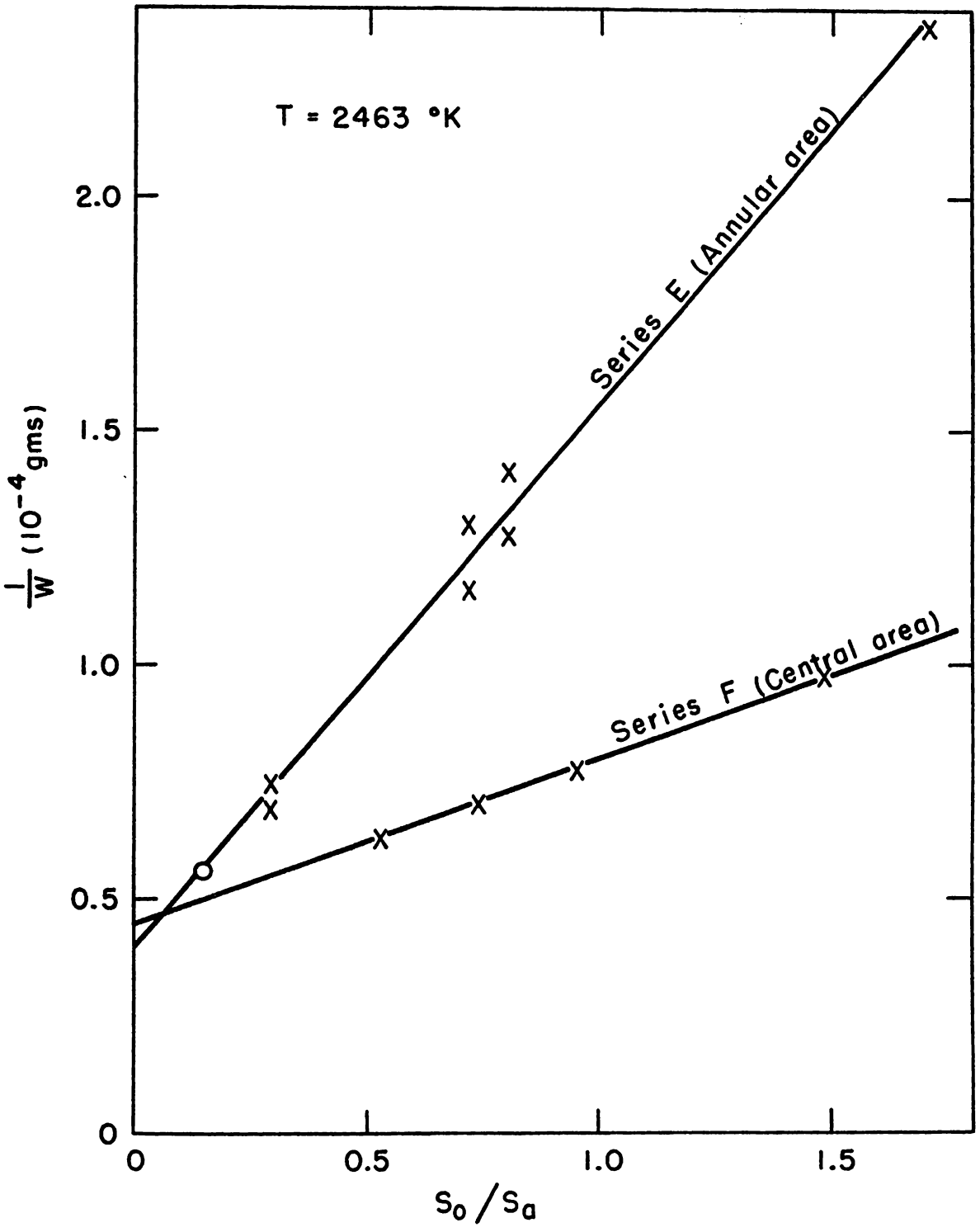

Figure 8

Results of the Inner Shield (Series E and F) Measurements; the Effect of Size and Location of the Evaporating Area on the Rate of Effusion in the Forward Direction

(The circles indicate a measurement obtained in an auxiliary effusion experiment with the same inner shield used in the series B measurements)

The linear relationship between $1/W$ and S_0/S_a in these expressions is not surprising in view of Eq. (25). The errors quoted are the probable errors. It is seen from Fig. 8 that both series have a common origin at $(S_0/S_a) = 0$ within the probable errors. The circle on the plot was obtained in an auxiliary experiment with the same inner shield as was used in the series B measurements. The quantity $(1/W)$ had the value 0.57. Comparison of this value with the common intercept indicates that there should be applied a correction factor of 1.305 for the weights of collected sublimates obtained with effusion cell No. 1 containing the inner tungsten shield.

Only a qualitative explanation for the difference in slope between the E-series and F-series can be given at the present time. If one has a cylindrical effusion cell containing a small evaporating surface of material different from the cell material, then material can leave the cell via two routes: direct evaporation and evaporation and subsequent reflection from the walls of the cell, provided the mean free path is large compared with the cell dimensions. If one is interested only in the amount which leaves the cell in some prescribed direction, then the first of these two routes may be absent. Let us assume the target is located in the forward direction. To show the qualitative behavior one divides the interior surface of the cell into the following parts. Let S_a represent the evaporating area of the material, S_0 represent the orifice area, S_r represent the reflecting area, and S_1 represent the area of the target projected through S_0 onto the bottom of the effusion cell. Then, in general, the total arrival rate, Z, at the target is given by a sum of terms of the type $Z(a,b,c,\ldots x, 0)$ which designates the contribution of molecules which evaporate from S_a and are reflected at S_b, S_c, . . . S_x and thence out S_0. If the evaporating area S_a is not part of S_1, that is, if it is not directly opposite the target, then the total arrival rate at the target from an annular evaporating area is

$$Z_A = Z(a, 1, 0) + Z(a, r, 1, 0) + Z(a, r, r, 1, 0) + \ldots \quad . \qquad (42)$$

If now the evaporating area is opposite the target, it is then part of S_1 and one must define $S_\rho = S_1 - S_a$ as the part of S_1 which is a reflecting surface. The total arrival rate at the target for the evaporating area located centrally is given by

$$Z_C = Z(a, 0) + Z(a, r, \rho, 0) + Z(a, r, r, \rho, 0) + \ldots \quad . \qquad (43)$$

Since terms involving the least number of reflections are largest because of geometrical considerations, one observes $Z_C > Z_A$. As the two evaporating areas, the central one and the annular one, are increased, they merge and both arrangements give the same arrival rate at the target. Hence, both series appear to have the same origin at $S_0/S_a = 0$.

The problem is less easily discussed quantitatively since it involves the solution of simultaneous integral equations. An initial attack has been made by G. H. Winslow[72] of Argonne National Laboratory. His analysis indicates that if these integral equations can be solved the solution would agree in detail with the observed results.

3. Comparison of Weights of Collected Sublimates Determined by Alpha Counting, Colorimetric Assay, and Direct Weighing

Initially it was thought that the weight of the collected sublimates could be measured by direct weighing on a microbalance. Accordingly some of the collected sublimates were assayed by direct weighing. Subsequently it was found that greater precision and probably greater accuracy could be obtained by alpha counting. As a check on the accuracy of the alpha counting, some of the collected sublimates were then assayed colorimetrically. Table II gives the results of the three independent methods. Natural isotopic abundance uranium was present on all targets.

The agreement between the weights obtained by the alpha-counting and colorimetric methods is exceptionally good when one considers the magnitudes of masses involved. Some of the discrepancy between the direct weighings and the other assays can be attributed to oxidation of the thin deposits. No explanation of the entire discrepancy is apparent at present.

Table II

COMPARISON OF α-COUNTING, COLORIMETRIC, AND DIRECT WEIGHING METHODS

Number	Weight of UO_2 in Micrograms		
	α-counting	Colorimetric	Direct Weighing
4	54.1	52.0	-
5	46.7	45.0	58
11	39.2	39.7	43
12	60.5	60.0	65
13	121.4	125.0	154
14	169.4	167.0	183

4. Calculation of the Vapor Pressure from Experimentally Determined Quantities

Calculations of the vapor pressure were carried out by means of Eq. (19). The molecular weight of the effusate was assumed to be that of UO_2 in view of arguments to be presented later. Assuming a 52% geometry for the proportional counter used, and using the values for the half-lives of U^{238}, U^{235}, and U^{234}(52, 9, 10) of 4.51×10^9 yr, 8.91×10^8 yr, 2.32×10^5 yr, respectively, and the isotopic composition of the natural uranium, one obtains the following relationship between counts per minute and weight in grams:

$$W = 1.447 \times 10^{-6} (c/m) \quad . \tag{44}$$

Sufficiently long counting times were used so that the probable error in c/m was ± 1.0% or less.

The orifice area S_0 was 0.0360 ± 0.0009 measured at room temperature by means of a calibrated microscope. The collimator radius r was measured by means of a telescopic gauge and a micrometer with the result that r = 0.9507 ± 0.0004 cm. The orifice-to-collimator distance was obtained by use of a cathetometer, with the result that d = 11.056 ± 0.006 cm. The geometry factor was then corrected for actual temperatures of exposure and the presence of the inner shield. Calculations showed the increase in S_0 due to thermal expansion to be the only significant factor to be considered at the exposure temperatures. The orifice-to-collimator distance, d, remained constant because the increase in height of the tungsten effusion cell No. 1 was almost exactly compensated by the decrease in length of the liquid nitrogen-cooled copper magazine (refer to Fig. 5). The decrease in radius of the stainless steel collimator was shown to be insignificant. Without introducing significant error, an average value of $S_0 = 0.0366$ cm^2 was used in all the calculations. The coefficient of thermal expansion of tungsten used in the above calculation was 4.0×10^{-6} °C^{-1}.(60) Substitution of these quantities into Eq. (19) yields the expression for the pressure, in mm Hg,

$$p_{mm} = (W/t)\, T^{1/2}\, (5.036 \times 10^3) \quad . \tag{45}$$

All vapor pressures calculated from Eq. (45) are referred to as series B-4 in Table VII (p. 69).

Additional vapor measurements carried out in the fused silica apparatus with effusion cell No. 1, but having a 10.675-cm orifice-to-collimator distance, are designated Series B-8 in Table VII. These pressures were calculated from the expression

$$p_{mm} = (W/t)\, T^{1/2}\, (4.694 \times 10^3) \quad , \tag{46}$$

which includes the inner shield correction factor. All series B data are represented on the combined vapor pressure plot (Fig. 13, p. 67) by triangles.

D. The Low Temperature (Series C) Effusion Measurements

Vapor pressure measurements over the temperature range 1300° to 1750°C were carried out in the apparatus designated in Fig. 9 as the Pyrex vapor pressure apparatus. This apparatus is adequately described by Erway and Simpson.[20] Uranium dioxide containing predominantly U^{233} was used to give greater sensitivity to the alpha counting method. The method of exposure of the condensation targets was similar to that of the high temperature measurements.

Effusion cell No. 2, shown schematically in Fig. 10, was machined from tantalum and contained a rather snug fitting X-ray density tungsten (19 g/cc) cup obtained from the Kulite Corporation. The crucible orifice was fabricated from a 3-mil tantalum sheet in which a round, well-defined hole had been carefully drilled. The tantalum sheet containing the orifice was then spot welded onto the crucible lid in numerous places to prevent warping of the orifice. The ideality of an orifice constructed in such a manner was evidenced by the ratio of orifice thickness to orifice diameter which was as small as 0.014. The problem of orifice clogging was not encountered at these low temperatures because the rate of effusion was small. X-ray density tungsten was considered necessary to hold the purified uranyl nitrate containing the 233 isotope which was introduced into the cup in the form of a highly concentrated solution. The slow evaporation of the solution to dryness resulted in the coverage of the entire inner surface of the tungsten cup with the solid nitrate, thus producing a very small ratio of orifice area to evaporating area. Conversion of the solid uranyl nitrate to UO_2 was accomplished as described previously.

Since the Pyrex vapor pressure apparatus was all glass and contained no ground glass joints, it was possible to attain vacua as low as 10^{-8} mm Hg. The residual pressure throughout all exposures never exceeded 2×10^{-7} mm Hg at the temperature of measurement.

Heating of the tantalum crucible was again carried out inductively. The temperature of the crucible remained constant to within two degrees as determined by the calibrated pyrometer No. 2, provided the exposure times were less than one hour. Over longer exposure times of two to three hours a slight decrease in the temperature of about 4 to 6 degrees was discernible. Therefore an average temperature was used in the calculations of vapor pressure.

The condensation coefficient of the effusate on the liquid nitrogen-cooled platinum targets was assumed in view of the measurements of Rauh and Thorn,[55] to be unity. They determined by actual measurement that the target temperature did not exceed 200°C with the oven at about 1700°C. Their "bouncing" experiment, similar to the one carried out in the fused silica vapor pressure apparatus, indicated a condensation coefficient of unity.

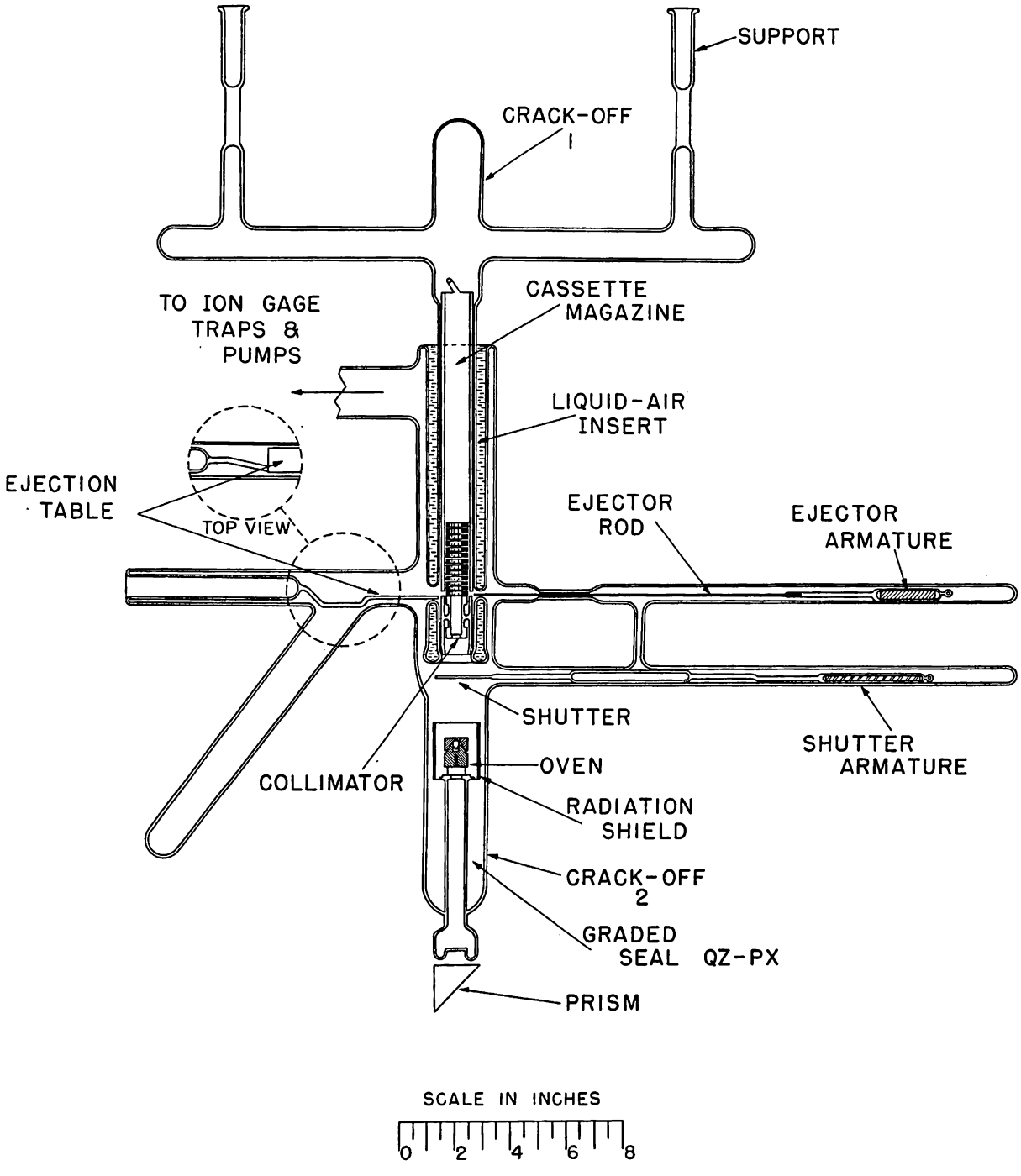

Figure 9

Schematic Diagram of the Pyrex Vapor Pressure Apparatus for Effusion Measurements at Temperatures Below 2000°K

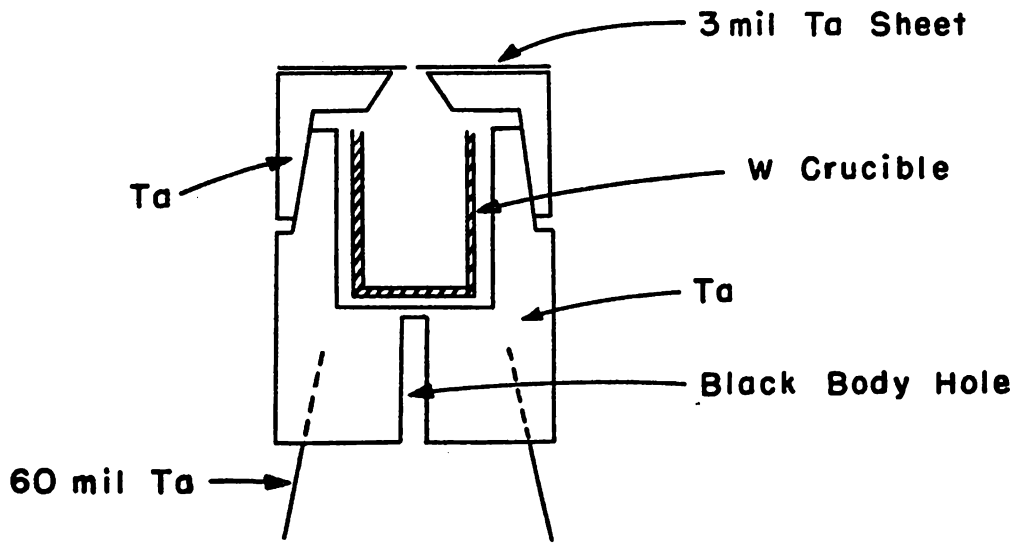

Figure 10

Schematic Diagram of Effusion Cell No. 2
Used with the Pyrex Vapor Pressure Apparatus

The expression relating the weight in grams of UO_2 on a given target with the value of c/m is given by

$$W = 1.058 \times 10^{-10} (c/m) \quad . \tag{47}$$

The half-life of U^{233} has been determined by Hyde(32) to be $1.62 \pm 0.01 \times 10^5$ years.

Room temperature measurements resulted in the following values for S_0, d, and r: $S_0 = 0.0272 \pm 0.0004$ cm^2, r = 0.8041 ± 0.0006 cm, and d = 11.895 ± 0.009 cm. From the value of the linear coefficient of thermal expansion for tantalum given by Sachs and Van Horn,(60) 6.5×10^{-6} deg^{-1}, the geometry factor as a function of temperature was calculated and incorporated with the constant term in Eq. (19) to yield

$$p_{mm} = (W/t)T^{1/2} G \quad , \tag{48}$$

where G varied linearly from 8.269×10^3 at 1325°C to 8.236×10^3 at 1725°C.

The geometry factor for the Pyrex apparatus (Fig. 9), in contrast to that of the fused silica apparatus (Fig. 5), showed significant temperature dependence. In addition to the increased orifice area with temperature, a significant decrease in the orifice-to-collimator distance d occurred due to the increase in height of the tantalum effusion cell No. 2. This increase in height was not compensated by a decrease in length of the Pyrex magazine, since the coefficient of thermal expansion of Pyrex is very small compared to that of metals.

Values of the vapor pressure calculated from Eq. (48) are designated as series C-1 and C-2 in Table VIII, p. 70. These data are represented by circles on the combined vapor pressure plot (Fig. 13, p. 67).

E. The Ultra-High Temperature (Series H) Effusion Measurements

Additional effusion measurements, at somewhat higher temperatures, were carried out in the fused silica apparatus (Fig. 5) over a temperature range 2162°C to 2550°C. Hence, considerable overlap occurred between the lower end of these measurements and the upper end of the series B measurements. Uranium dioxide of natural isotopic abundance was contained in tungsten effusion cell No. 3 shown in Fig. 11. The crucible in this case was well shielded on all sides and comparison of the black-body hole temperature with the cavity temperature proved them to be identical. The annular tungsten radiation shields were held in position by a slotted tantalum cover, similar to the case of effusion cell No. 1 (Fig. 6). A slotted cylindrical sheet of 5-mil tantalum served as a radiation shield for the sides of the crucible. The kinematic table upon which the crucible rested was fabricated from BeO, which possesses better high temperature refractory properties than does fused silica.

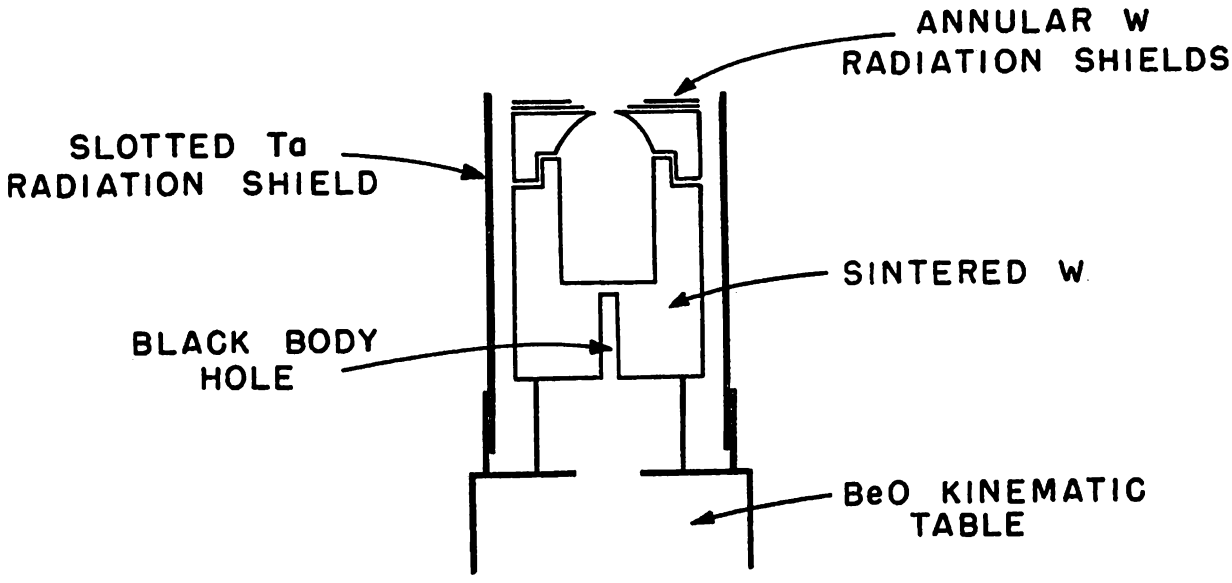

Figure 11

Schematic Diagram of Effusion Cell No. 3
Used for Effusion Measurements above 2400°K

The area of the orifice was measured to be 0.0161 ± 0.0004 cm^2 at room temperature; the collimator radius was 0.9507 ± 0.0004 cm; and the orifice-to-collimator distance was 11.286 ± 0.008 cm.

Calculations of the vapor pressure were made by means of the expression

$$p_{mm} = (W/t)T^{1/2}\,(8.973 \times 10^3) \quad . \tag{49}$$

Proper cognizance of the change in geometry factor with temperature was taken in the evaluation of the constant term in Eq. (49); the change in orifice area was the only significant factor involved and a value of 0.0164 cm^2 was used in calculating vapor pressures. Values of the vapor pressure calculated from Eq. (49), using the molecular weight of UO_2, are designated as series H-1 and H-2 in Table IX, p. 71, and are represented by x's on the combined vapor pressure plot, Fig. 13, p. 67. One significant difference between series H-1 and H-2 bears mention. Before the series H-2 measurements were carried out, the tungsten effusion cell No. 3 containing the UO_2 charge was initially heated at about 2800°K for about five minutes in order to melt the charge and increase its thermal conductivity. This initial melting probably reduced temperature gradients along the evaporating surface. Thus, the temperature observed in the black-body hole probably more nearly represented the temperature of the evaporating surface.

1. The Observed Melting Point of UO_2

Complete melting of UO_2 occurred at the highest temperature exposure of series H-1 which was 38° higher than the highest temperature exposure of the series B measurements where no melting occurred. Hence the melting point of UO_2 is between 2661°K and 2699°K. Spectrographic analysis of the molten residue indicated less than 0.2% tungsten and less than 0.5% silicon. It is believed that the presence of such small amounts of impurities would not appreciably lower the melting point. Thus, in view of the precision and accuracy involved in the temperature measurements of this investigation, the value obtained is probably closer to the true melting point than any of the values quoted in an earlier section of this thesis. The value of Friederich and Sittig[21] most nearly agrees with the result presently reported.

F. Miscellaneous Effusion Measurements

1. The Use of Tantalum as a Crucible Material

The vapor pressure of UO_2 was independent, within the deviation of 6 per cent, of whether the measurements were carried out in tungsten or in tantalum crucibles. Ten platinum condensation targets were exposed in the fused silica vapor pressure apparatus (Fig. 5) to the effusate

originating from a tantalum oven similar to effusion cell No. 2 (Fig. 10). No tungsten liner was present inside the crucible cavity and the UO_2 charge was placed in direct contact with the tantalum. The range of temperature over which exposures were made varied from 1847° C to 2151° C. The measurements were designated as series B-6 and B-7. The series B-6 measurements were carried out using a thin-edged orifice having an area of 0.1110 ± 0.0005 cm^2 measured at room temperature. The quantity r was 0.9507 cm, and d was 10.035 cm. The geometry factor, corrected for the average temperature of exposure, gave rise to the following expression from which values of the pressure were calculated:

$$p_{mm} = (W/t)T^{1/2}\,(1.023 \times 10^3) \quad . \tag{50}$$

The B-7 series of measurements was carried out using an orifice of about one-half the area as used in the B-6 series of measurements. Its area, measured at room temperature, was 0.0560 ± 0.0004 cm^2. The quantity r was 0.9507 cm and d was 11.615 cm. Values of the pressure of series B-7 were calculated from the following equation corrected for change in geometry:

$$p_{mm} = (W/t)T^{1/2}\,(2.710 \times 10^3) \quad . \tag{51}$$

In both series B-6 and B-7, the amount of natural abundance UO_2 on all targets was determined by α counting. The X-ray lattice parameter of both residues indicated a composition of $UO_{2.00}$. The primary vaporization data for series B-6 and B-7 are summarized in Table X, p. 72.

A change in the orifice area by a factor of two in the two series had no effect on the calculated vapor pressures. This indicates that the product αS_a in Eq. (25) is large compared with S_0. Hence the saturation pressure was measured. The combined data of both series were treated by the method of least squares to yield the equation

$$\log p_{mm} = 32,196 \pm 893/T + 12.029 \pm 0.390 \quad . \tag{52}$$

Precise measurement of the temperature, especially in series B-6, was extremely tedious because the central region of the black-body hole appeared darker than the edges of the hole. As a result of this central dark region, the measured temperature was somewhat lower than the true temperature. This would tend to reduce the discrepancy between the tungsten and tantalum measurements.

2. The Effusion Measurements on $U^{238}O_2$

Eight 1-mil thick aluminum condensation targets of 3/4" diameter were exposed in the fused silica vapor pressure apparatus (Fig. 5) with tungsten effusion cell No. 1 (Fig. 6) which contained depleted $U^{238}O_2$. The

molecular beam striking the target was collimated by a 9/16" i.d. annular nickel washer pressed against the aluminum target in the cassette and held in a fixed position by a phosphor bronze spring. Hence, the stainless steel collimator of the vapor pressure apparatus did not serve as the effective collimator. All exposures were carried out at a constant temperature for the same length of time. The constant temperature served as a means of viewing the constancy of the vapor pressure as a function of time. The expression giving the pressure as a function of experimentally observed quantities is

$$p_{mm} = (W/t)T^{1/2}\,(8.896 \times 10^{3}) \quad . \tag{53}$$

The above equation includes the corrections for the presence of the inner tungsten shield and for the change in geometry with temperature. A slight correction for the small temperature difference was made. Calculation showed the average pressure and the probable error at 2469°K to be

$$p_{mm} = (7.84 \pm 0.04) \times 10^{-2} \quad . \tag{54}$$

This average pressure is shown by the crossed square in the combined vapor pressure plot (Fig. 13) and the data are designated as series I-2 in Table VI. The last exposure in the table was excluded because the sample was exhausted during the subsequent exposure, and it is likely that the evaporating area became too small for saturation to be achieved. The constancy of the vapor pressure throughout the entire series, during which time an appreciable fraction of the initial oven charge was evaporated, indicates that the system UO_2 is invariant at constant temperature.

3. Vaporization of U_3O_8 in Vacuo

A sample of U_3O_8 weighing 0.04881 gram was heated inductively at about 1000°C in a vacuum of 10^{-3} mm Hg in a previously outgassed open platinum crucible, 1-1/4" high by 3/8" i.d. The sample was weighed before and after heating to determine the weight loss during the run. Four platinum dishes, mounted in cassettes in inverted positions in the copper magazine of the quartz vapor pressure apparatus (Fig. 5), were exposed to the effusate leaving the open crucible. Examination of the platinum dishes by the fluorophotometric method showed, at least qualitatively, the presence of uranium. A small amount of yellowish-brown condensate was present on the condenser wall. The condensate proved to be uranium in some form as evidenced by α counting. A sufficient quantity of this condensate was not present for direct oxygen determination. X-ray examination of the residue showed the presence of a single face-centered cubic phase, UO_{2+x}, having a lattice parameter of 5.4576 kx units. This value of a_0 corresponds to an

O/U value of 2.04 obtained from Fig. 3. During the period of heating, the sample lost 21.0 mg of material via vaporization. If one now assumes the total weight loss of the sample is attributable to molecular oxygen, i.e.,

$$U_3O_8(s) \longrightarrow 3UO_y(s) + \frac{8-3y}{2} O_2(g) \quad , \tag{55}$$

then one can calculate a value of y = 1.91, or O/U = 1.91, which is contradictory to the actual value of O/U = 2.04. If this discrepancy were due to experimental error in determining the weight loss of the sample, it would have amounted to an error of about 3 mg in the total weight loss, which is highly improbable.

Likewise, one can calculate that U_3O_8 does not vaporize under the experimental conditions investigated according to the over-all reaction

$$U_3O_8(s) \longrightarrow 1.04\ UO_{2.04}(s) + 1.96\ UO_3(g) \quad , \tag{56}$$

because the weight loss of the sample would have been almost 2/3 its original weight.

Hence, one might conclude that U_3O_8 does not decompose entirely by loss of oxygen, but the vapor contains a small fraction of a uranium-carrying species, probably $UO_3(g)$. The existence of such a gaseous molecule is also evidenced by Biltz and Mueller's data[2] and Brewer's analysis of their data.[7]

Undoubtedly the decomposition of U_3O_8 to UO_2 occurs in steps. The single datum reported here is not sufficient to permit the calculation of the partial pressures of $UO_3(g)$ and oxygen in any one of these steps. As a result, one could calculate only an "average pressure" of $UO_3(g)$, which is meaningless in the thermodynamic sense. However, Brewer, using the data given by Biltz and Mueller,[2] estimated the partial pressure of $UO_3(g)$ over $UO_{2.62}$ at 1600°K to be 10^{-5} atm. From this and other available thermodynamic data for solid UO_3, Brewer calculated 10^{-4} atm $UO_3(g)$ in equilibrium with solid UO_3 at 1600°K and 10^{-5} atm $UO_3(g)$ in equilibrium with solid UO_3 at 1450°K. These data, therefore, allow one to calculate a heat of sublimation for UO_3 which is 70.8 kcal mole^{-1}.

G. The Volatility of a Mixture of Uranium Metal and Uranium Dioxide (Series D)

The volatilities of two different mixtures of uranium metal and uranium dioxide were investigated as a function of time at a given temperature by determining the activity of a series of condensation targets which had been exposed to the effusate from each of the mixtures. All measurements were carried out in the fused silica vapor pressure apparatus (Fig. 5). Series D-1 was carried out at 2074°K. Tungsten effusion

cell No. 1 containing an X-ray density tungsten liner was initially charged with 10.3 mg of cleaned uranium metal in the form of wire, and 39.6 mg of the dioxide, which gave a value of O/U = 1.54 for the mixture. Both the metal and oxide were enriched in the U^{235} isotope, the exact isotopic composition being given in Section IV, B-1. It will be realized that the predominant α activity was from the U^{234}. The series of condensation targets was exposed for intervals of various times ranging from three to twenty minutes. During the exposures the residual pressure in the vacuum system decreased continuously from an initial value of 9×10^{-6} mm Hg down to a final value of 5×10^{-7} mm Hg. The volatility data are given in Table III and are shown in Fig. 12, the plot of c/m per one-minute exposure vs time in minutes. The average time, or "half time" of exposure, and the corresponding alpha count are represented by each of the experimental points. The residual pressure in the system, corresponding to the pronounced minimum in Fig. 12, was 2×10^{-6} mm Hg. The contents of the tungsten liner, upon exposure to the atmosphere after the experiment, showed the presence of both metal and oxide. The metal had melted during the exposures and had run to the bottom and sides of the tungsten liner since it is more dense than the oxide. X-ray examination of a sample taken from the interface between the two phases showed only the presence of $UO_{2.00}$.

In order to ascertain the effect on the mixture volatility of a varying residual pressure in the vacuum system, a second mixture experiment, designated series D-2, was carried out in the same apparatus (Fig. 5). In this series effusion cell No. 1 containing the X-ray density tungsten liner was initially charged with 6.8 mg of uranium metal and 13.3 mg of uranium dioxide. The tungsten liner had been previously outgassed at about 2200°C to remove any uranium remaining from series D-1. A constant residual pressure of about 4×10^{-7} mm Hg was obtained by a prolonged pumping and "flashing" technique during which time considerable amount of uranium metal and dioxide may have vaporized from the effusion cell. During all exposures, the residual pressure in the vacuum system remained constant at 4×10^{-7} mm Hg. The condensation targets were exposed for six-minute intervals over a total time of about three hours. The volatility data are given in Table III, and Fig. 12 gives the resulting plot of c/m per one-minute exposure vs time in minutes. Again the "half-time" of each exposure corresponding to a given alpha count is represented by the experimental points. Examination of the residue after exposure to the atmosphere showed no visible trace of uranium metal when the tungsten liner was viewed under a microscope. An X-ray analysis of the residue showed only the $UO_{2.00}$ cubic phase to be present.

Since only a three-degree difference in temperature occurred between the two series, they will be treated as if both were carried out at the same temperature. Series D-1 was obviously complicated by the constant decrease in background pressure, since all other conditions were maintained constant in both series. The weight loss data for both series

Table III

VOLATILITY DATA FOR URANIUM-URANIUM DIOXIDE MIXTURES

(Fused Silica Apparatus, Tungsten Effusion Cell No. 1, Enriched U^{235})

Series D-1			Series D-2		
No.*	(c/m)** per Minute	Average Time (Min)	No.*	(c/m)** per Minute	Average Time (Min)
1	23.1	5.0	22	34.1	8.0
2	13.7	13.0	23	33.9	20.0
3	9.6	21.0	24	32.9	32.0
4	9.6	29.0	25	26.3	44.0
5	10.7	38.0	26	20.5	56.0
6	13.1	47.0	27	16.1	68.0
7	14.9	55.0	28	13.8	80.0
8	17.0	64.5	29	11.9	92.0
9	19.9	74.5	30	10.9	104.0
10	31.4	85.0	31	10.8	116.0
11	36.3	98.5	32	10.2	128.0
12	39.2	119.5	33	10.0	140.0
			34	9.4	152.0
			35	9.2	164.0
			36	9.0	177.0

* Order of exposure.

** Corrected for background of 0.1 c/m.

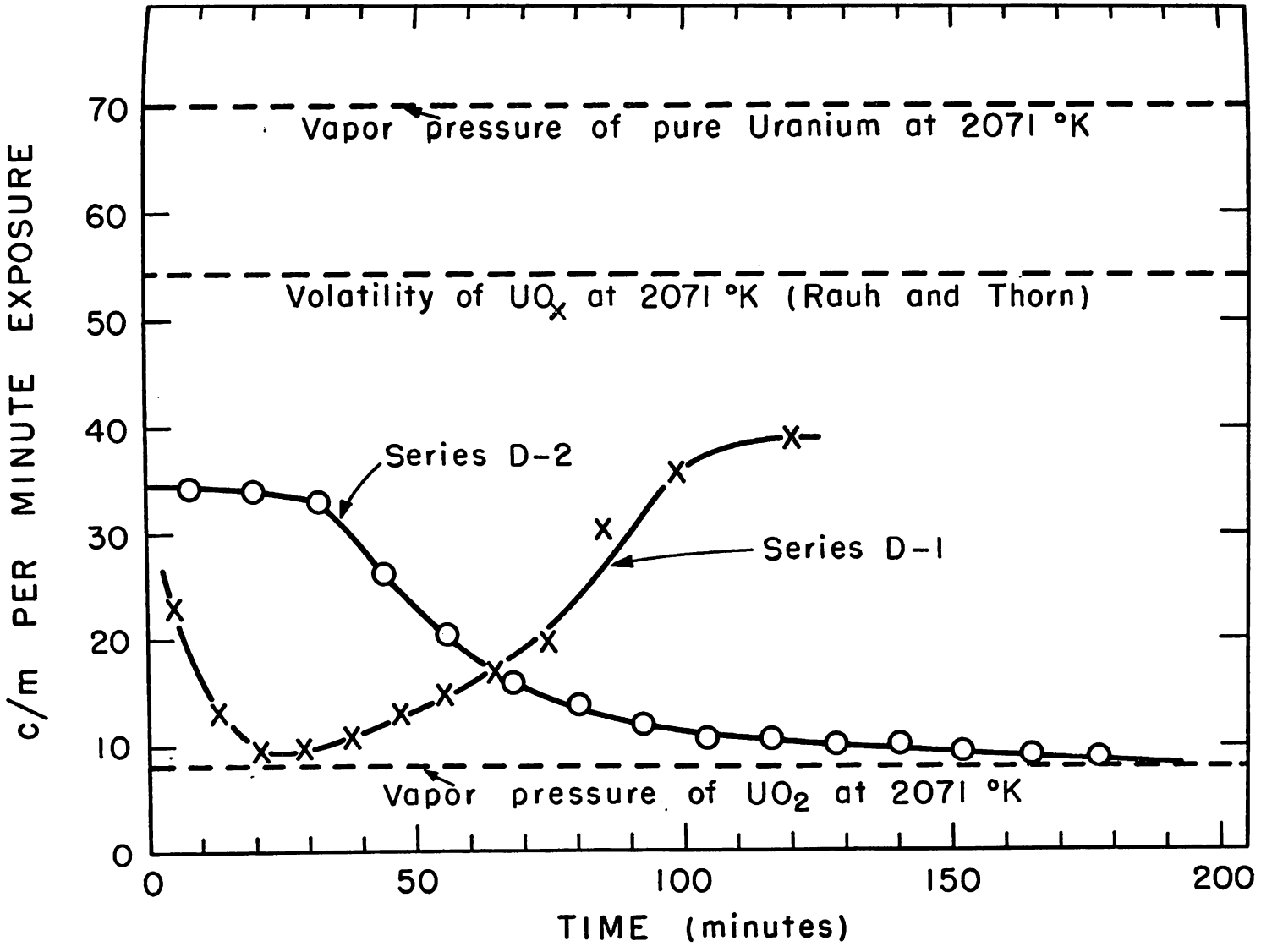

Figure 12

Plot of the Volatility of Uranium Metal-Uranium Dioxide Mixtures (Series D-1 and D-2) as a Function of Time

are summarized in Table IV. The final weights are uncertain to about ± 0.2 mg since it was very difficult to remove all the dioxide from the tungsten liner in order to weigh the residual metal and dioxide independently. The counting rate to be expected for pure uranium metal is shown as 70 c/m in Fig. 12, whereas a value of 54 c/m is to be expected for UO_x, the oxidized metal obtained from the measurements of Rauh and Thorn[55] at a temperature of 2071°K. Calculation shows that in series D-1 all the uranium should have been lost from the effusion cell in 106 minutes if it vaporizes at a pressure corresponding to the value of 70 c/m. If, however, it vaporizes at a pressure corresponding to 54 c/m (UO_x), 137 minutes would have been necessary to deplete the effusion cell of metal. A similar calculation for series D-2 yields times of 69.4 and 90.0 minutes for total loss of uranium vaporizing at pressures corresponding to 70 c/m and 54 c/m, respectively.

If one compares the areas under the curves in Fig. 12 with the respective weight losses of metal and dioxide, good agreement is obtained if a correction for the time of "flashing" in the case of series D-2 is considered. The total time of flashing was estimated to be 25 ± 10 minutes. The results are shown in Table V where all areas are given in the same arbitrary units.

The ratio of areas for the dioxide agrees quite well with the ratio of observed weight losses of the two series. If one calculates the weight of dioxide that should be lost, based on the vapor pressure of UO_2 at this temperature, a value of 1.2 mg is obtained. Hence, it appears that the presence of uranium metal does not affect the rate of evaporation of UO_2. The agreement between the ratio of areas under the curves and the observed ratio of uranium metal weight losses does not show as good agreement as in the case of UO_2. The reason for this may be associated with the phenomenon encountered in the inner shield measurements. The geometrical arrangement of metal with respect to the oxide was such that only an annular area of metal contributed to evaporation. Hence, direct evaporation did not occur in the direction of the target.

It is of interest to calculate a pressure corresponding to the initial portion of series D-2 in Fig. 12 and to compare this value with the vapor pressure of uranium metal at this temperature. One may assume a value for the molecular weight M = 235 in view of the weight loss data and calculate a value of about 1.14×10^{-3} mm Hg corresponding to this maximum volatility. This value of the pressure will not be in serious error as a result of this particular choice of M, since uranium constitutes the large majority of the mass of any oxide molecule one could postulate as being responsible for this volatility. The vapor pressure of pure uranium at this temperature, 2071°K, is 2.1×10^{-3} mm. Hence, the mixture volatility seems at least in qualitative agreement with the suppression of the uranium vapor pressure by an oxide found by Rauh and Thorn.[55] As it will

Table IV

SUMMARY OF WEIGHT LOSS DATA FOR URANIUM-URANIUM DIOXIDE MIXTURES

(Fused Silica Apparatus, Tungsten Effusion Cell No. 1, Enriched U^{235})

Series D-1 (T = 2074°K)

	Initial weight (mg)	Final weight (mg)	Weight loss (mg)
metal	10.3	6.6	3.7
dioxide	39.6	38.5	1.1

Initial O/U = 1.54

Series D-2 (T = 2071°K)

	Initial weight (mg)	Final weight (mg)	Weight loss (mg)
metal	6.8	0.2	6.6
dioxide	13.3	12.3	1.0

Initial O/U = 1.27

Table V

COMPARISON OF INTEGRATED RATE AND TOTAL AMOUNT VAPORIZED IN THE MIXTURE EXPERIMENTS

	Series	Area (arbitrary units)	Weight loss (mg)
metal	D-1	96	3.7
	D-2	140	6.6
dioxide	D-1	51	1.1
	D-2	44	1.0

become apparent in a later section of this thesis, this maximum volatility of the metal-oxide mixture will play a predominant role in showing that fragmentation is unimportant in the vaporization of $UO_2(s)$.

H. Tabulation of All Primary Vaporization Data

All the data comprising series B-4, B-8, C-1, C-2, H-1, H-2, and I-2 were plotted as shown in Fig. 13, p. 67. These data were taken with three different effusion cells, in two different apparatuses, using three different isotopic compositions. The temperature corrections were different; the geometries were different; the half-lives were different; yet the data fit together exceptionally well. One notices immediately that the plot appears to be linear from 1600° to about 2200°K, but shows positive curvature above 2200°K. Treatment of all data by the method of least squares[47] yielded two empirical equations:

$$\log p_{mm} = 13.340 - 3.7337 \times 10^4/T + 3.6700 \times 10^6/T^2 + 2.4638 \times 10^9/T^3 \quad , \tag{57}$$

and

$$\log p_{mm} = 14.739 - 4.3817 \times 10^4/T + 1.2157 \times 10^7/T^2 \quad . \tag{58}$$

Either of the above equations will give the continuous curve drawn through the experimental points in Fig. 13, although the former gives the better fit of the experimental data. One should remember that the above least squares treatment was performed with pressures calculated from the assumption that the molecular weight M = 270.08.

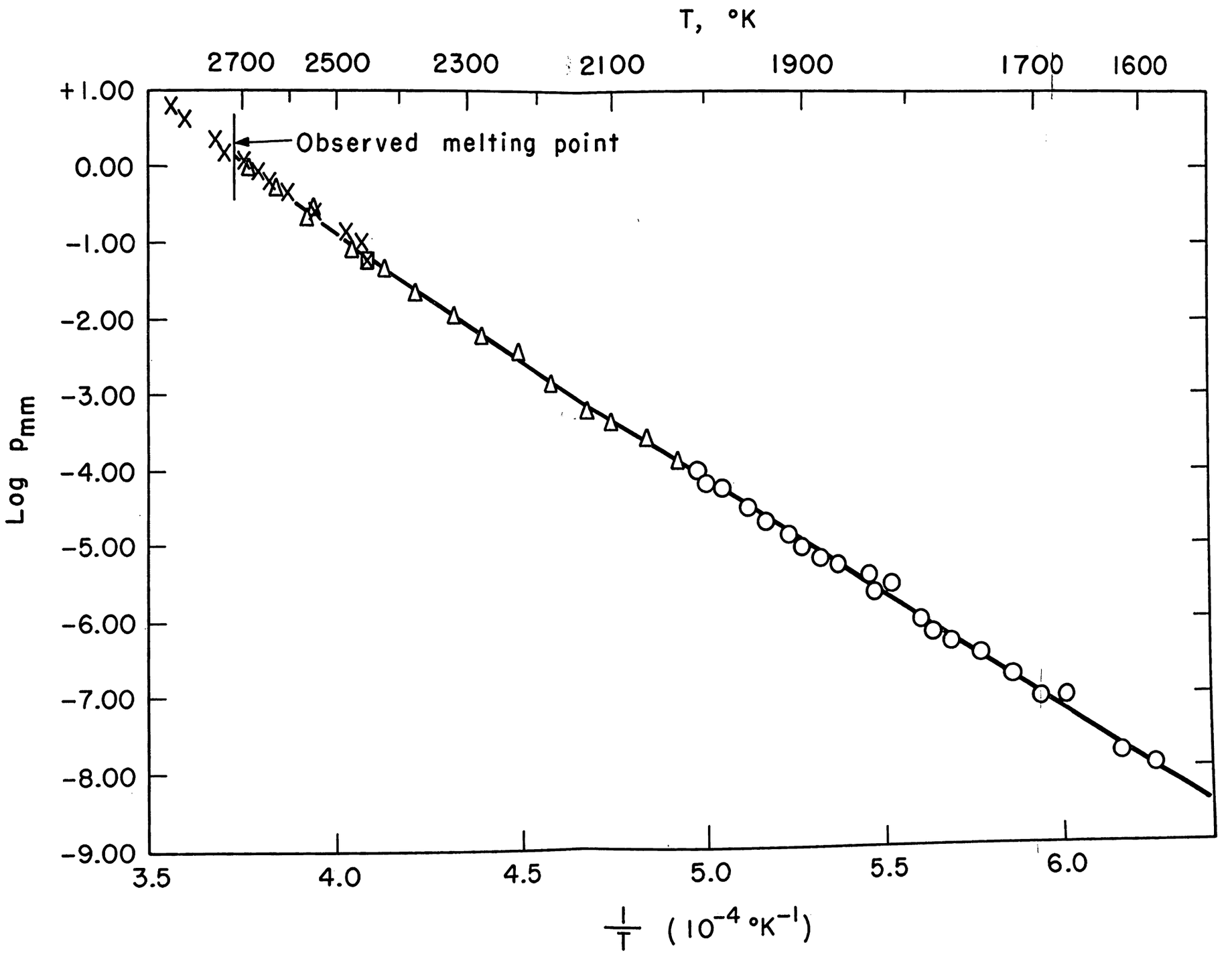

Figure 13

Log p vs. 1/T Plot for All Vapor Pressure Series

Table VI

VOLATILITY OF $UO_2(s)$ AS A FUNCTION OF TIME AT CONSTANT TEMPERATURE

Series I-2. (Fused Silica Apparatus, Tungsten Effusion Cell No. 1, Inner Shield, Sample Enriched in U^{238}.)

No.*	c/m**	W(10^{-6} gms)	t (sec)	T*** (°K)	$T^{1/2}$	p_{mm}	log p_{mm}	$1/T(10^{-4}\ °K^{-1})$
3	33.0	97.1	540	2469	49.690	7.95×10^{-2}	-1.100	4.050
4	32.2	94.7	540	2467	49.670	7.75×10^{-2}	-1.111	4.054
5	32.3	95.0	540	2467	49.670	7.77×10^{-2}	-1.109	4.054
6	31.6	92.9	540	2466	49.659	7.60×10^{-2}	-1.119	4.055
7	31.0	91.2	540	2469	49.690	7.47×10^{-2}	-1.127	4.050
8	32.6	95.9	540	2469	49.690	7.85×10^{-2}	-1.105	4.050
9	32.8	96.4	540	2469	49.690	7.89×10^{-2}	-1.103	4.050
11	31.1	91.5	540	2469	49.690	7.49×10^{-2}	-1.126	4.050

* Order of exposure.

** Corrected for background of 0.1 c/m.

*** A constant value of 29°, as determined by preliminary experiments, has been added to the corrected black-body temperature.

Orifice area, $S_0 = 0.0366 \pm 0.0009\ cm^2$. Orifice-to-collimator distance, d = 10.6571 ± 0.006 cm. Radius of collimator, r = 0.2813 ± 0.004 cm. Inner shield correction factor = 1.305. Average of all pressures is indicated by ⊠ in Fig. 13.

Table VII

HIGH TEMPERATURE (SERIES B) VAPORIZATION DATA FOR $UO_2(s)$

(Fused Silica Apparatus, Tungsten Effusion Cell No. 1, Inner Shield, Natural Uranium)

No.*	c/m**	W(10^{-6} gms)	t (sec)	T (°K)	$T^{1/2}$	p_{mm}	log p_{mm}	1/T(10^{-4}°K^{-1})
Series B-4								
18	205.0	296.6	300	2536***	50.359	2.51×10^{-1}	-0.601	3.943
19	410.9	594.6	300	2608***	51.069	5.10×10^{-1}	-0.293	3.834
20	308.5	446.4	120	2661***	51.586	9.66×10^{-1}	-0.015	3.757
21	119.7	173.2	1020	2424***	49.235	4.21×10^{-2}	-1.376	4.125
22	170.2	246.3	780	2478***	49.779	7.92×10^{-2}	-1.102	4.036
23	77.1	111.6	1200	2378***	48.765	2.28×10^{-2}	-1.641	4.205
24	17.0	24.7	8700	2133***	46.184	6.60×10^{-4}	-3.180	4.688
25	34.3	49.6	8700	2181***	46.701	1.34×10^{-3}	-2.873	4.585
26	78.7	113.9	4500	2279***	47.739	6.09×10^{-3}	-2.216	4.388
27	88.6	128.2	2880	2320***	48.166	1.08×10^{-2}	-1.967	4.310
1	160.0	231.5	300	2550***	50.498	1.96×10^{-1}	-0.707	3.922
Series B-8								
28	4.93	7.1	6000	2065†	45.442	2.52×10^{-4}	-3.598	4.843
29	40.40	58.5	3600	2228†	47.202	3.60×10^{-3}	-2.444	4.488
30	4.55	6.6	10800	2031†	45.067	1.29×10^{-4}	-3.888	4.924
31	5.93	8.6	4500	2104†	45.870	4.12×10^{-4}	-3.386	4.753

The geometry measurements for Series B-8 are identical with those of Series I-2, except $r = 0.9507 \pm 0.0004$.

*Order of exposure.

**Corrected for background of 0.1 c/m.

***Temperature correction applied as in series I-2.

†Temperature correction applied as in Series B-4.

Orifice area, $S_o = 0.0366 \pm 0.0009$ cm^2.

Orifice-to-collimator distance, $d = 11.056 \pm 0.006$ cm.

Radius of collimator, $r = 0.9507 \pm 0.0004$ cm.

Inner shield correction factor = 1.305.

All data represented by Δ in Fig. 13.

Table VIII

LOW TEMPERATURE (SERIES C) VAPORIZATION DATA FOR $UO_2(s)$

(Pyrex Apparatus, Tantalum Effusion Cell No. 2, Sample Enriched in U^{233})

Series C-1

No.*	c/m**	W (grams)	t (sec)	T*** (°K)	$T^{1/2}$	p_{mm}	log p_{mm}	$1/T(10^{4}\,°K^{-1})$
1	272.3	2.881×10^{-8}	2400	1833	42.813	4.07×10^{-6}	-5.391	5.455
2	549.8	5.817×10^{-8}	2100	1902	43.611	9.56×10^{-6}	-5.020	5.258
3	56.0_8	5.933×10^{-9}	5520	1736	41.667	3.55×10^{-7}	-6.450	5.760
4	1.90_6	2.017×10^{-10}	3900	1624	40.299	1.65×10^{-8}	-7.782	6.158
5	12.5_1	1.324×10^{-9}	4500	1687	41.073	9.58×10^{-8}	-7.019	5.928
6	161.0	1.703×10^{-8}	5100	1785	42.249	1.12×10^{-6}	-5.952	5.602
7	1039.3	1.010×10^{-7}	600	1985	44.553	5.93×10^{-5}	-4.227	5.038
8	1283.2	1.358×10^{-7}	720	2000	44.721	6.67×10^{-5}	-4.176	5.000
9	1536.9	1.626×10^{-7}	1800	1958	44.250	3.16×10^{-5}	-4.500	5.107
10	400.9	4.242×10^{-8}	2700	1865	43.185	5.34×10^{-6}	-5.272	5.362
11	119.9	1.269×10^{-8}	6000	1777	42.154	7.06×10^{-7}	-6.151	5.627
Series C-2								
12	13.90	1.471×10^{-9}	4500	1666	40.817	1.06×10^{-7}	-6.976	6.002
13	299.8	3.172×10^{-8}	3600	1814	42.591	2.97×10^{-6}	-5.527	5.513
14	351.8	3.722×10^{-8}	1800	1883	43.393	7.10×10^{-6}	-5.149	5.311
15	855.7	9.053×10^{-8}	1500	1938	44.023	2.10×10^{-5}	-4.678	5.160
16	590.0	6.242×10^{-8}	1500	1916	43.772	1.44×10^{-5}	-4.841	5.219
17	181.0	1.924×10^{-8}	2700	1829	42.766	2.41×10^{-6}	-5.617	5.467
18	78.0	8.252×10^{-9}	5100	1758	41.929	5.38×10^{-7}	-6.270	5.688
20	840.4	8.891×10^{-8}	5106	1586	target was contaminated - discarded			
21	24.67	2.610×10^{-9}	4500	1709	41.340	1.90×10^{-7}	-6.721	5.851
22	1.55	1.640×10^{-10}	4200	1600	40.000	1.23×10^{-8}	-7.910	6.250
23	840.4	8.891×10^{-8}	306	2010	44.833	1.03×10^{-4}	-3.987	4.975

The geometry measurements for series C-2 are identical with series C-1.
All data are represented by O in Fig. 13.

*Order of exposure.

**Corrected for background of 0.1 c/m.

***Preliminary experiments indicated cavity and black-body temperatures were identical.

Room temperature orifice area, $S_0 = 0.0272 \pm 0.0004$ cm^2.

Room temperature orifice-to-collimator distance, $d = 11.895 \pm 0.009$ cm.

Room temperature radius of collimator, $r = 0.8041 \pm 0.0006$ cm.

Table IX

ULTRA-HIGH TEMPERATURE (SERIES H) VAPORIZATION DATA FOR $UO_2(s)$

(Fused Silica Apparatus, Tungsten Effusion Cell No. 3, Natural Uranium)

Series H-1

No.*	c/m**	W(10^{-6} gms)	t (sec)	T*** ($^{\circ}K$)	$T^{1/2}$	p_{mm}	log p_{mm}	$1/T(10^{-4}{}^{\circ}K^{-1})$
13	83.9	121.4	420	2488	49.881	1.29×10^{-1}	-0.888	4.019
14	99.5	144.0	240	2538	50.379	2.71×10^{-1}	-0.567	3.940
15	130.2	188.4	180	2588	50.872	4.78×10^{-1}	-0.321	3.864
16	173.8	251.5	180	2617	51.156	6.41×10^{-1}	-0.193	3.821
17	144.0	208.4	120	2638	51.362	8.00×10^{-1}	-0.097	3.791
18	217.3	314.4	120	2688	51.652	1.21	+0.084	3.748
19	55.7	80.6	72	2697	orifice clogged - not used			
20	258.5	374.0	120	2699	51.952	1.453	+0.162	3.705
Series H-2								
1	42.2	61.1	600	2384	48.827	4.46×10^{-2}	-1.351	4.195
2	60.2	87.1	480	2435	49.346	8.04×10^{-2}	-1.095	4.107
3	65.8	95.2	360	2463	49.628	1.18×10^{-1}	-0.929	4.060
4	411.3	595.2	120	2720	52.154	2.321	+0.364	3.676
5	375.9	543.9	60	2778	52.707	4.287	+0.632	3.600
6	255.9	370.3	30	2809	53.000	5.870	+0.769	3.560

The geometry measurements for series H-2 are identical with series H-1.

*Order of exposure.

**Corrected for background of 0.1 c/m.

***Same as for Series C-1.

Orifice area, $S_0 = 0.0164 \pm 0.0004$ cm^2

Orifice-to-collimator distance, $d = 11.286 \pm 0.008$ cm.

Radius of collimator, $r = 0.9507 \pm 0.0004$ cm.

All data are represented by X in Fig. 12.

Table X

VAPORIZATION DATA FOR $UO_2(s)$ (TANTALUM EFFUSION CELL)

(Fused Silica Apparatus, Natural Uranium)

Series B-6

No.*	c/m**	W(10^{-6} gms)	t (sec)	T*** (°K)	$T^{1/2}$	p_{mm}	log p_{mm}	$1/T(10^{-4}\ °K^{-1})$
16	45.6	66.0	3000	2147	46.336	1.04×10^{-3}	-2.982	4.658
28	96.2	139.2	900	2271	47.656	5.21×10^{-3}	-2.283	4.403
29	122.5	177.3	360	2378	48.764	2.46×10^{-2}	-1.610	4.205
30	88.8	128.5	1320	2242	47.350	4.72×10^{-3}	-2.327	4.460
31	54.6	81.6	1500	2199	46.893	2.61×10^{-3}	-2.583	4.548
Series B-7								
17	82.4	119.2	2700	2247	47.402	5.67×10^{-3}	-2.246	4.450
32	216.3	313.0	900	2393	49.942	4.71×10^{-2}	-1.327	4.179
33	92.0	133.1	1200	2316	48.125	1.45×10^{-2}	-1.840	4.318
34	125.5	181.6	780	2375	48.734	3.08×10^{-2}	-1.512	4.211
35	115.8	167.6	420	2424	49.233	5.32×10^{-2}	-1.274	4.125

*Order of exposure.

**Corrected for background of 0.1 c/m.

***Constant values of 111° and 32°, as determined by preliminary experiments, have been added to the corrected black-body temperatures to give cavity temperatures for series B-6 and B-7, respectively.

Orifice area (series B-6) = 0.1110 ± 0.0005 cm^2.

Orifice area (series B-7) = 0.0560 ± 0.0004 cm^2.

Radius of collimator, r = 0.9507 ± 0.0004 cm (same for both series).

Orifice-to-collimator distance, d = 10.035 ± 0.007 cm (series B-6).

Orifice-to-collimator distance, d = 11.615 ± 0.008 cm (series B-7).

VI. ANALYSIS AND INTERPRETATION OF THE DATA

A. Vaporization Phenomena of the UO_2 Phase

The congruency of the evaporation of $UO_2(s)$ has been demonstrated previously. It remains to deduce the processes important in vaporization. For UO_2, the possibility of vaporization to the elements can be readily examined since the free energy of formation of UO_2 is known as a function of temperature up to 1500°K[16] and the vapor pressure of liquid uranium has been established over the temperature range 1630° to 1970°K.[55] The calculation is shown below at 1500°K.

$$UO_2(s) = U(\ell) + O_2(g); \quad \Delta F°/T = 131.80 \text{ e.u.} \tag{59}$$

$$U(\ell) = U(g); \quad \Delta F°/T = 45.08 \text{ e.u.} \tag{60}$$

Summation of these equations gives,

$$UO_2(s) = U(g) + O_2(g); \quad \Delta F°/T = 176.88 \text{ e.u.} \tag{61}$$

The equilibrium constant for the reaction in question is,

$$K = p_U p_{O_2} = p_U^2 = p_{O_2}^2 \quad . \tag{62}$$

Since $\Delta F°/T = -4.576 \log K$, the equilibrium partial pressures of U(g) and $O_2(g)$ may be conveniently calculated. The same calculation can be performed at 2000°K by extrapolation of the free energy of formation data of the oxide.

In a similar fashion, the equilibrium partial pressures of U(g) and O(g) may be calculated at 1500°K. Thus one writes

$$UO_2(s) = U(g) + 2O(g); \quad \Delta F°/T = 225.72 \text{ e.u.} \tag{63}$$

For this case

$$K = p_U p_O^2 = 4p_U^3 = \tfrac{1}{2} p_O^3 \quad . \tag{64}$$

Calculations for this process can also be carried out at 2000°K by extrapolation of the necessary data. The results of these calculations are given in Fig. 14. Since the measured volatility of UO_2 is 10^4 times greater than the volatility calculated on the basis of decomposition to the elements, one concludes that these processes are not important at these temperatures and that gaseous oxide molecules must be of importance in the equilibrium vapor phase above $UO_2(s)$.

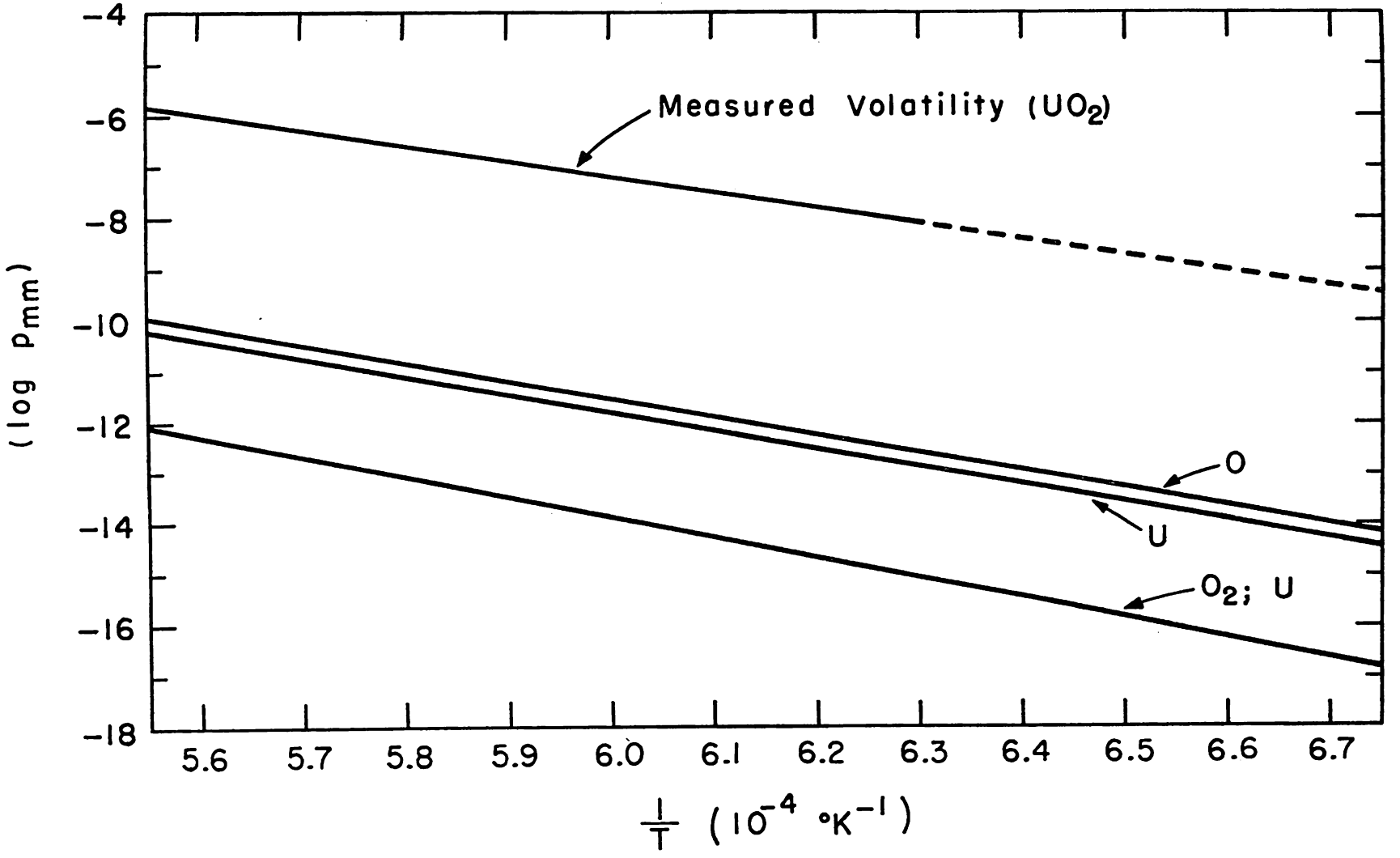

Figure 14

The Partial Pressures of the Gaseous Elements in Equilibrium with UO_2(s)

1. The Linear Region of log p vs. 1/T

Inspection of Fig. 13 shows that log p vs. 1/T appears to be very nearly linear over a 600° temperature range from 1600 to 2200°K. An extrapolation of this line fails, however, to contain the highest temperature points. The results will be interpreted in terms of two independent vaporization reactions. Consider first the low temperature range over which the plot is linear.

The predominant process occurring in the temperature range 1600° to 2000°K is undoubtedly the formation of $UO_2(g)$. X-ray diffraction patterns of sublimates collected on quartz targets at a temperature of about 800°C indicated the presence of the UO_2 cubic phase only. Spectrographic analysis indicated the absence of tungsten or any of its oxides. The absorption spectrum (see Addendum) of these sublimates also was characteristic of the UO_2 phase. However, X-ray diffraction patterns of sublimates condensed at temperatures < 400°C indicated that the collected sublimates were amorphous. Direct oxygen analysis of these sublimates proved them to have a composition of about U_3O_8. This is not surprising in view of the thermodynamic instability of $UO_2(s)$ at room temperature with respect to oxidation to $U_3O_8(s)$. Since the $UO_2(g)$ was condensed on the cold target in a very active amorphous state, rapid oxidation of the collected sublimates probably occurred when air was admitted to the apparatus after a series of exposures. Additional evidence that UO_2 was oxidized in this process was furnished by the observation of a sharp color change in the rather large amount of sublimate that had condensed on the fused silica condenser wall. The color change was from brown to black; bulk UO_2 is brown; bulk U_3O_8 is black.

If the higher temperature points did not exist, one would be inclined to pass a linear least-squares line through the points from 1600° to 2000°K, and to calculate a heat and entropy of sublimation from the slope and intercept, respectively. The linear least-squares equation is,

$$\log p_{mm} = (-30.019 \pm 0.335) \times 10^3/T + 10.865 \pm 0.197 \quad . \qquad (65)$$

The effective heat of sublimation over this temperature range is 137.4 ± 1.6 kcal mole^{-1} and the entropy of sublimation is 36.5 ± 0.9 e.u.

Rehn and Cefola[56] reported measurements of the vapor pressure of UO_2 at one hundred degree temperature intervals from 1873° to 2273°K. Their pressures are larger than those reported here by a factor of ten. They did, however, report a heat of sublimation of 137 kcal mole^{-1}. Apparently their measurements contained either an error that was proportional to the pressure which did not, therefore, influence the slope of the vapor pressure plot, or their measured temperatures were too low by nearly 150° over the entire experimental range.

One knows that over a temperature range of 400° the heat of sublimation will not remain constant and the plot of log p vs 1/T will be curved instead of linear. One may express the heat of sublimation as a linear function of the temperature over the temperature range in question as

$$\Delta H_T = \Delta H_0 + \Delta C_p T \quad , \tag{66}$$

where ΔH_0 is an integration constant having the dimensions cal mole^{-1}. The relationship

$$\left(\frac{\partial(\Delta F°/T)}{\partial T}\right)_p = -\frac{\Delta H^o}{T^2} \quad , \tag{67}$$

may be used with Eq. (66) to obtain

$$\log p_{atm} - (\Delta C_p/R) \log T = -\Delta H_0/4.576T + I \quad , \tag{68}$$

in which p is the vapor pressure in atmospheres and I is a constant of integration. The left-hand side of Eq. (68) is commonly designated as $-\Sigma$, which, when plotted against 1/T, yields a value of ΔH_0 from the slope. In order to calculate values for $-\Sigma$, one must either possess a knowledge of ΔC_p for the sublimation process or be able to estimate it. For the sublimation of $UO_2(s)$, ΔC_p was not known so it had to be estimated. Kelley[37] gives the heat capacity of $UO_2(s)$ from 298°K up to 1500°K:

$$C_p = 19.20 + 1.62 \times 10^{-3} T - 3.96 \times 10^5 T^{-2} \quad . \tag{69}$$

From this expression one calculates a value of C_p equal to 21.45 cal deg^{-1} mole^{-1} at 1500°K. The heat capacity of $UO_2(g)$ if it is assumed to be a nonlinear and classically fully excited molecule would be 14 cal deg^{-1} mole^{-1}. It is more likely to be about 12 cal deg^{-1} mole^{-1} in view of the measured heat capacities of such triatomic molecules as $H_2O(g)$ and $CO_2(g)$, which possess vibrational degrees of freedom that are not fully excited over at this temperature. The electronic contribution to the heat capacity of $UO_2(g)$ at 1500°K may be as large as 1 or 2 cal deg^{-1} mole^{-1}. Hence, it does not seem unreasonable to estimate a value of 13.5 cal deg^{-1} mole^{-1} for C_p of $UO_2(g)$ and, therefore, ΔC_p is equal to -8 cal deg^{-1} mole^{-1} for the sublimation process, $UO_2(s) \rightarrow UO_2(g)$, over the temperature range 1600° to 2000°K.

In the absence of more reliable data this value was assumed in the calculation of ΔH_0. Figure 15 gives the Σ-plot for UO_2 obtained by means of Eq. (68). The value of ΔH_0 evaluated from the slope is equal to 151.5 ± 1.7 kcal mole^{-1}. From the least-squares constants obtained from the Σ-plot treatment, the heat of sublimation for the process $UO_2(s) \longrightarrow UO_2(g)$ over the temperature range 1600° to 2000°K is given by

$$\Delta H^o_T = 151{,}500 - 8T \quad , \tag{70}$$

while the entropy of sublimation for the same process is given by

$$\Delta S^{o}_{T} = -18.42 \log T + 96.36 \quad . \tag{71}$$

At 1800°K, ΔH^{o} = 137.1 kcal mole^{-1} and ΔS^{o} = 36.4 e.u. mole^{-1}.

Equations (68), (70), and (71) give the pressure, the heat of sublimation, and the entropy of sublimation over the temperature range 1600 to 2000°K. How far beyond these temperature limits the equations apply depends, of course, on how well the ΔC_p has been estimated. In the absence of experimental heat capacity data for $UO_2(g)$, the necessary thermodynamic data must be estimated in order to extrapolate heats and entropies to lower temperatures.

Kelley[37] gives 23,750 cal mole^{-1} as $(H^{o}_{1500} - H^{o}_{298})$ and 30.82 e.u. for $(S^{o}_{1500} - S^{o}_{298})$ for $UO_2(s)$. A graphical integration of the data of Jones, Gordon, and Long[35] gives 2,725 cal mole^{-1} as $(H_{298} - H_0)$ for $UO_2(s)$. The entropy, S^{o}_{298} = 18.63 e.u. for $UO_2(s)$. It is estimated, that $(H^{o}_{1500} - H^{o}_{298})$ is 14,400 cal mole^{-1}, that $(S^{o}_{1500} - S^{o}_{298})$ is 19.31 e.u., that $(H^{o}_{298} - H^{o}_{0})$ is 2,100 cal mole^{-1}, and that S^{o}_{298} is 64.6 e.u. for $UO_2(g)$. The uncertainties in these values are unknown and may be large.

These values may be used together with values of ΔH^{o}_{T} and ΔS^{o}_{T} at 1500°K calculated from equations (70) and (71) to give

$$\Delta H^{o}_{298} = 159{,}650 \text{ cal/mole},$$

$$\Delta H^{o}_{0} = 160{,}275 \text{ cal/mole},$$

and

$$\Delta S^{o}_{298} = 49.37 \text{ cal/deg/mole}.$$

The entropy of sublimation of UO_2 determined in this work is in the range to be expected for simple sublimation processes. The entropies of sublimation of ThO_2[28,62] and PuO_2[53] are about the same as the value found in this work.

It is now possible to construct a thermodynamic cycle involving UO_2, as shown in Fig. 16. The heat of formation of $UO_2(s)$ at 0°K, ΔH^{o}_{0}, was estimated to be -258.6 kcal mole^{-1} from the thermodynamic data given by Coughlin.[16] Rauh and Thorn[55] calculated the heat of sublimation of uranium at 0°K, $\Delta H^{o}_{0}(U)$, to be 116.6 kcal mole^{-1}. The heat of sublimation of $UO_2(s)$ at 0°K, $\Delta H^{o}_{0}(UO_2)$, is 160.3 kcal mole^{-1} as estimated from the slope of the Σ-plot, Fig. 15, and the estimated thermodynamic data for $UO_2(g)$. The dissociation energy of oxygen, $D_0(O_2)$, is given by Gaydon[22] as 116.9 kcal mole^{-1}. These data enable one to calculate a dissociation energy for $UO_2(g)$ to the gaseous atoms at 0°K, $D_0(UO_2)$, which is 331.8 kcal mole^{-1} or 14.4 e.v.

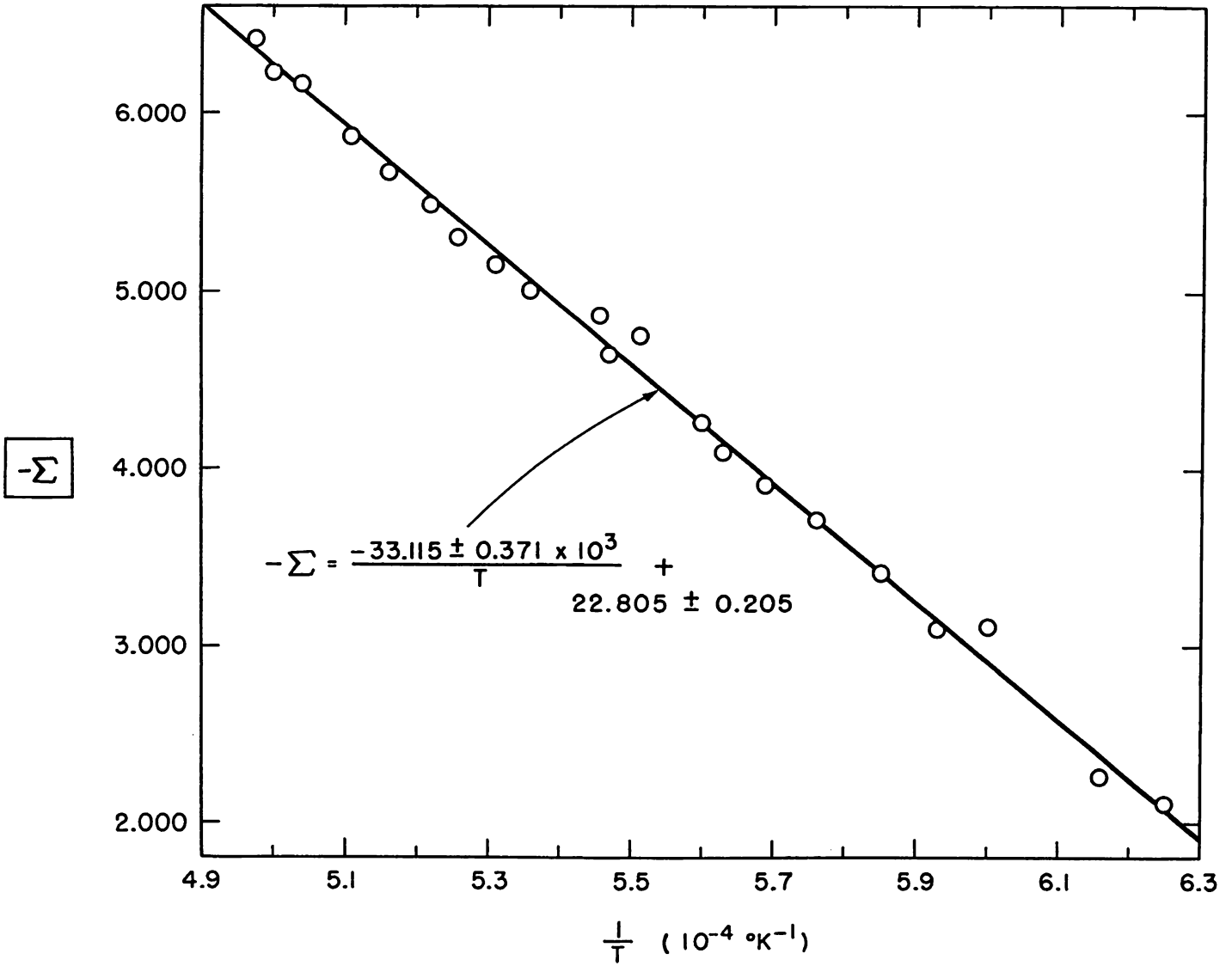

Figure 15

Plot of $-\Sigma$ vs. $1/T$ for Uranium Dioxide

$[-\Sigma = \log p_{atm} - (\Delta C_{p/R} \log T]$

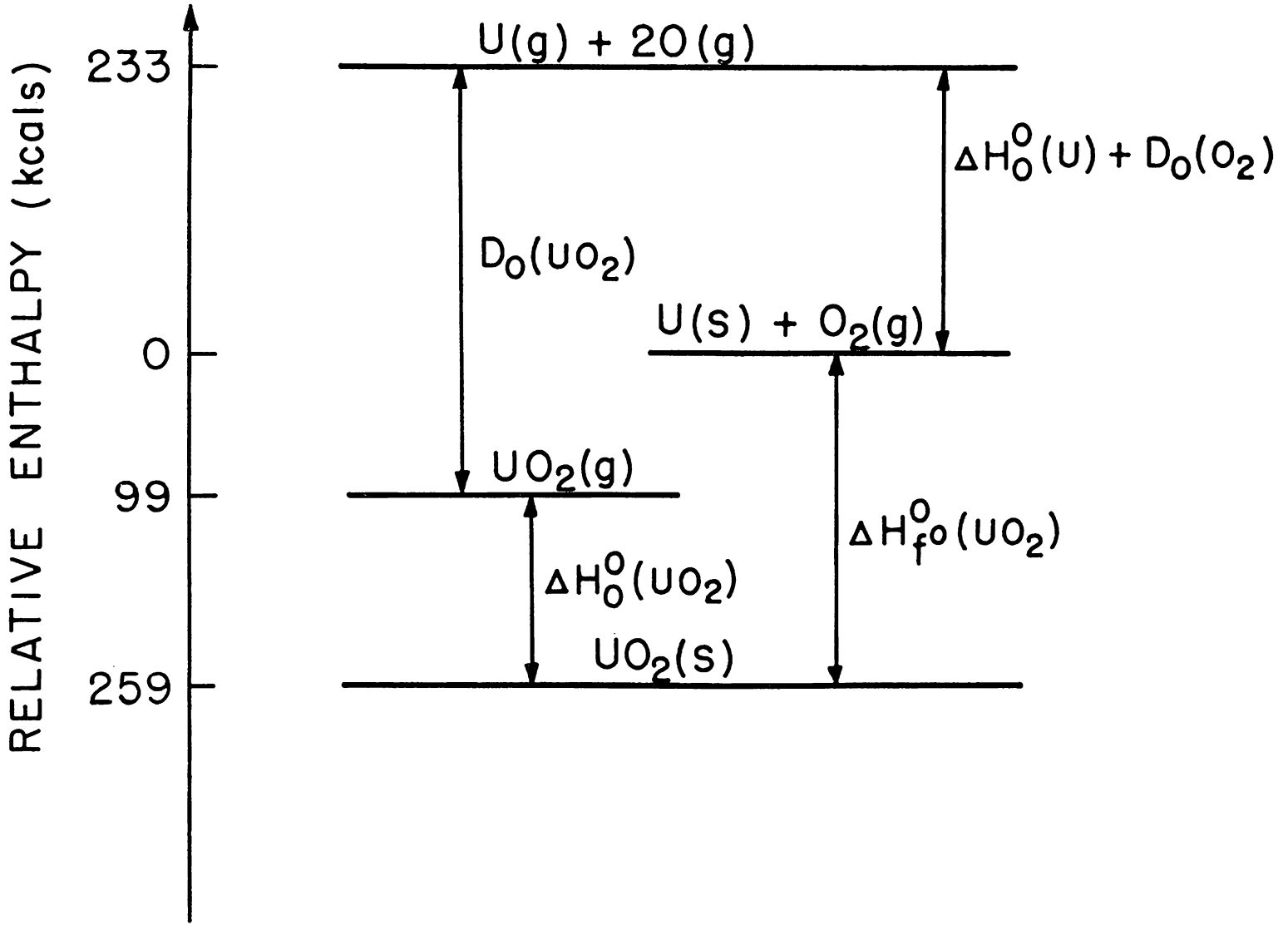

Figure 16

Thermodynamic Cycle Involving Uranium Dioxide

2. Analysis of the Curved Region of log p vs. 1/T

From an inspection of Fig. 13 one readily discerns that the vapor pressure plot shows positive curvature at the higher temperatures. As was pointed out previously, curvature may arise from ΔC_p, exceeding the upper limit of the effusion method, experimental error, and other vaporization processes. The quantity ΔC_p for all known oxide vaporization processes is negative and usually falls within the range -5 to -15 cal $mole^{-1}$ deg^{-1}. Therefore, ΔC_p causes curvature in the negative direction.

The employment of the effusion method over pressure regions where deviations from molecular flow become pronounced might also give rise to curvature. Several ratios of mean free path to orifice diameter were calculated at given temperatures over the range of discernible curvature using Eq. (20). The value of the average collision diameter for the vapor molecules was assumed to be 5 Å. The results are shown in Table XI. The work of Mayer and Johnson clearly validates the use of the effusion method at these values of λ/d. Hence, it would seem improbable that the curvature in log p vs. 1/T could have been caused by exceeding the upper limit of the effusion method.

Table XI

RATIO OF MEAN FREE PATH TO ORIFICE DIAMETER AT VARIOUS TEMPERATURES

$1/T$ $(10^{-4}\ °K^{-1})$	T(°K)	λ/d
4.60	2174	100
4.30	2326	10
4.05	2469	1.0
3.70	2703	0.1

One also might argue that the curvature arises from systematic or basic errors in the effusion measurements. The principal source of error associated with all the measurements probably lies in the determination of the temperature. If the curvature were due to error in measurement of the temperature, this error must have been as large as 200° at about 2600°K. This seems very unlikely in view of the calibrated pyrometer used and the precision one can obtain in temperature measurements with an optical pyrometer even at these high temperatures. Consequently, the only plausible explanation of the curvature is given by the postulation of one or more additional processes

such as polymerization, fragmentation, ionization, or reaction with the crucible, which become important at the higher temperatures. Proceeding on this basis one may then analyse the data in the following manner.

The least-squares equation for the vapor pressure of UO_2, corrected for ΔC_p, is that obtained in the Σ-plot treatment [see Eqs. (68), (70), and (71)],

$$\log p_{mm}\,(UO_2) = -33{,}115/T - 4.026 \log T + 25.686 \quad . \tag{72}$$

The partial pressure of $UO_2(g)$ calculated from Eq. (72) was subtracted from the total volatility calculated on the basis of M = 270.08 and obtained from the empirical least-squares Eq. (57) to give the pressure corresponding to the second vaporization process designated as process 2; the results are embodied in the following least-square equation:

$$\log p_{mm} = 38{,}221/T + 14.207 \tag{73}$$

The results of these calculations are shown in Fig. 17. It should be pointed out that Eq. (73) is necessarily based on the molecular weight of the vaporizing species being that of UO_2 and must therefore be corrected when applied to processes in which the molecular weight does not correspond to that of UO_2.

The following ~~congruent~~ vaporization processes were postulated to account for process 2:

Case I. $UO_2(s) = UO(g) + \left(\frac{1-\alpha}{2}\right) O_2(g) + \alpha\, O(g)$;

Case II. $UO_2(s) = 1/2\ U_2O(g) + (3-3\alpha)/4\ O_2(g) + (3/2)\,\alpha\, O(g)$;

Case III. $UO_2(s) = 1/2\ UO(g) + 1/2\ UO_3(g)$;

Case IV. $UO_2(s) = 1/3\ U(g) + 2/3\ UO_3(g)$;

Case V. $UO_2(s) \not\rightarrow UO_2^+(g) + e^-(g)$;

Case VI. $UO_2(s) = UO_2(g)$,

and $UO_2(s) = UO(s) + \left(\frac{1-\alpha}{2}\right) O_2(g) + \alpha O(g)$,

and $UO(s) = UO(g)$;

Case VII. $2UO_2(s) = (UO_2)_2(g)$;

Case VIII. $3UO_2(s) + 2W(s) = 3U(g) + 2WO_3(g)$.

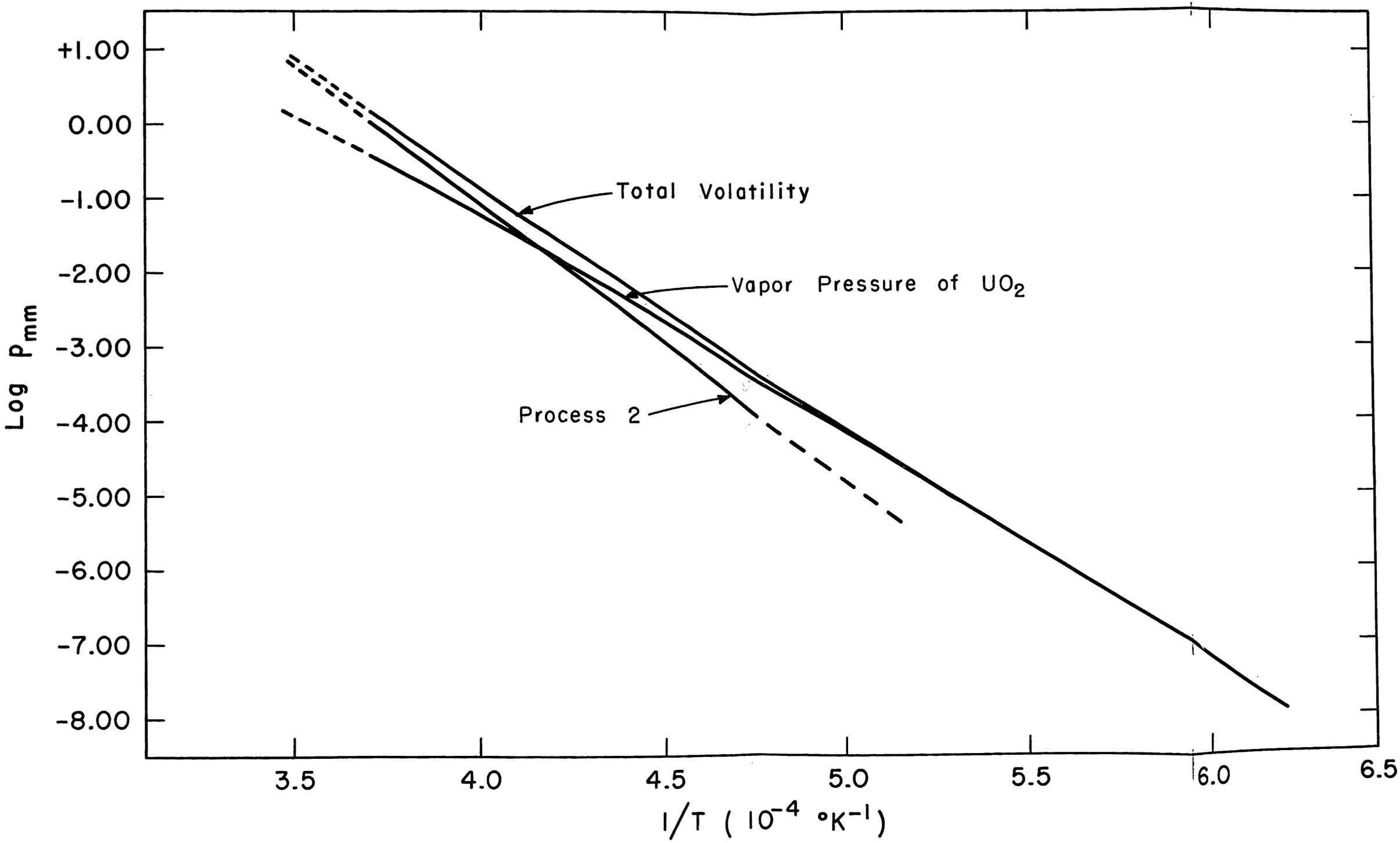

Figure 17

Plot Showing the Vapor Pressure of Uranium Dioxide, the Total Volatility of Uranium Dioxide, and the Calculated Pressure for the Process (Designated as Process 2) that Becomes Important at High Temperatures

a. Case I: Formation of UO(g). The equilibrium constant for Case I may be written as follows:

$$K_I = p_{UO} p_{O_2}^{(1-\alpha)/2} \cdot p_O^{\alpha} \quad , \tag{74}$$

where α is the fractional decomposition of oxygen molecules to oxygen atoms. Since K_I is a constant at a given temperature, an infinite number of combinations of values for p_{UO}, p_{O_2}, and p_O exist as long as the solid composition is not specified. However, if one assumes the solid phase to be constantly subliming at the composition $UO_{2.00}$ the following relationships necessarily hold:

$$p_{O_2} = \left(\frac{1-\alpha}{2}\right) p_{UO} \quad , \tag{75}$$

and

$$p_O = \alpha p_{UO} \quad . \tag{76}$$

Substitution of these relationships into Eq. (74) gives

$$K_I = \left(\frac{1-\alpha}{2}\right)^{(1-\alpha)/2} (\alpha)^{\alpha} (p_{UO})^{(3+\alpha)/2} \quad . \tag{77}$$

The total oxygen pressure is given by

$$p_{oxy} = \frac{(1+\alpha)}{2} p_{UO} \quad , \tag{78}$$

whereas the total pressure is given by

$$p_t = \frac{(3+\alpha)}{2} p_{UO} \quad . \tag{79}$$

If one assumes that Case I gives rise to the increased volatility of UO_2 at higher temperatures, then a value of p_{UO} at any given temperature may be calculated from Eq. (73), since only the UO(g) would have been collected on the condensation targets. The small difference between the molecular weights of UO and UO_2 is insignificant and will be ignored. One can then evaluate K_I once a method of calculating α is established. This can be done by considering the following equilibrium:

$$O_2 = 2\ O \quad . \tag{80}$$

The equilibrium constant for this process is

$$K_{oxy} = p_O^2/p_{O_2} = \frac{(2\alpha/1+\alpha)^2\, p_{oxy}}{(1-\alpha)/(1+\alpha)} \quad . \tag{81}$$

Substitution of p_{oxy} from Eq. (78) into Eq. (81) yields

$$K_{oxy} = (2\alpha^2/1-\alpha)p_{UO} \quad . \tag{82}$$

The above quadratic equation can be solved for α. Since the quantities under the radical are both large it is useful to expend it in series. Thus

$$\alpha = 1 - (2p_{UO}/K_{oxy}) + (8p_{UO}^2/K_{oxy}^2) - \cdots \quad . \tag{83}$$

If process 2 is represented by Case I, then one can calculate the pressure of UO in equilibrium with the mixture of metal and dioxide at 2071°K, and compare it with the value observed in the mixture experiment. To do this one first calculates a value of α from Eq. (83) at 2071°K. The value for K_{oxy} at this temperature is 1.46×10^{-6} atm determined from the available thermodynamic data for oxygen. The value of p_{UO} is calculated directly from Eq. (73). The value of α thus obtained is 0.91 which now enables one to calculate from Eq. (77) a value of 1.00×10^{-14} atm for K_I. Using this value of K_I, one obtains $\Delta F°/T = 64.1$ e.u. It is now possible to calculate the equilibrium pressure of UO(g) above the mixture via the two equations,

$$UO_2(s) = UO(g) + 0.045\ O_2(g) + 0.91\ O(g); \quad \Delta F°/T = 64.1 \text{ e.u.}, \tag{84}$$

and

$$0.045\ O_2(g) + 0.91\ O(g) + 1/2\ U(\ell) + 1/2\ UO_2(s); \quad \Delta F°/T = -54.0 \text{ e.u.} \tag{85}$$

The value of $\Delta F°/T$ in Eq. (85) was obtained from data given by Coughlin.[16] Summation of the above equations yields the equation for the process under consideration. Thus one obtains

$$1/2\ UO_2(s) + 1/2\ U(\ell) = UO(g); \quad \Delta F°/T = +10.1 \text{ e.u.} \tag{86}$$

If process 2 is represented by Case I, the equilibrium constant calculated from the last equation should equal the equilibrium pressure of UO(g) above the mixture of metal and oxide. The calculation gives 6.21×10^{-3} atm or 4.72 mm Hg. The maximum pressure observed above the metal-oxide mixture was only 1.14×10^{-3} mm. Therefore, Case I cannot be the correct process to account for the increased volatility of $UO_2(s)$ at high temperatures.

b. Case II: Formation of $U_2O(g)$. The calculations necessary to show that Case II cannot account for the increased volatility of $UO_2(s)$ at higher temperatures are similar to those for Case I. The reaction under consideration at 2071°K is

$$1/2\ UO_2(s) + 3/2\ U(\ell) = U_2O(g);\quad \Delta F°/T = -41.7\ \text{e.u.} \tag{87}$$

From the above value of $\Delta F°/T$ one calculates a value of $p_{U_2O} = 2 \times 10^{10}$ atm which clearly eliminates Case II as a reasonable explanation.

c. Case III: Formation of $UO(g)$ and $UO_3(g)$. For the equilibrium constant for Case III one writes

$$K_{III} = p_{UO}^{1/2} \cdot p_{UO_3}^{1/2} \quad . \tag{88}$$

If one specifies congruent sublimation of the solid phase then $p_{UO} = p_{UO_3}$ necessarily follows. Since all the effusate would have been condensed on the targets, the total measured pressure p for process 2 is given by

$$p = 2p_{UO} = 2p_{UO_3} \quad . \tag{89}$$

Hence, the equilibrium constant K_{III} becomes $p/2$, and $\Delta F°/T$ evaluated at 2071°K is equal to 34.0 e.u. To test the compatibility of Case III with the observed volatility of the metal-oxide mixture at 2071°K, the following four equations are necessary:

$$2UO_2(s) = UO(g) + UO_3(g);\quad \Delta F°/T = +68.0\ \text{e.u.} \tag{90}$$

$$3/2\ O_2(g) + 3/2\ U(\ell) = 3/2\ UO_2(s);\quad \Delta F°/T = -126.4\ \text{e.u.} \tag{91}$$

$$UO_3(g) = UO_3(s);\quad \Delta°F/T = -7.5\ \text{e.u.} \tag{92}$$

$$UO_3(s) = U(\ell) + 3/2\ O_2(g);\quad \Delta F°/T = +80.2\ \text{e.u.} \tag{93}$$

The necessary thermodynamic data for the evaluation of $\Delta F°/T$ for Eqs. (91) and (93) were extrapolated from data given by Coughlin.[16] $\Delta F°/T$ for Eq. (92) was evaluated from the estimated vapor pressure data of UO_3 given by Brewer.[7] Summation of the above four equations gives:

$$1/2\ UO_2(s) + 1/2\ U(\ell) = UO(g);\quad \Delta F°/T = 14.3\ \text{e.u.} \tag{94}$$

The calculated pressure of UO(g) in equilibrium with the metal-oxide mixture is 7.5×10^{-4} atm or 5.7×10^{-1} mm Hg, compared to the experimental value of 1.14×10^{-3} mm Hg. In view of the extrapolations involved in obtaining $\Delta F°/T$ values for Eqs. (91) and (93), and of the uncertainty involved in the value of $\Delta F°/T$ for Eq. (92), one cannot rigorously exclude Case III. However, it would seem quite probable that Case III does not account for the increased volatility of $UO_2(s)$ at higher temperatures, based on the available thermodynamic data.

d. Case IV: Formation of U(g) and UO_3(g). Case IV cannot be directly related to the experimentally measured volatility of the uranium-uranium dioxide mixture, but its volatility can be calculated at 2071°K and compared with the experimentally observed volatility for process 2 (Fig. 17) at this temperature. To accomplish this calculation one writes the four equations:

$$UO_2(s) = U(\ell) + O_2(g); \quad \Delta F°/T = + 84.3 \text{ e.u.} \tag{95}$$

$$1/3\ U(\ell) = 1/3\ U(g); \quad \Delta F°/T = + 8.5 \text{ e.u.} \tag{96}$$

$$3/2\ UO_3(s) = 2/3\ UO_3(g); \quad \Delta F°/T = + 5.0 \text{ e.u.} \tag{97}$$

$$O_2(g) + 2/3\ U(\ell) = 2/3\ UO_3(s); \quad \Delta F°/T = - 53.5 \text{ e.u.} \tag{98}$$

Summation of these equations gives the desired process. Thus one writes

$$UO_2(s) = 1/3\ U(g) + 2/3\ UO_3(g); \quad \Delta F°/T = + 44.3 \text{ e.u.} \tag{99}$$

The equilibrium constant for this process at 2071°K is

$$K_{IV} = 2.1 \times 10^{-10} = p_U^{1/3} \cdot p_{UO_3}^{2/3} \quad . \tag{100}$$

If one assumes the composition of the solid to remain fixed, then $p_U = 1/2\ p_{UO_3} = p/3$, where p would be the measured pressure if Case IV occurred. The value of p which one calculates from K_{IV} at 2071°K is 4.0×10^{-10} atm or 3.0×10^{-7} mm Hg. The pressure for process 2 that one calculates at 2071°K from Eq. (73) is 5.9×10^{-5} mm Hg. Hence, Case IV gives rise to a calculated pressure that is about 100 times less than the actual pressure for process (2) and one concludes that Case IV does not explain the positive curvature in log p vs. 1/T (Figs. 13 and 17). Again, one should exercise caution in view of the extrapolations of thermodynamic data and the estimation of the UO_3 vapor pressure data involved in the calculations. Therefore, one is justified only in saying that Case IV appears improbable as based on the available thermodynamic data.

e. Case V: Formation of UO_2^+(g). The possibility of an appreciable number of UO_2^+(g) ions which give rise to the curved region in Fig. 13 was examined experimentally. Three condensation targets were exposed to the effusate from tungsten effusion cell No. 1 (Fig. 6) in the fused silica apparatus (Fig. 5) at 2473°K which is definitely in the region of curvature. The three targets were exposed in succession with voltages of +22, 0, and -22, with reference to the crucible, impressed on them. All three targets showed the same weight gain within experimental error as determined by alpha counting. Since any UO_2^+(g) ions formed would leave the effusion cell with an average energy of about 1/5 of an electron volt, it was assumed that +22 volts should repel them from the target and, hence, they would not be collected. Therefore, in view of these experimental results Case V can be eliminated as possible explanation for the curved region in Fig. 13.

f. Case VI: Formation of UO(s). If UO_2 were to vaporize according to the reactions listed as Case VI, one might expect to find evidence of UO(s) in the residue after heating UO_2(s) to a high temperature. This would certainly be the case if UO(s) were thermodynamically stable at room temperature and its vapor pressure were comparable to that of UO_2(s). However, if UO(s) were thermodynamically stable only at very high temperatures, then one might not observe it at room temperature with conventional X-ray diffraction techniques. Previous work in the uranium-oxygen system, as shown by Fig. 1, seems to indicate that UO(s) is found, if at all, only at temperatures greater than 1200°C. Hoch and Johnston[28] found that ThO(s) was formed when a mixture of thorium metal and thorium dioxide, ThO_2, was heated at 1850°C. Their findings are based on the appearance of a new cubic phase evidenced by high-temperature X-ray diffraction patterns. The X-ray patterns also show that the ThO(s) phase completely disappeared, and the Th and ThO_2 phases reappeared, at lower temperatures. Since the high temperature behavior of ThO_2(s) may be very similar in many respects to that of UO_2(s) it would seem reasonable to introduce Case VI as a possible explanation of the high temperature behavior of UO_2(s).

Let us assume that UO_2(s) undergoes partial decomposition to UO(s) at very high temperatures to form, at a fixed temperature, an invariant system composed of two condensed phases and a vapor phase. If effusion measurements are then carried out on the system, both UO_2(g) and UO(g) will contribute to the equilibrium vapor above the two solid phases and both will be condensed out on condensation targets. Hence, the total volatility minus the UO_2(s) vapor pressure will yield the vapor pressure of UO(s) which will then correspond to process 2, Fig. 17. The slight difference between the molecular weights of UO and UO_2 can be shown to be insignificant for the purpose of this calculation. The constant volatility obtained in the I-2 series (Table VI) indicates that the rate of formation of the UO(s) must be slightly larger than its rate of effusion out of the orifice. Series H-2 indicates that the UO_2(s) is never completely converted to UO(s) because the oven charge in this series of measurements was held at a temperature of about 2800°K for about 5 minutes before exposures of condensation targets at somewhat lower temperatures were carried out. If all the UO_2(s) had been converted to UO(s) the H-2 series points would have fallen on the curve designated as process 2, Fig. 17, a result which was not observed. Hence, if Case VI is a reasonable explanation, both UO_2(s) and UO(s) were present in the effusion oven throughout all of the series H-2 and I-2 exposures. Making the assumption that process 2, Fig. 17, represents the vaporization of UO(s), one can calculate the pressure of UO(g) that would exist in equilibrium with a mixture of uranium metal and uranium dioxide at 2071°K. To do this one writes the equations:

$$UO(s) = UO(g); \quad \Delta F°/T = +32.6 \text{ e.u.} \tag{101}$$

$$U(\ell) + 1/2\ O_2(g) = UO(s);\quad \Delta F°/T = -41.3 \text{ e.u.} \tag{102}$$

$$1/2\ UO_2(s) = 1/2\ O_2(g) + 1/2\ U(\ell);\quad \Delta F°/T = +42.1 \text{ e.u.} \tag{103}$$

Summation of these three equations gives

$$1/2\ UO_2(s) + 1/2\ U(\ell) = UO(g);\quad \Delta F°/T = +33.4 \text{ e.u.} \tag{104}$$

The standard heat and entropy of formation of UO(s) were estimated by Brewer[7] and these values were used to make the calculation of $\Delta F°/T$ for Eq. (102). From the value of $\Delta F°/T = 33.4$ e.u. for Eq. (104), one can calculate the pressure of UO(g) in equilibrium with the metal-oxide mixture to be 5.0×10^{-8} atm or 3.8×10^{-5} mm Hg; experimentally one observed a pressure of 1.14×10^{-3} mm Hg. Again one must proceed with caution in drawing conclusions in view of the possible error in $\Delta F°/T$ for Eq. (102). However, an error as large as 7 or 8 e.u. in $\Delta F°/T$ for Eq. (104) would still give results in harmony with the experimental pressure of the mixture.

If the process 2 curve in Fig. 17 represents the vaporization of UO(s), then the average heat of sublimation over the temperature range 2200° to 2700°K calculated from the slope of Eq. (73) is 174.9 kcal mole^{-1}, and the average change in entropy associated with this process, as obtained from the intercept of Eq. (73), is 51.9 e.u. mole^{-1}. Such a value for the change in entropy associated with the simple vaporization process, $UO(s) \rightarrow UO(g)$, seems unreasonably large. In general, the change in entropy accompanying a simple vaporization process ranges from about 30 to 40 e.u. for refractory substances. The change in entropy associated with the simple vaporization of UO_2, $UO_2(s) \rightarrow UO_2(g)$, was found to be about 36 e.u. Hence, from the entropy considerations above, one must view Case VI as a very unlikely interpretation of the curvature in log p vs. 1/T (Fig. 13).

Additional support to this last statement is obtained from the calculation of the equilibrium oxygen atom pressure associated with the following reaction at 2500°K:

$$UO_2(s) = UO(s) + O(g) \quad . \tag{105}$$

In order to make this calculation one writes the equations:

$$UO_2(s) = U(\ell) + O_2(g);\quad \Delta F°/T = 62.9 \text{ e.u.} \quad , \tag{106}$$

$$U(\ell) + 1/2\ O_2(g) = UO(s);\quad \Delta F°/T = -30.6 \text{ e.u.} \quad , \tag{107}$$

$$1/2\ O_2(g) = O(g);\quad \Delta F°/T = 8.3 \text{ e.u.} \tag{108}$$

Summation of these equations yields the desired equation, namely, Eq. (105) with a value of $\Delta F°/T = + 40.6$ e.u. The equilibrium pressure of oxygen atoms is found to be 1.02×10^{-9} atm or 7.8×10^{-7} mm Hg. The sources of the necessary thermodynamic data for the above calculation have been previously cited. Clearly if the equilibrium pressure of oxygen atoms is only about 1×10^{-6} mm Hg and if UO(s) vaporizes at a pressure of the order of 0.1 mm, as indicated in Fig. 17, then UO(s) would be leaving the effusion cell by a factor of 10^5 more rapidly than it is being formed from the decomposition of $UO_2(s)$. Therefore, in view of the above arguments, Case VI is not a reasonable interpretation of process 2.

g. Case VII. Formation of the Dimer, $U_2O_4(g)$. If $UO_2(s)$ were to vaporize at very high temperatures according to the expression listed as Case VII, then one can neither prove or disprove the existence of the dimer, $U_2O_4(g)$, on the basis of the data submitted in this thesis alone. The criterion used to reject Cases I, II, and III, namely the observed volatility of the metal-dioxide mixture (series D-2), is thermodynamically unrelated to the existence of $U_2O_4(g)$. In fact, there are no available thermodynamic data that can be employed either to confirm or refute the existence of the dimer.

Nevertheless, arguments can be presented which would indicate that, if $U_2O_4(g)$ existed in the equilibrium vapor above $UO_2(s)$, it would be of importance only at very high temperatures and would be of little or no importance at lower temperatures. Brewer[5] has reasoned that for high boiling substances the dimer will be important only at high temperatures whereas the monomer will be the principal vapor species at low temperatures. For low boiling substances this situation is exactly reversed. Stevens[65] finds $UO_2^+(g)$ to be the predominant ionic species in his mass spectrometer when $UO_2(s)$ is vaporized from a tantalum filament at temperatures up to about 2200°K. Regions of higher temperature have not been investigated by this means.

Hence, in view of these arguments and the lack of any other reasonable process to account for the high temperature vaporization behavior of $UO_2(s)$, let us treat process 2, Fig. 17, as resulting from the vaporization of $UO_2(s)$ to form $U_2O_4(g)$.

In order to carry out this treatment one must consider in some detail the relationships between pressure, amount, and rate of effusion of the monomer and dimer in the equilibrium vapor leaving the effusion cell. In the effusion experiments one actually measured the total number of moles of uranium u collected on the target. The assumption was then made that the vaporizing species was $UO_2(g)$ and all pressures p_e were then calculated based on Eq. (8). Hence, the defining equation for p_e is

$$u = p_e (2\pi M_1 RT)^{-1/2} \quad , \qquad (109)$$

Where M_1 is the molecular weight of UO_2. Actually both monomer and dimer are assumed to be present in the vapor. If u = the total number of gram atoms of uranium effusing per cm^2 per sec; u_1 = the number of gram atoms of uranium in $UO_2(g)$ effusing per cm^2 per sec, and u_2 = the number of gram atoms of uranium in $U_2O_4(g)$ effusing per cm^2 per sec, then $u = u_1 + u_2$. The numbers of moles of $UO_2(g)$ and $U_2O_4(g)$ effusing per cm^2 per sec are u_1 and $1/2\ u_2$, respectively. In view of Eq. (8) one can write that

$$u_1 = p_1 (2\pi M_1 RT)^{-1/2} \quad , \tag{110}$$

and

$$1/2\ u_2 = p_2 (2\pi M_2 RT)^{-1/2} = p_2(2)^{-1/2}(2\pi M_1 RT)^{-1/2} \quad , \tag{111}$$

where M_1, p_1 and M_2, p_2 are the molecular weights and pressures of the monomer and dimer, respectively.

From Eqs. (109), (110), and (111) and the uranium balance one can derive a relationship among p_e, p_1, and p_2, viz.,

$$p_e - p_1 = (2)^{1/2}\ p_2 \quad . \tag{112}$$

It will be remembered that Eq. (73) was obtained by subtracting p_1 from p_e to obtain p_2 at various temperatures. Therefore, this equation can be easily modified to yield the correct pressure of the dimer by the appropriate correction involving $2^{1/2}$. Obviously, only the constant term will be affected and it will be less by an amount 1/2 log 2. Eq. (73) thus corrected becomes

$$\log p_{mm} = - 38{,}221/T + 14.056 \tag{113}$$

Eq. (113) applies over the temperature range 2200° to 2700°K. The heat ΔH_2^o and entropy ΔS_2^o of sublimation of $UO_2(s)$ to $U_2O_4(g)$ as calculated from the slope and intercept of Eq. (116) are 174.9 kcal $mole^{-1}$ and 51.1 e.u., respectively.

If the curvature in Fig. 17 is caused by $U_2O_4(g)$, the heat of dissociation of the dimer ΔH_D^o, is readily calculable from the summation of the following equations and their respective heats. At 2450°K one has

$$2\ UO_2(s) \longrightarrow 2UO_2(g); \quad 2\ \Delta H_1^o = 263.8 \text{ kcal mole}^{-1} \quad , \tag{114}$$

$$U_2O_4(g) \longrightarrow 2UO_2(s); \quad - \Delta H_2^o = - 174.9 \text{ kcal mole}^{-1} \quad . \tag{115}$$

Thus one obtains

$$U_2O_4(g) \longrightarrow 2UO_2(g); \quad \Delta H_D^o = 88.9 \text{ kcal mole}^{-1} \quad . \tag{116}$$

The change in entropy associated with the dissociation of the dimer to yield $2UO_2(g)$ is found similarily and is 16.6 e.u. at 2450°K.

The respective amounts of monomer and dimer in the equilibrium vapor is related to the pressures p_1, and p_2 by the equation

$$\frac{p_1}{p_2} = 2\alpha/(1-\alpha) \qquad (117)$$

where α is the fractional dissociation of $U_2O_4(g)$ to $2UO_2(g)$. The quantity α, explicitly solved in terms of p_1 and p_2, is

$$\alpha = p_1/(2p_2 + p_1) \quad . \qquad (118)$$

At 2200°K, α = 0.44, while at 2700°K, α = 0.11.

h. Case VIII. Reaction with the Effusion Cell. One must bear in mind the possibility of a reaction between the charge and the material of construction of the effusion cell. The formation of U(g) or UO(g), along with $WO_3(g)$ or other gaseous tungsten oxides, might account for increased volatility at high temperatures.

The large entropy change of about 52 e.u. accompanying process 2 is somewhat difficult to account for on the basis of a simple vaporization process, i.e., $MO_y(s) \longrightarrow MO_y(g)$. Reaction with the crucible material to form two volatile species would be expected to have a large entropy change associated with it.

Two lines of evidence indicate that appreciable reaction with the effusion cell did not occur. First, the vaporization results with tantalum effusion cells were very nearly the same as with tungsten effusion cells. Second, the amount of tungsten leaving the effusion cell would have been comparable with the amount of uranium. During several target exposures, the total quantities of both tungsten and uranium oxides would have been present in large amounts on the condenser wall. There was no visual evidence indicating a large quantity of tungsten oxide deposition which would have been dark blue in color. Furthermore, spectroscopic analysis showed no tungsten on the condensation targets and only insignificant quantities on the walls of the vapor pressure apparatus. Tungsten was present in the residue in an amount less than 0.2%. Hence, it appears that reaction with the effusion cell cannot account for the curvature in the plot of log p vs. 1/T, as shown in Fig. 13.

In summarizing the above treatments, one can say that the high temperature vaporization behavior of $UO_2(s)$ is explainable on the basis of Case VII, the formation of $U_2O_4(g)$. One can further state that Case VII represents the most reasonable process of the eight cases that were postulated to explain this very interesting high temperature phenomenon. Cases III

and IV cannot be rigorously excluded in view of the uncertainties in the thermodynamic quantities for UO_3. Experiments of a more direct nature would, therefore, be desirable in order to identify the molecular species giving rise to the curvature in log p vs. $1/T$ in Fig. 13. Such valuable data might be obtained from momentum detection experiments similar to those of Weber and Plantenberg,[70] or from velocity selection experiments similar to those carried out by Ko.[39] The mass spectrometer might also serve as a useful tool in identifying the vapor species in equilibrium with $UO_2(s)$ at high temperatures.

B. Vaporization Phenomena of Metal-Metal Dioxide Mixtures

Figure 18 is an attempt to classify the general volatility-time behavior of metal-metal dioxide mixtures according to the types of processes that might occur when the mixture is heated in an effusion cell at a given temperature in vacuo. The oxide MO_2 is assumed to yield $MO_2(g)$ upon vaporization.

The type of behavior indicated by curve 1 is that of no appreciable reaction between equimolar amounts of metal M and the dioxide MO_2. Both are then free to vaporize at their respective vapor pressures $\overset{\circ}{p}_M$ and $\overset{\circ}{p}_{MO_2}$. Usually $\overset{\circ}{p}_M$ is larger than $\overset{\circ}{p}_{MO_2}$ for almost all oxides. Thus,

$$\left.\begin{aligned} &M(s \text{ or } \ell) = M(g) \\ \text{and} \\ &MO_2(s) = MO_2(g) \end{aligned}\right\} . \qquad (119)$$

A marked decrease in volatility results when the evaporating surface of the metal is no longer large enough to maintain the saturation vapor pressure of the metal inside the effusion cell.

Curve 2 shows the behavior of an equimolar mixture containing an easily oxidizable metal. The vapor pressure of the metal is suppressed by the presence of a closely adhering oxide skin which forms on its surface as a result of residual oxygen in the vacuum system. Again, no reaction occurs and the principal gaseous species in equilibrium with the condensed phases are M(g) and $MO_2(g)$, i.e.,

$$\left.\begin{aligned} &M(\text{oxide-coated}) = M(g) \\ \text{and,} \\ &MO_2(s) = MO_2(g) \end{aligned}\right\} . \qquad (120)$$

Appreciable reaction between equimolar amounts of M and MO_2 to form a stable gaseous oxide MO is shown by curve 3. If appreciable MO(g) is formed, the initial observed volatility must necessarily be greater than

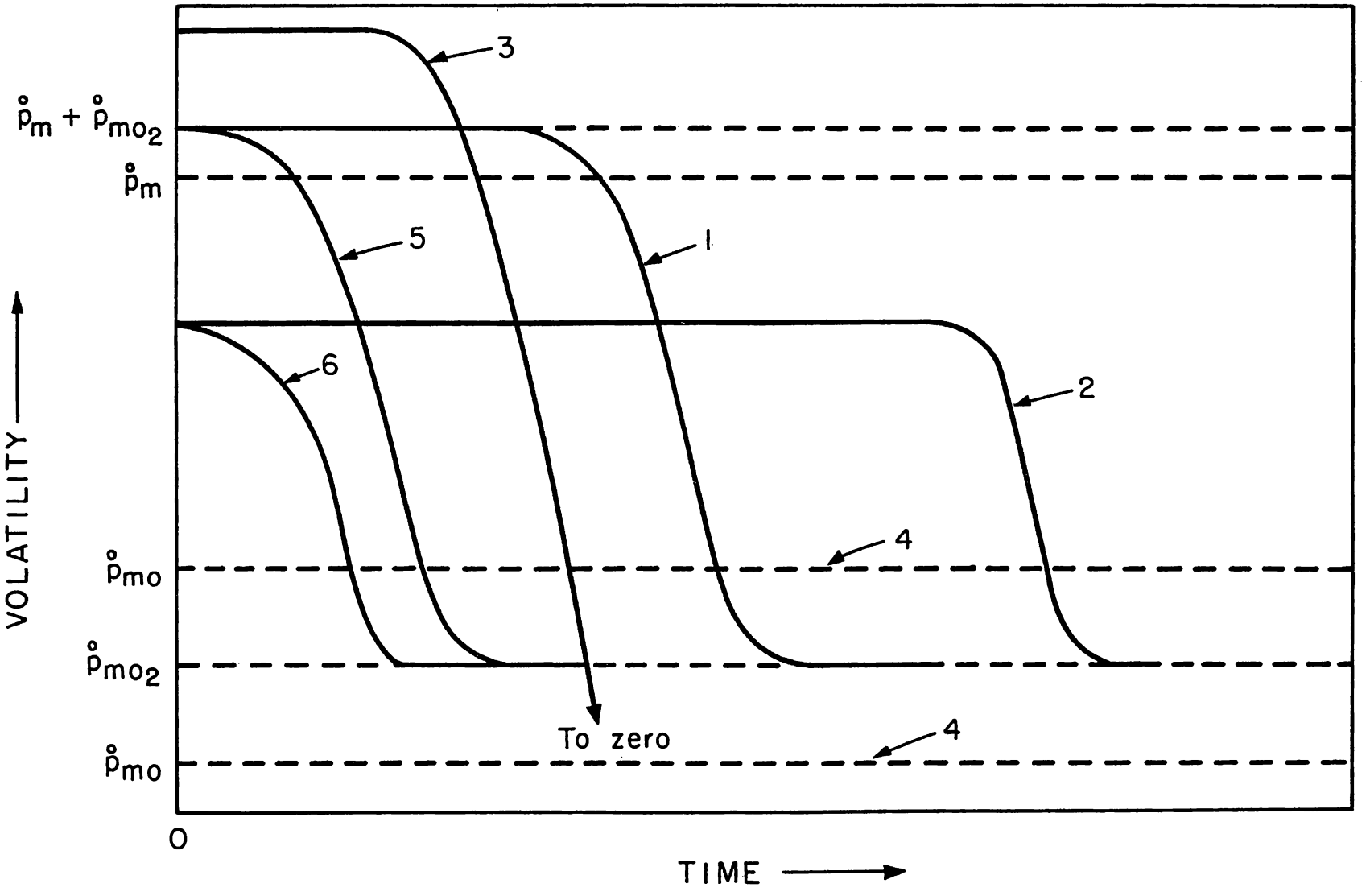

Figure 18

General Volatility vs. Time Behavior of Metal-Metal Dioxide Mixtures

the sum of the vapor pressures of M and MO_2, and reaction occurs according to the equation:

$$M\ (s \text{ or } \ell) + MO_2(s) = 2MO(g) \quad . \tag{121}$$

Curve 4 represents the complete reaction between equimolar amounts of M and MO_2 to form the relatively nonvolatile solid oxide MO. The observed volatility of the mixture represents the vapor pressure of MO(s) which may be either more or less volatile than $MO_2(s)$. Two curves numbered 4 are shown. Hence, reaction occurs according to the equation:

$$M\ (s \text{ or } \ell) + MO_2(s) = 2MO(s) \quad . \tag{122}$$

Two other processes of significance are indicated by curves 5 and 6. Curve 5 represents the volatility-time behavior of a mixture containing only a small amount of pure metal and a large amount of oxide which undergoes no reaction. The amount of metal present in the mixture is insufficient to maintain the saturation vapor pressure of the metal. Hence, the initial volatility decreases rapidly with time. Curve 6 indicates the similar behavior of a mixture containing a small amount of oxide-coated metal and a large amount of oxide.

Specific cases could occur which would involve one or more combinations of the various types of behavior cited here. Such cases would be necessarily complicated and volatility-time measurements might have to be supplemented by other data in order to determine the exact nature of the processes occurring. Solid and gaseous oxides of different stoichiometry than MO (such as M_2O and M_2O_3) might be formed, but the volatility-time behavior in such cases would be similar to that shown by curves 3 and 4.

1. Interpretation of the Uranium-Uranium Dioxide Mixture Volatilities

The principal vapor species above the series D-2 metal-dioxide mixture were U(g) and $UO_2(g)$ as is evident from the weight loss data given in Tables III and IV. Hence, it appears that no chemical reaction occurred between the metal and dioxide. The uranium vapor pressure is suppressed by the presence of an oxide skin, a result similar to the findings of Rauh and Thorn.[55] The volatility-time behavior shown by series D-2 (Fig. 12) is indicated by curve 2 in Fig. 18.

The anomalous behavior of the series D-1 measurements (Fig. 12) is no doubt associated with the constantly changing background pressure which controlled the rate of formation of the oxide skin. At the beginning of the series, when the background oxygen pressure was 9×10^{-6} mm Hg, the rate of formation of the oxide skin was large compared to its net rate of evaporation and the rate of evaporation of uranium was thereby initially suppressed. At the minimum in the c/m vs. time

curve, where the background pressure was 2×10^{-6} mm Hg, the rate of formation of the oxide skin just equaled its net rate of evaporation. A further decrease in the background pressure caused the increased volatility with increased time.

It should be pointed out that the interpretation by Rauh and Thorn of the mechanism suppressing the vapor pressure of uranium is probably not quite correct in that the oxide skin which formed on the surface of the liquid was assumed to be impervious. This being the case, the volatility of the oxide-coated liquid should reach a minimum when the entire surface of the liquid becomes covered with a monolayer of the oxide. This minimum should then correspond to the vapor pressure of the oxide which they designated UO_x. On the basis of this investigation, the oxide UO_x is, in all probability, UO_2. This minimum volatility is almost a factor of ten larger than the vapor pressure of UO_2 at the temperatures of their measurements. Hence, it seems quite probable that the presence of the oxide monolayer did not completely suppress the vaporization of the metal, and that the volatility of this oxide-covered liquid really is due to the sum of the oxide vapor pressure and the pressure resulting from diffusion of U(g) through the oxide skin. To test the validity of this hypothesis, one would have to carry out the measurements on the uranium vapor pressure at higher oxygen pressures, and, therefore, at greater thicknesses of the oxide skin. Such measurements might enable one to calculate quantitatively the rate of diffusion of U(g) through various thicknesses of the oxide skin according to classical diffusion theory. For thicknesses of the order of monolayers, the measurements would have the further interesting aspects in that quantum theory should be applicable and one might then be able to obtain an insight into the nature of diffusion on the basis of atomic concepts.

C. Discussion and Summary of Errors

Equation (19) gives the vapor pressure p explicitly in terms of constants and experimentally determined quantities. The uncertainty in p calculated from this equation may result from four kinds of errors. (1) An inherent error is one originating from an inaccurate knowledge of some constant not measured in the experiment. (2) A systematic error is one that arises from an uncertainty in a measured quantity, which uncertainty affects all calculated values of p in a nonrandom manner. (3) A statistical error is one arising from purely statistical fluctuations in equally reliable measurements. (4) A basic error is one originating from failure of the experimental method employed to fulfill a condition demanded by theory. The basic errors involved in the effusion method are discussed in Section IV-1. In order to discuss the remaining kinds of error involved in the calculation of a vapor pressure, Eq. (19) is rewritten so as to show the kind of error associated with each group of terms, viz.,

$$p = \underbrace{\left[j\left(\frac{2\pi R}{M}\right)^{1/2} \right]}_{\text{inherent errors}} \cdot \underbrace{\left[\frac{d^2 + r^2}{r^2 S_0} \right]}_{\text{systematic errors}} \cdot \underbrace{\left[\frac{(c/m)\, T^{1/2}}{t} \right]}_{\text{statistical errors}}, \quad (126)$$

where all quantities have been previously defined except j, which is the conversion factor from counts per minute to grams of UO_2. The particular group of terms in the respective error brackets is purely arbitrary and the author recognizes, for example, that errors of both a systematic and inherent nature are to be found in the temperature. All errors that are discussed are probable errors unless otherwise specified. The probable error of a function $Z = f(z_1, z_2, \cdots)$ is defined by the expression,[3]

$$R_Z = [(\partial Z/\partial z_1)^2 r_1^2 + (\partial Z/\partial z_2)^2 r_2^2 + \cdots]^{1/2} \quad , \quad (127)$$

where r_1, r_2, etc. are the probable errors in z_1, z_2, etc.

1. Inherent Errors in the Vapor Pressure

The uncertainty in the gas constant R is considered to be negligible in this discussion. The molecular weight M of the vaporizing species in all calculations of p was assumed to be that of UO_2, and no significant uncertainty in M resulted below 2000°K. Above 2000°K, proper cognizance of the variation in the molecular weight of the effusing vapor was taken. The constant j originates from the conversion of counts per minute to grams of UO_2 for a collected sublimate and directly involves the half-lives of radioactive species. For the U^{233} exposures, the probable error in the half-life is ± 0.6%, and the percentage isotopic composition is known within a probable error of 0.02%, which is negligible. Similar magnitudes of errors are involved in consideration of other isotopes. The total inherent probable error is then approximately ± 0.6% at temperatures below 2000°K.

2. Systematic Errors in the Vapor Pressure

The geometry factor was corrected for the changes occurring in d, r, and S_0 due to their respective expansions and contractions at the various temperatures of measurement. (Refer to Section V.) The error introduced in this correction is due to the uncertainties in the respective linear coefficients of thermal expansion and can be shown to be negligible. The errors incurred in the room temperature measurements of d, r, and S_0 are quoted in Section V and are also considered negligible in this discussion.

3. Statistical Errors in the Vapor Pressure

The uncertainty associated with c/m arises from three sources: (a) the statistical fluctuation in the total number of observed counts, (b) the uncertainty in the counting time, and (c) the error resulting from resolution losses and drift of the counter. Sources (b) and (c) are insignificant and the largest probable error associated with (a) for all targets is ± 1.3%.

In computing the probable error in t, the exposure time of a target, a probable error of ± 0.01 minute in starting, and ± 0.01 minute in terminating the exposure was assumed. The probable error in any one value of t was taken as the square root of the sum of the squares of these errors, viz., ± 0.014 minute. For the shortest exposure of 2.00 minutes, the error involved is 0.7%. Since all other times of exposure were considerably longer, the probable error in t can be considered negligible.

In determining the statistical uncertainty involved in the measurement of the temperature T, one must consider the following four experimental steps involved in every assignment of a value to T: (1) the calibration of the optical pyrometer based on the freezing point of copper by means of rotating sectors, (2) the determination by means of the pyrometer of the transmissivity of the window and prism combination used in viewing the effusion cell, (3) the determination of the apparent temperature of the black-body hole, and (4) the comparison of black-body hole with cavity temperature. To get some idea of the magnitudes of the uncertainties involved in these observations let us consider the measurement of one particular temperature (target No. 23, series C-2). This particular exposure was chosen since it represents about the best precision obtained. The average pyrometer reading in this particular case was 1710°C, which was determined from seven independent measurements. The probable error in the average temperature was calculated to be ± 0.7°. The transmissivity of the interposed window and prism combination yielded the result that

$$1/T_a - 1/T = (0.116 \pm 0.002) \times 10^{-4}\ \text{deg}^{-1} \quad . \qquad (128)$$

Calculation of the probable error in T using the previously calculated probable error in T_a and the above expression yields a value of ± 1.5°. The black-body hole temperature and the cavity temperature agreed within an estimated probable error of ± 1.0°. The calculation of the probable error associated with the calibration of the pyrometer at this temperature proceeds as follows. The probable error in the effective wavelength λ_e is estimated to be ± 0.1 mμ. The measurements of the sector transmissivities were quite precise and the probable error associated with their respective transmissivities is considered to be zero. In view of these errors and the probable error involved in the two sector measurements necessary to extrapolate the calibration curve from the copper point to the desired temperature (assuming a probable error of ± 0.7% at the copper point) one calculates a probable error associated with the calibration procedure of about ± 2.4°. The total per cent probable error associated with the measurement of temperature is the square root of the sum of the squares of the errors for all involved processes, namely, ± 0.17%.

Consider now the probable error in the calculated values of p arising from the measurements indicated in the third bracket of Eq. (126) alone. Since the percent probable error in the temperature is much smaller

than that for the counting, it can be shown that the percent probable error in the result is essentially that of the counting, which is about one per cent. This value is to be compared with statistical error obtained by making a number of successive exposures at a constant temperature, such as the I-2 series, Table VI. After the individual values given in Table VI were normalized to a temperature of 2469°K, the average value obtained was $(7.84 \pm 0.043) \times 10^{-2}$ mm Hg. The probable error of a single observation was 1.4 per cent. The agreement is good.

It should be remembered that the errors above specifically exclude basic, systematic, and inherent errors. The scatter of the vapor pressure points shown in Fig. 13 is not caused entirely by the statistical error previously calculated since errors as large as 25% in the vapor pressure occur for those points showing greatest deviation from the least-squares curve. Consequently these large errors must be classed as indeterminate.

VII. SUMMARY AND CONCLUSIONS

A high temperature, high vacuum investigation of the vaporization processes of uranium dioxide has been carried out over the temperature range 1600° to 2800°K by means of the effusion method. Prior to this investigation effusion measurements extending over such a large range of high temperature and pressure were unknown. The use of various radioactive isotopes of uranium made it possible to carry out these measurements.

It has been demonstrated that UO_2 vaporizes congruently over the entire range of investigation by the observation that the vapor pressure is unique at constant temperature, as evidenced by series I-2, and that the composition of the residues after appreciable vaporization was always found to be $UO_{2.00}$ by X-ray lattice parameter measurement and direct oxygen analysis.

A plot of log p vs. 1/T for all the data is linear from 1600° to about 2200°K, but shows a definite positive curvature above this latter temperature. An empirical equation which has been fitted to all the data by the method of least-squares is

$$\log p_{mm} = 13.340 - \frac{3.7337 \times 10^4}{T} + \frac{3.6700 \times 10^6}{T^2} + \frac{2.4638 \times 10^9}{T^3} \quad (57)$$

This equation was obtained in order to permit a quick calculation of the rate of evaporation. In order to simplify its use for that purpose, a molecular weight corresponding to UO_2 was employed, even though UO_2 may be the less important vapor species at higher temperatures. Therefore, the use of this equation, together with this molecular weight, will yield the observed rate of vaporization.

Over the temperature range 1600° to 2000°K, $UO_2(s)$ vaporizes predominantly to $UO_2(g)$. The vapor pressure over this range of temperature is represented by the least-squares equation

$$\log p_{mm} = -\frac{33,115}{T} - 4.026 \log T + 25.686 \quad . \quad (72)$$

The average heat and entropy of sublimation for $UO_2(s)$ to $UO_2(g)$ over this temperature range are 137.1 ± 1.6 kcal mole^{-1} and 36.4 e.u., respectively. The value for ΔH_0°, the heat of sublimation of $UO_2(s)$ to $UO_2(g)$ at absolute zero, is 160.3 ± 5.0 kcal mole^{-1}. From the calculated and available thermodynamic data a dissociation energy for $UO_2(g)$ to its gaseous atoms is found to be 14.4 ev at 0°K.

The positive curvature in log p vs. 1/T above 2200°K probably does not result from exceeding the upper limit of the effusion method. This conclusion was reached after a study of infrequently cited molecular beam

investigations. The positive curvature was then reasoned to result from the presence of another vaporization process. Eight vaporization processes were proposed to explain the positive curvature in log p vs. 1/T. The processes involving the formation of UO(g), $U_2O(g)$, UO_2^+ (g), and UO(s) were shown to be impossible by calculations and additional experiments. The processes involving the formation of UO(g) and UO_3(g), and U(g) and UO_3(g) were regarded as unlikely in view of the available thermodynamic data. Even though extrapolation and estimation of thermodynamic data could have introduced considerable uncertainty in the calculated results, this uncertainty was probably not sufficiently large to alter the conclusions reached unless the thermodynamic quantities for UO_3 are in serious error. Experimental evidence eliminated reaction of UO_2 with the effusion cell as the cause of the increased volatility at the higher temperatures.

To account for the positive curvature in log p vs. 1/T at high temperatures the existence of the dimer, U_2O_4(g), was postulated. The least-squares equation obtained for the vapor pressure of UO_2(s) vaporizing to U_2O_4(g) is

$$\log p_{mm} = -\frac{38,221}{T} + 14.358 \quad . \tag{113}$$

The heat of dissociation of the dimer to $2UO_2$(g) was found to be 88.9 kcal $mole^{-1}$ at 2450°K.

From the observation that melting of the over charge had occurred at 2426°C or below, but not at 2388°C, one concludes that the melting point lies between these limits; the value chosen is 2405°C.

Specially designed experiments demonstrated that the location of the evaporating surface inside the effusion cell markedly affects the rate of effusion in the forward direction, if this area is comparable with the orifice area.

The absorption spectrum of thin films of UO_2(s) has been measured from 4000 to 8000 Å.

The vaporization behavior of the reliably established uranium oxides at about 900°K is summarized in the total pressure vs. composition phase diagram shown in Fig. 19. The dioxide, UO_2, is the only known uranium oxide which vaporizes congruently.

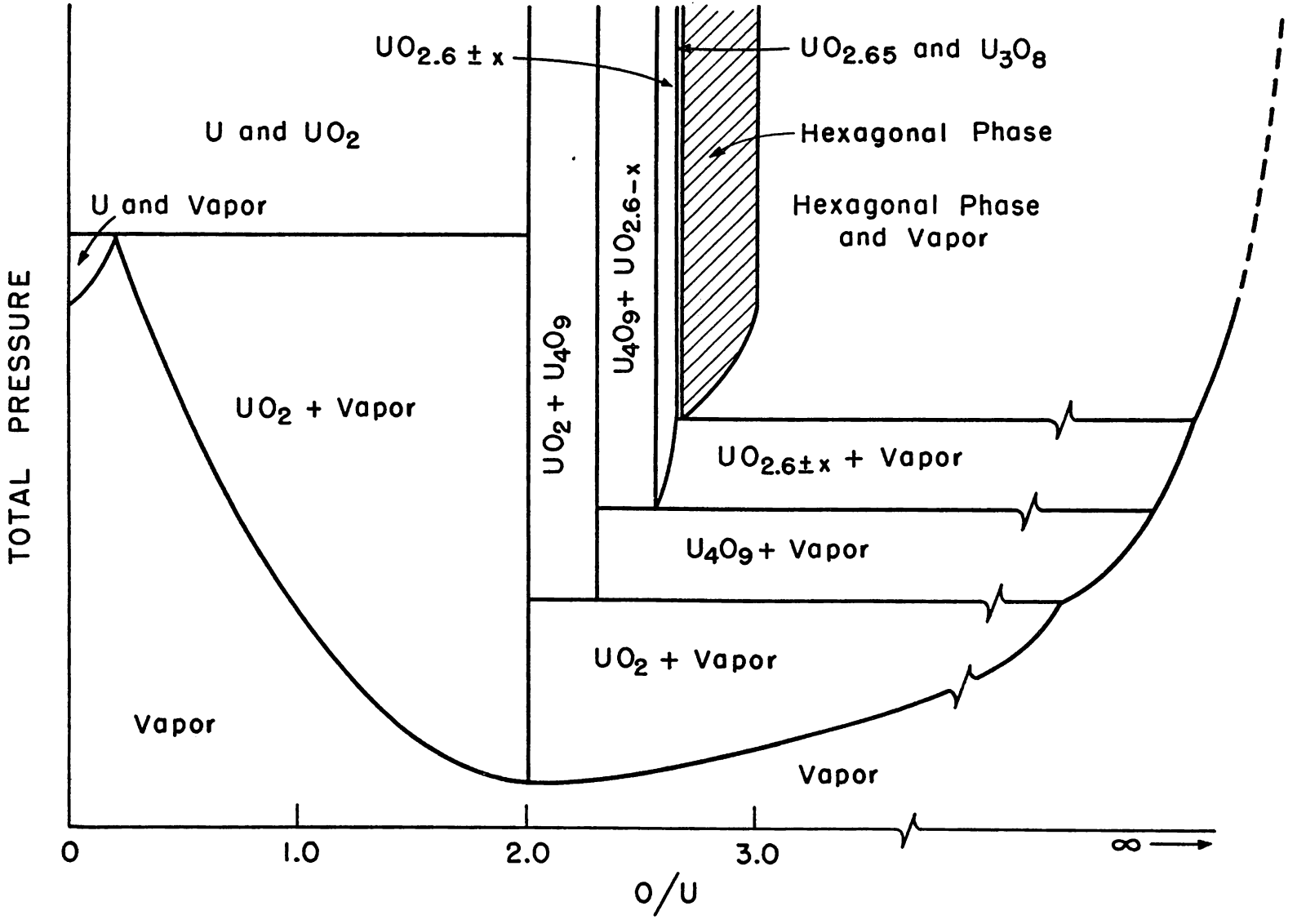

Figure 19

The Phase Diagram of the Uranium-Oxygen System Showing Total Pressure vs. Composition at a Constant Temperature, 900°K

VIII. SUGGESTIONS FOR FUTURE RESEARCH

There remain several unsolved problems concerning both the uranium-oxygen system and other aspects encountered in this research. Further investigations are necessary to prove or disprove the existence of the dimer in the equilibrium vapor above $UO_2(s)$ at temperatures greater than 2200°K. Such investigations might include the direct examination of the average molecular weight of the vapor by means of a momentum detector or a velocity selector. Additional information as to the nature of the vapor species might be obtained from mass spectrometric studies.

Volatility-time curves should be obtained for mixtures of uranium metal and dioxide heated at temperatures in the region of 2200° to 2500°K in an attempt to find UO(s). Additional information about the formation and stability range of UO(s) could be obtained from a high temperature X-ray diffraction study of these mixtures. Since ThO(s) is stable at high temperatures only, this author suspects a similar behavior for UO(s).

The absorption spectrum of uniform thin films of $UO_2(s)$ prepared by condensation of vapor on cooled targets should be studied as a function of film thickness and as a function of the target temperature. This investigation could be extended to include the effect of dissolved oxygen, i.e., the formation of the UO_{2+x} phase, upon the absorption spectrum.

A method should be devised whereby the partial pressure of oxygen in equilibrium with a known composition of the UO_{2+x} phase can be measured at various temperatures. A knowledge of both the equilibrium oxygen pressure and the solid composition would enable one to calculate the activity of oxygen in the UO_{2+x} phase. It may also be possible to establish more reliably the pressure vs. composition phase diagram of the uranium-oxygen system by such a method, at least at low temperatures where numerous solid phase transformations are known to occur as shown in Fig. 1.

The vaporization of U_3O_8 and lower oxides between U_3O_8 and UO_2 requires additional study since it appears that vaporization of U_3O_8 and lower oxides is somewhat complicated by a small but significant loss of uranium which may be carried as $UO_3(g)$. Reliable measurements of the vapor pressure of UO_3 would be useful in interpreting this loss of uranium in terms of $UO_3(g)$, and also in re-evaluating the high temperature vaporization behavior of $UO_2(s)$.

Further fundamental investigations dealing with the effusion method are necessary. The upper limit of the method has not been unequivocally established. One might employ an effusion cell containing a thin-edged orifice and measure the spatial distribution of effusing Cs atoms as a function of source pressure by means of a surface ionization detector. Similarly, the spatial distribution of effusate from a channeled orifice could be measured.

Measurements of the effect of location and size of the evaporating area should be carried out at temperatures where the mean free path is quite small. This would mean almost all molecules leaving the effusion cell would originate from the gas phase and the beam intensity in the forward direction should be independent of the location of the evaporating area. Similar measurements should also be performed at very large mean free paths. The cavity of the effusion cell should be spherically shaped to enable one to perform conveniently the integrations involved in the calculation of the arrival rate or beam intensity at a given point in the 2π solid angle above the plane of the orifice. A comparison of the spatial distributions outside the orifice obtained with both annular and central evaporating areas, comparable in magnitude to the orifice area, should be quite revealing.

IX. ADDENDUM

THE ABSORPTION SPECTRUM AND COLOR OF URANIUM DIOXIDE SUBLIMATES

The room temperature absorption spectrum of solid uranium dioxide was measured in the region 4000 to 8000 Å. A uniform thin film (0.2 mg/cm^2) of uranium dioxide, as evidenced by X-ray diffraction lines, was deposited on a 1-mm quartz condensation target by exposing the target to the molecular beam originating from an inductively heated effusion cell. The exposure was carried out in the fused silica vapor pressure apparatus (Fig. 5) fitted with a water-cooled, fused silica cold-finger attachment that accommodated a single condensation target. The temperature of the target during the exposure was estimated to be about 800°C. A recording Cary spectrophotometer was used for measuring the absorption spectrum. Figure 20 shows the absorption spectrum thus obtained. Maxima occur at 7500 Å and 5200 Å; a partially hidden maximum occurs at 4500 Å. The fundamental absorption band begins at about 4300 Å and extends beyond 3500 Å where a maximum optical density of 2.4 was recorded. The optical density was still increasing at this wavelength. Gruen[26] had previously found a maximum at 6500 Å and had mistakenly identified a 5200 Å maximum with the beginning of the continuous absorption band which actually begins at about 4300 Å as shown by this investigation. Effusate collected at a temperature <400°C was shown to be U_3O_8 by direct oxygen analysis and the measured absorption remained constant from 8000 to about 4000 Å. For wavelengths less than 4000 Å, a slightly increased absorption was noted.

Thin uniform films of UO_2(s) condensed on liquid nitrogen-cooled platinum targets show very interesting variations in color, depending upon their thickness. These colors vary in the following order of increasing thickness: light tan, purple, blue, yellow, green, and red violet. It is possible to estimate with good accuracy the weight of material on a given platinum target from its color.

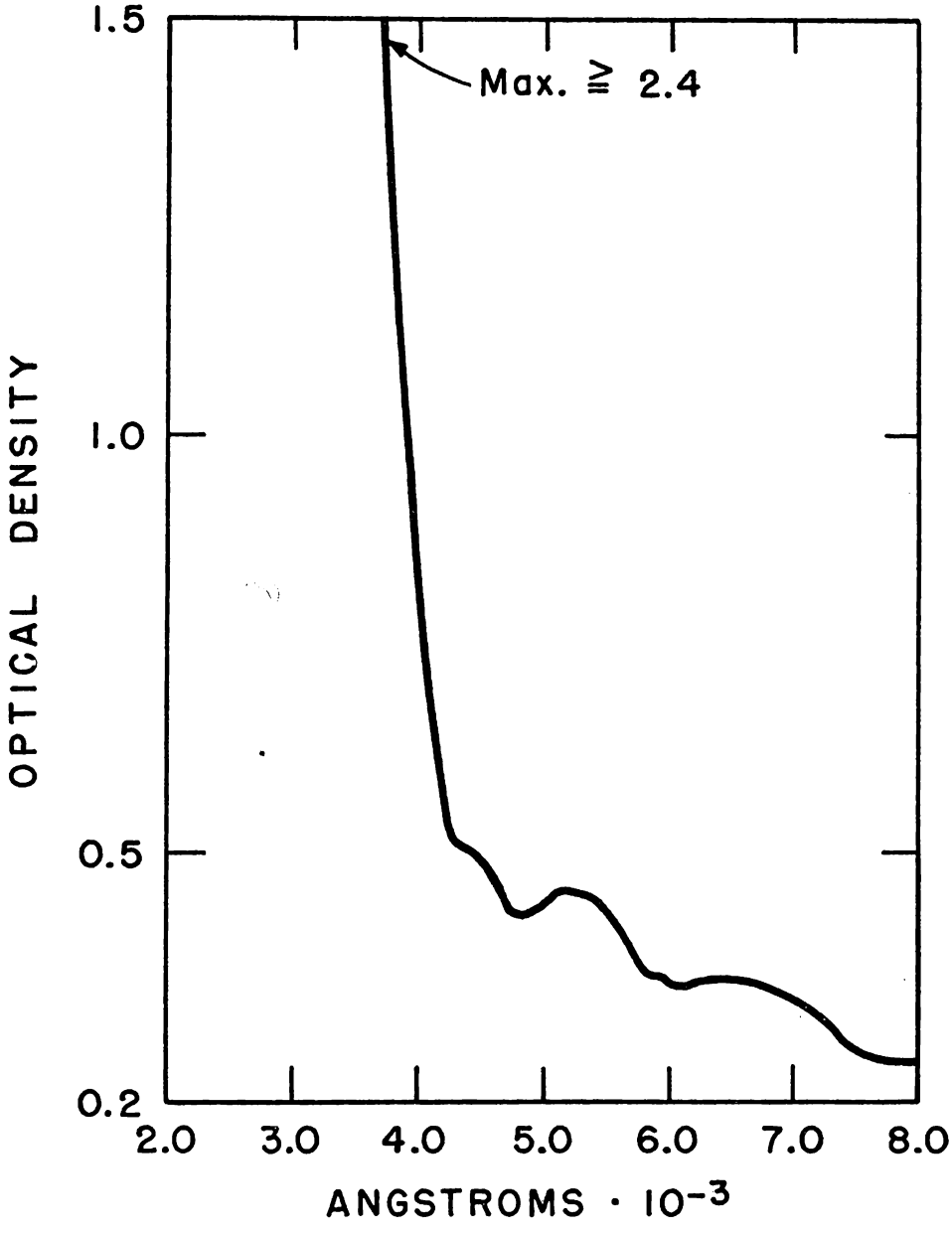

Figure 20

The Absorption Spectrum of Solid Uranium Dioxide

X. APPENDICES

RELATION AMONG ATOMIC PERCENT O, WEIGHT PERCENT O, AND ATOMIC RATIO IN THE URANIUM-OXYGEN SYSTEM

O/U	Atomic Percent Oxygen	Weight Percent Oxygen	O/U	Atomic Percent Oxygen	Weight Percent Oxygen	O/U	Atomic Percent Oxygen	Weight Percent Oxygen	O/U	Atomic Percent Oxygen	Weight Percent Oxygen	O/U	Atomic Percent Oxygen	Weight Percent Oxygen	O/U	Atomic Percent Oxygen	Weight Percent Oxygen
0.00	0.000	0.000	0.50	33.33	3.252	1.00	50.00	6.299	1.50	60.00	9.161	2.00	66.67	11.85	2.50	71.43	14.39
0.02	1.961	0.134	0.52	34.21	3.378	1.02	50.49	6.417	1.52	60.32	9.271	2.02	66.89	11.96	2.52	71.59	14.49
0.04	3.846	0.268	0.54	35.06	3.503	1.04	50.98	6.535	1.54	60.63	9.382	2.04	67.11	12.06	2.54	71.75	14.58
0.06	5.660	0.402	0.56	35.90	3.628	1.06	51.46	6.652	1.56	60.94	9.492	2.06	67.32	12.16	2.56	71.91	14.68
0.08	7.407	0.535	0.58	36.71	3.753	1.08	51.92	6.769	1.58	61.24	9.602	2.08	67.53	12.27	2.58	72.07	14.78
0.10	9.090	0.668	0.60	37.50	3.878	1.10	52.38	6.886	1.60	61.54	9.712	2.10	67.74	12.37	2.60	72.22	14.88
0.12	10.71	0.800	0.62	38.27	4.001	1.12	52.83	7.003	1.62	61.83	9.821	2.12	67.95	12.48	2.62	72.38	14.98
0.14	12.28	0.932	0.64	39.02	4.125	1.14	53.27	7.119	1.64	62.12	9.931	2.14	68.15	12.58	2.64	72.53	15.07
0.16	13.79	1.057	0.66	39.76	4.249	1.16	53.70	7.234	1.66	62.41	10.04	2.16	68.35	12.68	2.66	72.68	15.17
0.18	15.25	1.196	0.68	40.48	4.372	1.18	54.13	7.350	1.68	62.69	10.15	2.18	68.55	12.78	2.68	72.83	15.27
0.20	16.67	1.327	0.70	41.18	4.494	1.20	54.54	7.465	1.70	62.96	10.26	2.20	68.75	12.89	2.70	72.97	15.36
0.22	18.03	1.458	0.72	41.68	4.617	1.22	54.95	7.580	1.72	63.24	10.37	2.22	68.95	12.99	2.72	73.12	15.46
0.24	19.35	1.588	0 74	42.53	4.739	1.24	55.36	7.695	1.74	63.50	10.47	2.24	69.14	13.09	2.74	73.26	15.56
0.26	20.63	1.718	0.76	43.18	4.861	1.26	55.75	7.810	1.76	63.77	10.58	2,26	69.33	13.19	2.76	73.41	15.65
0.28	21.88	1.849	0.78	43.82	4.983	1.28	56.14	7.923	1.78	64.03	10.69	2.28	69.51	13.29	2.78	73.55	15.75
0.30	23.08	1.977	0.80	44.44	5.104	1.30	56.52	8.037	1.80	64.28	10.80	2.30	69.70	13.39	2.80	73.68	15.84
0.32	24.24	2.106	0.82	45.05	5.225	1.32	56.90	8.151	1.82	64.54	10.90	2.32	69.88	13.49	2.82	73.82	15.94
0.34	25.37	2.235	0.84	45.65	5.345	1.34	57.26	8.264	1.84	64.79	11.01	2.34	70.06	13.59	2.84	73.96	16.03
0.36	26.47	2.363	0.86	46.24	5.465	1.36	57.63	8.378	1.86	65.03	11.12	2.36	70.24	13.69	2.86	74.09	16.13
0.38	27.54	2.491	0.88	46.81	5.585	1.38	57.98	8.498	1.88	65.28	11.22	2.38	70.41	13.79	2.88	74.23	16.22
0.40	28.57	2.619	0.90	47.37	5.706	1.40	58.33	8.603	1.90	65.52	11.33	2.40	70.59	13.89	2.90	74.36	16.32
0.42	29.58	2.746	0.92	47.92	5.825	1.42	58.68	8.714	1.92	65.75	11.43	2.42	70.76	13.99	2.92	74.49	16.41
0.44	30.56	2.871	0.94	48.45	5.944	1.44	59.02	8.827	1.94	65.99	11.54	2 44	70.93	14.09	2.94	74.62	16.50
0.46	31.51	3.000	0.96	48.98	6.063	1.46	59.35	8.938	1.96	66.22	11.64	2.46	71.10	14.19	2.96	74.75	16.60
0.48	32.43	3.126	0.98	49.49	6.181	1.48	59.68	9.050	1.98	66.44	11.75	2.48	71.26	14.29	2.98	74.87	16.69
															3.00	75.00	16.78

Expressions used in the construction of this table were:

$$\text{At. \% O} = \frac{(O/U) \cdot 100}{1 + (O/U)} \qquad \text{Wt. \% O} = \frac{16/238\ (O/U) \cdot 100}{16/238\ (O/U) + 1}$$

APPENDIX II

FREE ENERGY FUNCTIONS FOR $UO_2(s)$ AND $UO_2(g)$

T (°K)	$-\left(\frac{F^\circ_T - H^\circ_{298}}{T}\right)_s$	$-\left(\frac{F^\circ_T - H^\circ_{298}}{T}\right)_g$
1500	24.12	75.33
1600	25.77	76.11
1700	27.88	76.84
1800	28.70	77.54
1900	30.03	78.20
2000	31.29	78.83

$\Delta H^\circ_{298} = 159.7$ kcal mole^{-1}

XI. BIBLIOGRAPHY

1. Alberman, K. B., and Anderson, J. S., J. Chem. Soc. 1949 S303, Suppl. Issue 2.

2. Biltz, W., and Mueller, H., Z. anorg. Chem., 163, 257 (1927)

3. Birge, R. T., Am. J. Phys., 7, 351 (1939).

4. Boulle, A., Compt. rend. 229, 214 (1949).

5. Brewer, L., Paper 7, Chemistry and Metallurgy of Miscellaneous Materials: Thermodynamics, N.N.E.S. IV-19B, McGraw-Hill Book Co., Inc., New York (1950).

6. Brewer, L., Bromley, L. A., Gilles, P. W., and Lofgren, N. L., "The Thermodynamic Properties and Equilibria at High Temperatures of Uranium Halides, Oxides, Nitrides, and Carbides," N.N.E.S. VIII-6, McGraw-Hill Book Co., Inc., New York (1949).

7. Brewer, L., Chem. Rev. 52, 1 (1953).

8. Brewer, L., and Mastick, D. F., J. Chem. Phys. 19, 834 (1950).

9. Clark, F. L., Spencer-Palmer, H. J., and Woodward, R. N., British Atomic Energy Project Reports, Br-522, October, 1944 [See Seaborg, G. T., and Perlman, I., Revs. Mod. Phys. 20, 585-667 (1948)].

10. Chamberlain, O., Williams, D., and Yuster, P., Phys. Rev. 70, 580 (1946).

11. Chupka, W. A., Personal Communication, Argonne National Laboratory, Lemont, Illinois.

12. Clausing, P., Physica 9, 65, (1925).

13. Clausing, P., Z. Physik 66, 471 (1930).

14. Clausing, P., Ann. Physik 12, 961 (1932).

15. Clower, E. W., Doctoral Thesis, University of Illinois, Urbana, Illinois, 1954.

16. Coughlin, J. P., Bur. Mines Bull., p. 542 (1954).

17. Crawford, J. A., Paper 16.55, The Transuranium Elements, N.N.E.S. IV-14B, McGraw-Hill Book Co., Inc., New York (1949)

18. Cunningham, B. B., Ghiorso, A., and Jaffey, A., Paper 16.3, The Transuranium Elements, N.N.E.S. IV-14B, McGraw-Hill Book Co., Inc., New York, 1949.

19. Dawson, J. K., and Lister, M. W., J. Chem. Soc., 1950, Part 3, 2181.

20. Erway, N. D., and Simpson, O. C., J. Chem. Phys., 18, 953 (1950).

21. Friederich, E., and Sittig, L., Z. anorg, u. allgem. Chem. 145, 127 (1925).

22. Gaydon, A. G., Dissociation Energies and Spectra of Diatomic Molecules, Dover Publications, Inc., New York, 1950.

23. Greenwood, H., J. Chem. Soc. 93, Part II, 1492 (1908).

24. Gronvold, H., and Haraldsen, H., Nature 162, 69 (1948).

25. Groves, W. O., Hoch, M., and Johnston, H. L., J. Phys. Chem. 59, 127 (1955).

26. Gruen, D., J. Am. Chem. Soc. 76, 2117 (1954).

27. Hering, H., and Perio, P., Bull. soc. chim. France, p. 351 (1952).

28. Hoch, M., and Johnston, H. L., J. Am. Chem. Soc. 76, 4833 (1954).

29. Hoekstra, H. R., and Katz, J. J., Anal. Chem. 25, 1608 (1953).

30. Hoekstra, H. R., Siegel, S., Fuchs, L. H., and Katz, J. J., J. Phys. Chem. 59, 136 (1955).

31. Huber, E., Holley, C., and Meierkord, E., J. Am. Chem. Soc. 74, 3406 (1952).

32. Hyde, E. K., Paper 19.15, The Transuranium Elements, N.N.E.S. IV-14B, Part II, McGraw-Hill Book Co., Inc., New York, 1954.

33. Jaffey, A., Argonne National Laboratory Report 4875, September, 1952.

34. Johnson, T. H., Phys. Rev. 31, 103 (1928).

35. Jones, W. M., Gordon, J., and Long, E. A., J. Chem. Phys. 20, 695 (1952).

36. Katz, J. J., and Rabinowitch, E., The Chemistry of Uranium, N.N.E.S. VIII-5, Part I, McGraw-Hill Book Co., Inc., New York, 1951, pp. 244-345.

37. Kelley, K. K., Bur. Mines Bull. 476 (1949).

38. Kiess, C., Humphreys, C., and Laun, D., J. Research Nat. Bur. Standards, 37, 57 (1946).

39. Ko, C. C., J. Franklin Inst. 217, 173 (1934).

40. Knauer, F., and Stern, O., Z. Physik 39, 774 (1926).

41. Knudsen, M., Ann. Physik 28, 75 (1909).

42. Ibid., 999 (1909).

43. Ibid., 29, 179 (1909).

44. Knudsen, M., The Kinetic Theory of Gases, Meuthen, Ltd., London, 1934.

45. Lambertson, W. A., and Gunzel, F. H., Jr., AECD Report-3465, June, 1952.

46. Langmuir, I., Phys. Rev. 2, 329 (1913).

47. Margenau, H., and Murphy, G. M., The Mathematics of Physics and Chemistry, D. Van Nostrand Co., Inc., New York, p. 481.

48. Mayer, H., Z. Physik 52, 235 (1928).

49. Ibid., 58, 373 (1929).

50. Mayer, J., and Mayer, M. Statistical Mechanics, J. Wiley and Sons, Inc., New York, 1940, p. 18.

51. Moore, G. E., and Kelley, K. K., J. Am. Chem. Soc. 69, 2105 (1947).

52. Nier, A. O., Phys. Rev. 55, 150 (1939).

53. Phipps, T. E., Sears, G. W., and Simpson, O. C., J. Chem. Phys. 18, 724 (1950).

54. Price, G. R., Ferretti, R. J., and Schwartz, S., Anal. Chem. 25, 322 (1953).

55. Rauh, E. G., and Thorn, R. J., J. Chem. Phys. 22, 1414 (1954).

56. Rehn, J., and Cefola, R., Report CK-1240, January 19, 1944. (See reference 36).

57. Rodden, C. J., and Warf, J. C., Analytical Chemistry of the Manhattan Project, N.N.E.S. VIII-1, McGraw-Hill Book Co., Inc., New York, 1950, Chapter I.

58. Ruff, O., and Gocke, O., Z. angew. Chem. 24, 1459 (1911).

59. Rundle, R. E., Baenzinger, N. C., Wilson, A. S., and MacDonald, R. A., J. Am. Chem. Soc. 70, 99 (1948).

60. Sachs, G., and Van Horn, K. R., Practical Metallurgy, American Society of Metals, 1943, p. 2.

61. Seaborg, G. T., and Katz, J. J., The Actinide Elements, N.N.E.S. IV-14A, McGraw-Hill Book Co., Inc., New York, 1949, p. 612.

62. Shapiro, E., Phys. Rev. 78, 352 (1950).

63. Simpson, O. C., Thorn, R. J., and Winslow, G. H., Argonne National Laboratory Report-4264, May 6, 1949.

64. Stern, O., Z. Physik 66, 471 (1920).

65. Stevens, C., Personal Communication, Argonne National Laboratory, Lemont, Illinois.

66. Stimson, H. F., J. Research Nat. Bur. Standards 42, 209 (1948).

67. Thorn, R. J., Argonne National Laboratory Report-5417, March 21, 1955.

68. Tingwaldt, C., and Hoffmann, F., Optische Pyrometrie, Edwards Brothers, Inc., Ann Arbor, Michigan, 1944.

69. Wahlin, H. B. Phys. Rev. 39, 183 (1932).

70. Weber, A. H., and Plantenberg, Sister Gonzaga O.S.B., Phys. Rev. 69, 649 (1946).

71. Wheatley, Q. de L., Doctoral Thesis, University of Kansas, Lawrence, Kansas (April, 1954).

72. Winslow, G. H., Personal Communication, Argonne National Laboratory, Lemont, Illinois.

ACKNOWLEDGEMENTS

The author is extremely indebted to Professor Paul W. Gilles for his patience, understanding, and guidance throughout the author's academic training and this research. It was through his efforts that the necessary arrangements were made at Argonne National Laboratory where this research was carried out.

To Dr. Robert J. Thorn, who directed this research at Argonne National Laboratory, the author warmly extends his gratitude for the encouragement, interest, and guidance he so willingly gave.

In addition, the author wishes to acknowledge the following:

Drs. O. C. Simpson, and G. H. Winslow, and Mr. E. G. Rauh of Argonne National Laboratory whose timely suggestions and criticisms proved invaluable in this work.

Dr. S. Siegel and Miss L. Wiersema of Argonne National Laboratory for their assistance in analyzing the numerous X-ray diffraction patterns necessary throughout this investigation.

Mr. B. Holt and Dr. H. R. Hoekstra of Argonne National Laboratory for performing numerous oxygen analyses.

Argonne National Laboratory for the opportunities and services afforded the author under the Participating Institutions Program carried out in conjunction with the University of Kansas.